Aus dem Bereich Med. Biophysik

Theoretische Medizin und Biowissenschaften

der Medizinischen Fakultät

der Universität des Saarlandes, Homburg/Saar

Killing efficiency of natural killer cells is boosted by physical contact with T cells

Dissertation zur Erlangung des Grades eines Doktors der
Naturwissenschaften

der Medizinischen Fakultät

der UNIVERSITÄT DES SAARLANDES

2023

vorgelegt von: Xiangda Zhou

geb.am: 07.10.1987 in Jilin, China

<div align="center">Index</div>

1. Abstract

Natural killer (NK) cells are killer cells from the innate immune system responsible for eliminating pathogen-infected or tumorigenic cells. T cells are the central players in the adaptive immune system, including T helper CD4$^+$ T cells and cytotoxic CD8$^+$ T cells. However, how the interaction between NK cells with T cells influences NK cell killing efficiency still largely unknown. To tackle this question, in this work, I co-cultured primary NK cells with activated T cells and examined NK cell killing efficiency. I found that an *in vitro* co-culture with activated T cells, both CD4$^+$ and CD8$^+$, greatly enhances the killing efficiency of homologues NK cells against different types of tumor cell lines. Co-culture with T cells did not affect NK cells on the expressions of cytolytic proteins (perforin and granzymes) or the degranulation of lytic granules. Instead, T cell co-culture greatly enhanced speed and persistence of NK cell migration as well as NK cell infiltrating capability into 3D collagen matrices. The T cell-induced NK activation can be achieved in 24-hour-co-culture and lasts for several days. I have further identified that physical contact between NK and T cells is indispensable. Blockade of IL-2 receptor using neutralizing antibody abolished enhancement in NK cell killing boosted by T cells. Nether conditional medium from activated T cells nor addition of IL-2 could resemble the extent of T cell boosted NK cell killing, indicating that local IL-2 plays a critical role in this regard. Moreover, ICAM-1/LFA-1 interaction is also involved in boosting NK cell functions by T cells. Surface molecule profiling from CyTOF analysis revealed distinct subsets in T cell boosted NK cells. RNAseq data show that cytoskeletal elements and related molecules as well as metabolic pathways were significantly altered by T cell co-culture. These findings extend the understanding of the T-NK cell interaction mechanism and provide valuable insights into the link between important players from both innate and adaptive immunity.

1. Zusammenfasung

Natürliche Killerzellen (NK) sind zelluläre Bestandteile des angeborenen Immunsystems, die eine wichtige Rolle bei der Beseitigung von mit Krankheitserregern infizierten oder tumorbildenden Zellen spielen. Auf der anderen Seite sind T-Zellen die Hauptakteure des adaptiven Immunsystems, zu denen CD4$^+$ T-Helferzellen und zytotoxische CD8$^+$ T-Zellen gehören. Obwohl die Interaktion zwischen NK-Zellen und T-Zellen die Tötungseffizienz der NK-Zellen beeinflusst, ist dieser Mechanismus noch weitgehend unerforscht. Im Rahmen dieser Studie habe ich primäre NK-Zellen mit aktivierten T-Zellen in einer Ko-Kultur untersucht, um die Auswirkungen auf die Tötungseffizienz der NK-Zellen zu untersuchen. Die Ergebnisse zeigen, dass die In-vitro-Kokultur mit aktivierten T-Zellen, sowohl CD4$^+$ als auch CD8$^+$, die Tötungseffizienz der NK-Zellen gegen verschiedene Tumorzelllinien signifikant erhöht. Es wurde festgestellt, dass diese Ko-Kultur weder die Expression von zytotoxischen Proteinen wie Perforin und Granzyme noch die Degranulation der lytischen Granula beeinflusst. Stattdessen erhöht die Ko-Kultur mit T-Zellen die Geschwindigkeit und Ausdauer der Migration der NK-Zellen sowie deren Fähigkeit, in dreidimensionale Kollagenmatrizes einzudringen. Die Aktivierung der NK-Zellen durch T-Zellen kann bereits innerhalb von 24 Stunden in der Ko-Kultur erreicht werden und hält mehrere Tage an. Des Weiteren wurde festgestellt, dass der direkte physische Kontakt zwischen NK- und T-Zellen unerlässlich ist. Die Blockade des IL-2-Rezeptors mit einem neutralisierenden Antikörper hebt die Verstärkung der NK-Zellabtötung durch T-Zellen auf. Weder das konditionierte Medium von aktivierten T-Zellen noch die Zugabe von IL-2 allein konnten das Ausmaß der verstärkten NK-Zellabtötung durch T-Zellen erreichen, was darauf hinweist, dass lokales IL-2 in diesem Zusammenhang eine entscheidende Rolle spielt. Darüber hinaus spielt die Interaktion von ICAM-1/LFA-1 eine bedeutende Rolle bei der Verstärkung der NK-Zellfunktionen durch T-Zellen. Durch die Anwendung der CyTOF-Analyse konnten Oberflächenmolekülprofile erstellt werden, die unterschiedliche Untergruppen in den NK-Zellen aufzeigten, die durch T-Zellen verstärkt wurden. Zusätzlich zeigten RNAseq-Daten signifikante Veränderungen in Elementen des Zytoskeletts, verwandten Molekülen und Stoffwechselwegen durch die Ko-Kultur mit T-Zellen. Diese Erkenntnisse erweitern das Verständnis des Interaktionsmechanismus zwischen T- und NK-Zellen und liefern wertvolle Informationen über die Verbindung zwischen den maßgeblichen Akteuren des angeborenen und des adaptiven Immunsystems.

2. Introduction

The immune system, an exquisite "defense line" generated in millions of years of evolution, has helped us human beings to survive countless threats opposed by pathogenic microbes and abnormal cell proliferation like tumors. Our bodies' health relies on an effective immune response which requires a sophisticatedly orchestrated network involving more than 10 major types of immune cells. Previous investigations about how immune cells collaborate, locate targets and eliminate threats have helped us to make great progress on immunotherapy against tumor. In this study, we focus on the T cell-induced NK cell function promotion. Investigations were carried out to expand our knowledge about how the two major players from both adaptive and innate immunity interact and achieve a higher NK killing efficiency against tumor cells. These findings may provide positive insights for future anti-tumor research.

2.1 An overview of the immune system

The immune system is a well-developed network that involves sophisticated cellular and molecular orchestration among immune cells or between the immune system and somatic cells in the host body. For the survive of the host, there are three challenges for the immune system to take: 1) to recognize non-self or abnormal cells and mount destructive reaction correspondingly; 2) to form immunologic memory in order to response promptly when the body is re-exposed to the same pathogens; 3) to avoid immune response against self which is known as the immune tolerance. To address these challenges, a large number of immune cells with diverse functions are derived. Most of the immune cells are produced and matured in bone marrow (T cells complete development in thymus) after early childhood. Some of these cells undergo a process of sophisticated secondary education and then circulate in the extracellular fluid to patrol the body [1, 2].

There are two fundamental arms of the immune system, innate immunity and adaptive immunity. Innate immunity is an organization of cells and molecules that take effect immediately or shortly (within several hours) after the host is exposed to infectious agents [3]. In spite of how many times the host encounters the pathogen, the innate responses occur to the same extent. Besides the constitutively active physical barriers formed by epithelium, fatty acids, mucus, and cilia that reject inhaled or ingested particles, the innate defense mainly depends on cellular components include phagocytic cells such as neutrophils, monocytes, and macrophages; cells that produce inflammatory mediators including basophils, mast cells, and eosinophils (exert anti-parasite activities); antigen-presenting dendritic cells; natural killer (NK) cells [4-6]. The molecular components of innate immunity are comprised of soluble factors including cytokines such as the interferons (modulate immune cell functions), acute-phase

proteins, and complement cascade proteins [7-10].

Adaptive immunity, on the other hand, depends on antigen-specific defense mechanisms anchored by the antigen-driven clonal expansion of T and B lymphocytes [5, 11]. B cells are matured in bone marrow [2] responsible for producing antibodies, which neutralize pathogens or induce ADCC to destroy pathogen or aberrant cells. T cells are matured in thymus [12]. They are phenotypically characterized by the surface expression of the transmembrane T-cell receptors (TCR) that specifically bind to antigens presented by antigen-presenting cells (APCs) [13-15]. T cell populations are comprised of CD4^{+} and CD8^{+} T cells. In cell-mediated immune responses, T cells are activated by the foreign antigen presented by APCs. Most activated CD4^{+} T cells serve as helper cells to facilitate activation of other immune cells, for example B cells, NK cells, and CD8^{+} T cells by their cytokine secretion [16]. While activated CD8^{+} T cells, also known as cytotoxic T lymphocytes, can directly eliminate aberrant cells in an antigen-dependent manner [17].

2.2 All for kill: Killing machinery of natural killer cells

To eliminate pathogen-infected or tumorigenic cells, two particular groups of immune cells act as key players: cytotoxic T lymphocytes (CTLs) and NK cells. CTLs are effector CD8^{+} T cells, belonging to the adaptive immune system. Using TCRs and CD8 molecules, cytotoxic T lymphocytes recognize antigens presented by MHC class I molecules on the target cell surface. In comparison, NK cells kill target cells in an antigen-independent manner. Despite of the difference in the mechanisms for target recognition, cytotoxic T lymphocytes and NK cells share very similar killing machineries to eliminate their target cells.

NK cells, as the name suggests, possess cytotoxic capacity without prior activation by any antigen. NK cells have a pivotal role in eradicating tumorigenic and pathogen-infected cells. NK cells are phenotypically characterized by the absence of TCR/CD3 on their surface [18] and the surface expression of CD16 (Fc-γRIII, binds to the Fc region of IgG) and CD56 (neural cell adhesion molecule) . To find their target cells, NK cells need to patrol tissues, where they encounter complicated and dynamic three-dimensional (3D) environments [19-23]. NK cells recognize the cognate target cells by a sophisticated repertoire of activating and inhibitory receptors [24]. Once target cells are identified, NK cells form a tight contact with the target cells, termed immunological synapse (IS), to orient their killing machinery towards the target cells [25, 26]. NK cells mainly adopt two killing mechanisms to eliminate targets: cytotoxic protein-containing lytic granules as well as Fas/FasL pathway. NK cells can also initiate killing via ADCC, i.e., forming an IS with antibody-bound target cells through the Fc receptor CD16.

2.2.1 To kill or not to kill: target cell recognition by NK cells

There are many models proposed to explain how NK cells recognize their target cells. One of the first theories is the "missing-self" hypothesis, which is based on the fundamental concept that NK cells can be activated when encountering viral-infected or malignant cells with diminished or absent "self" MHC I molecule expression [27, 28]. However, experimental evidence shows how NK cells respond to their target cells is determined by a sophisticated balance between the intracellular signals triggered by serials of germline-encoded activating and inhibitory receptors expressed on the NK cell surface [24]. The MHC I receptors on NK cells do not regulate the NK activation in a binary behavior. They act like "rheostat" to dampen the signal of activating receptors rather than a "switch-off" [29]. NK cells are found capable to eliminate target cells when the activating signals from the engagement of multiple or highly potent activating NK receptors overwhelm the inhibitory signal from MHC I ligation [29-32].

Later, a sophisticated model suggests that NK cell activation is a result of competition between activating versus inhibitory signals mediated by activating and inhibitory receptors, respectively. To date, a wide repertoire of activating receptors has been defined on NK cells [29, 33-35]. In humans, the activating receptors mainly include natural cytotoxicity receptors (NCRs), NKG2D, and the Fc-γ receptor CD16. NCRs encompass NKp30 (CD337), NKp44 (CD334) and NKp46 (CD335). Engagement of NK activating receptors with their ligands triggers recruitment of downstream effector molecules to further transduce activation signals. For instance, CD16 binds to CD3ζ or FcRγ, NKp30 and NKp46 binds to CD3ζ, and NKp44 binds to DAP12 [36, 37].

Inhibitory mechanisms to harness activation of activating receptors are necessary since normal cells could also express ligands of the activating receptors under some circumstances [38]. To this purpose, NK cells express a panel of inhibitory receptors that bearing immunoreceptor tyrosine-based inhibition motifs (ITIMs). The majority of inhibitory receptors fall to two categories: C-type lectin domain family (e.g., NKG2A/CD159a, CD161/NKR-P1) and immunoglobulin superfamily (e.g., KIRs, LIRs) [29, 34, 39, 40]. The inhibitory receptors usually bind to MHC class I molecules that are expressed by most healthy somatic cells to prevent NK cells from destroying innocent cells. Under physiological circumstances, healthy cells express adequate number and density of inhibitory receptor ligands that provide sufficient inhibitory signal even when some activating signals are triggered at the same time [41-45]. In comparison, on abnormal cells, expression of inhibitory receptor ligands is downregulated while expression of activating receptor ligands is upregulated, tipping the balance towards activation to initiate the corresponding killing events.

2.2.2 Engaging target: Immunological synapse (IS) formation

The formation of an IS is a prerequisite for NK killing [46, 47]. IS formation involves a series of continuous and subsequential events. When NK cells get in contact with their cognate target cells, fundamental changes take place in NK cells. Surface molecules at the contact site are quickly attributed to spatially segmented structures, termed supramolecular activation clusters (SMACs). Depending on the distance from the center, there are central SMAC (cSMAC) and peripheral SMAC (pSMAC) [46, 48, 49]. Meanwhile, the cytoskeleton undergoes considerably radical rearrangements. Cortical actin forms a ring-like structure at the pSMAC. Microtubule organizing center (MTOC) is translocated from the uropod (rear part of NK cells) to the vicinity of the IS. Cytotoxic protein-containing lytic granules are also concentrated at the IS and are subsequently released into the cleft, leading to the destruction of target cells.

A tethering-like contact between the NK and the target is formed upon target recognition. Though still not yet well understood, selectin family members and CD2 are believed to play important roles in initiating the contact [50-52]. CD2 is found accumulated at the NK-target contact site within 5 minutes [48] and suggestively contribute to potentiate activation signals in NK cells [53, 54]. The transient contact can be converted to a stable conjugation if activation signals over-compete inhibitory signals. Compelling evidence shows that the interaction between lymphocyte function-associated antigen 1 (LFA-1) on NK cells and ICAM-1 on target cells is indispensable to stabilize/seal the contact [48] and the subsequent actin reorganization at the pSMAC [55].

Actin network plays a key role in maturation and functionality of the IS. Actin can be polymerized into a branched meshnetwork mediated by Arp2/3 or into bundle arrays mediated by formins [56-58]. Actin nucleator Arp2/3 is recruited to the side of an existing actin filament by associating transiently with the activator Wiskott–Aldrich syndrome protein (WASP) [59]. And after the detachment of the WASP, the Arp2/3 complexes nucleate a new branched actin filament t at a 70◦ angle [56, 60]. Therefore, WASP is of necessity to the characteristic shape changes that NK cells adopt soon after IS formation [48, 61-63]. Formin-mediated formation of actin bundles relies highly on profilin-dependent transport of actin monomer on the barbed end for actin elongation [64] .

Polarization of MTOC to the IS is one of the hallmarks of IS formation, essential for enrichment of lytic granules at the IS. Upon target recognition, prior to MTOC polarization, lytic granules are rapidly converged to the MTOC and in a dynein dependent manner [65]. Consequently, along with MTOC polarization towards the IS, lytic granules are also enriched at the IS. By inserting the microtubule plus-ends into the actin network accumulated at the IS, forces are generated to facilitate the MTOC reorientation [66].

Intact functionality of the cytoskeleton is also required for delivery of lytic granules to dock on the plasma membrane at the IS and the subsequent release. Studies using CTLs shows that

transport lytic granules to the IS can be dependent or independent of plus-end microtubule motor protein kinesin [67, 68]. In the latter case, lytic granules delivery is suggestively mediated by myosin II [69]. Release of lytic granules in NK cells is dependent on intact activity of myosin IIA, but myosin IIA is not involved in MTOC reorientation and lytic granule enrichment at the IS [69]. Actomyosin contractility would provide sufficient mechanical forces to allow lytic granules to pass through the F-actin meshwork.

2.2.3 Bullets: cytotoxic proteins

Lytic granules are the major mechanism employed by NK cells to eliminate their target cells [25, 26]. Lytic granules contain cytotoxic proteins mainly pore-forming perforin and serine protease granzymes, which are indispensable to lyse target cells. To avoid lysing NK cells themselves, perforin is stored in an inactivate form in lytic granules mainly owing to the acidic environment. Once released into the cleft, the neural pH in vicinity of target cells allows perforin to insert into target cell plasma membrane and oligomerize to form pores. Granzymes are internalized into target cells to activate caspase cascades and induce target cell apoptosis [26].

The pore-forming protein perforin was first discovered in 1985 [70]. Perforin precursor is synthesized in the ER. With 555 amino acids, 65 kDa, perforin is composed of multiple domains [71]. The N-terminal sequence of perforin is comprised with a signal peptide and the membrane attack complex/perforin (MACPF) domain, which is responsible for cytolytic activity [72]. The N-glycosylation sites are required for locating the perforin molecules from Golgi to lytic granules [73]. The C-terminus, on the other hand, is composed of an EGF-like domain and a CD2 domain, which facilitate perforin to incorporate into plasma membranes in a calcium-dependent way [74]. Once being sorted into lytic granules, the last 20 amino acids of the perforin C-terminus are cleaved by cathepsin L, resulting in the full activation of perforin [75]. However, in the lytic granules, perforin is inactivated mainly due to the acidic pH. If the acidic pH is elevated to neutral pH by concanamycin A, perforin is hydrolysed by DFP-sensitive proteases in the lytic granules [76]. Furthermore, in the lytic granules, the perforin activity is additionally inhibited by calreticulin and binding to serglycin [77].

In NK cells, the perforin gene is transcribed constitutively [78, 79]. However, subsets of NK cells differ in the perforin expression level. Compared to CD56^{bright} NK cells, CD56^{dim} subset express higher level of perforin and are more cytotoxic. It is reported that engagement of NK activating receptor NKp30 drastically induces nuclear factor-κB (NF-κB) activity [80], which contributes to regulating perforin expression in NK cells [81]. Transcription factor Eomesodermin (Eomes) is responsible for the perforin expression in cooperation with T-bet. The perforin mRNA level is found drastically reduced in Eomes-deficent murine NK cells [82, 83].

Granzymes belong to the serine protease family. So far, five granzymes have been identified in humans with different substrate specificity [84]. Granzyme A and granzyme K display tryptase-like activity; granzyme B (GzmB) is an asp-ase; granzyme H and granzyme M have chymotrypsin-like (chymase) activity. All granzymes are synthesized as pro-enzymes. Among all granzymes, GzmB is the most apoptotic one [85]. Through the mannose-6-phosphate receptor (MPR) pathway, the inactive precursor of GzmB is sorted to the lytic granules [86, 87], where two amino acids at the N-terminus of GzmB are cleaved predominantly by cathepsin C and possibly also by cathepsin H to gain the full protease activity [88-90]. The active GzmB is tightly packed in a complex with serglycin, which is a proteoglycan with protease-resistant peptide core, to inhibit GzmB cytolytic activity in lytic granules [91].

When released into a cytolytic IS, GzmB enters the target cells to induce apoptosis. There are mainly two pathways mediating GzmB entry: GzmB can be transferred into the cytoplasma of the target cells by going through the pores made by perforin [92] or by endocytosis. Compelling evidence shows that perforin is necessary for GzmB entry but not sufficient. Intracellular Ca^{2+} influx in target cells induced by formation of perforin pores is also required for GzmB to enter target cells [93]. Interestingly, GzmB mutants, which cannot bind to heparan-sulfate-containing membrane receptors for endocytosis, can enter the cytosol of target cells with a similar efficacy as wild type GzmB [94], suggesting that endocytosis mediated by heparan sulphate containing receptors on target cell membrane is dispensable for GzmB delivery into target cells [94].

GzmB mainly initiate apoptosis of the target cells by triggering caspase activation. GzmB directly cleave caspase 3 and also release caspase inhibition, both of which are required for GzmB-dependent apoptosis [95]. By cleaving caspase substrates such as Bid (BH3-interacting dominant death agonist), GzmB unleashes cytochrome c into the cytoplasma [96], where cytochrome c interacts with apoptosis proteinase-activating factor (Apaf)-1 and caspase 9 to further activate caspase 3 to trigger apoptosis [97]. Furthermore, GzmB can directly cleave Rho associated coiled-coil containing protein kinase 2 (ROCK2) to induce blebbing of target cells independent of caspase activation [98] and is also found play a role in the 70 kilodalton heat shock protein 70 (Hsp 70)-mediated perforin-independent apoptosis [99].

2.3 NK cell migration

NK cells have to infiltrate and patrol tissues in order to locate their target cells. An intact motility is of great importance for NK cells to execute their killing function [19, 20]. The migration of NK cells relies heavily on the integrity and rearrangement of their cytoskeleton. During migration, actin-rich protrusions are formed at the leading edge, whereas the MTOC is located at the uropod, the rear part of the cells. Myosin IIA mediated actomyosin contractility is required for retraction of uropod to allow cells move forward. Under physiological conditions,

NK cells need to migrate in 3D environments in most cases. Physical and chemical features of 3D environments can also greatly modulate NK migration.

2.3.1 Cytoskeleton is a key factor of cell migration

The cytoskeleton consists of three major types of protein: actin filaments, microtubules and intermediate filaments. Functions of actin filaments and microtubule network in immune killer cells especially CTLs have been intensively investigated. Actin cytoskeleton along with actomyosin contractility is essential to maintain the cell shape and generate forces for cell migration [100]. Microtubules serve as intracellular tracks with help of the motor proteins to enable transportation of intracellular organelles or vesicles to their desired destinations. Intermediate filaments are involved in maintaining cell shape and withstand mechanical stress [101]. However, the role of intermediate filaments in CTLs or NK cells remains largely unexplored.

Actin is one of the main components of the NK cell cytoskeleton. During NK cell migrating or conjugating with target cells, actin is found undergo polymerization and depolymerization and switch between the globular monomer stage (G-actin) and the filamentous stage (F-actin) bidirectionally [102]. As a highly conserved protein that expressed abundantly in most eukaryotic cells, actin participates and plays critical roles in many aspects of cell functions such as cell migration, cell shape maintenance and transcriptional regulation of polarity [103]. In NK cells, the actin filaments are dynamically reorganized according to the signals from the surface activating or inhibitory receptors. The activity of central nucleating factors such as the actin-related protein 2 and 3 (Arp2/3) complex and formins controls the direct nucleation of actin [101, 102]. Nucleating-promoting factors, for example, Wiskott–Aldrich Syndrome protein (WASp) family and WAVE2 are in responsible for regulation of nucleating factors [104-106]. Proteins like Coronin 1A work as the depolymerizing factors that antagonize Arp2/3-induced actin branching which is found crucial for NK lytic granule release [107].

Actomyosin contractility is essential for killer cell migration. Myosin IIA, an actin motor protein, plays a critical role in regulating the functions of T-cells and NK cells [108]. Abrogation of myosin IIA activity suppresses T-cell motility through a deficient uropod retraction [109]. Myosin II is considered to play central roles in the generation of the contractile force essential for cell migration [58, 110, 111]. Myosin II activity relies on the myosin light chain (MLC) phosphorylation. Myosin light chain kinases (MLCK) as well as Rho-associated protein kinase (ROCK) are the two major types of enzymes that participate in the MLC phosphorylation [112-114].

Microtubule filaments also play critical roles in NK effector function. They are expressed in all eukaryotic cells and are involved in intracellular trafficking, cell mitotic, cell migration, and

cell shape maintenance [115]. Microtubules are long (up to 5 mm) polymers that of the highest stiffness in cytoskeleton components [116]. A single microtubule is a hollow cylinder-shaped molecule with a diameter of 24 nm that is assembled with 13 protofilaments made up of α and β-tubulin heterodimers. The microtubules are originated from the MTOC [117]. The end which anchored at the MTOC is defined as the microtubule minus-end and in contrast, the end in which the microtubule grows is defined as the plus-end. When the microtubule extends, α and β-tubulin heterodimers are added to the plus-end. After the tubulin dimer is incorporated into the microtubule, a β-tubulin-bound guanosine triphosphate (GTP) cap of stabilizing properties is formed upon the growing tip. Due to the GTPase activity of tubulin, the GTP-tubulin under the cap is converted to guanosine diphosphate (GDP)-tubulin which is unstable [118]. Molecular motor proteins such as Dynein can help to the stabilize the plus-end [119]. On the other hand, microtubule depolymerases such as proteins from Kinesin family (Kinesin-13, 8, and 14) can remove the cap at the plus-end which leads to enhanced microtubule depolymerization [119-121]. These molecules regulating the stabilizing and destabilizing of microtubules are called microtubule-associated proteins (MAPs) [122, 123]. The synergy of a broad range of MAPs determines the dynamic of microtubules [123-125].

Among the three major types of cytoskeleton components, intermediate filaments (IFs) are the softest. They are distributed in cytoplasm widely and can crosslink with each other or with other cytoskeletal proteins such as actin and microtubule filaments [126]. In human genome, a large family with over 65 genes that each are cell-type specific, encodes IF proteins, in both cytosol and nucleus [127, 128]. These IFs are classified into six groups according to the similarities between their sequence of rod-like domain [128]. The type III IF protein vimentin, is a major IF component found in fibroblasts, smooth muscle cells, and leukocytes [127, 129]. In smooth muscle cells and fibroblasts, the deficiency of vimentin reduces the cell moving velocity and cell contraction force while an upregulation of vimentin expression promotes cell motility [129-132]. Vimentin is also reported to regulate the focal adhesion dynamics at the protrusions of moving cells [132]. In human PBMCs and mouse lymphocytes, the absence of vimentin is related to an impaired trans-endothelial migration and downregulated adhesion molecule [129]. Besides vimentin, lamins from the type IV IF proteins, a major component of the nuclear membrane, is reported to regulate the nucleus rigidity in tumor cells [128, 133, 134]. Since the size of the nucleus affects the migration efficiency when the cell is squeezing through 3D matrix fibers. Evidence suggests that lamins impact cell motility by regulating the nucleus rigidity. However, the role of IFs in NK function remains largely elusive.

2.3.2 Other factors that affect NK migration

Optimized motility is a prerequisite enabling NK cells to locate their target cells in a timely

manner. Cell migration modes fall into two main categories: mesenchymal and amoeboid migration. Leukocytes including NK cells often employ the amoeboid migration mode. During migration, the cell can switch between some submodes such as blebbing and gliding [135, 136]. Notable, the core of the amoeboid migration anchored on the cell-scale retrograde actin flow driven by the contractile forces in the actin network from the rear [137-140]. The cell locomotion is driven by the unspecific friction force generated from the indirect interaction between the actin filaments flow and the surrounding ECM. The MTOC is found always located at uropod of migrating T cells [141]. It's worth noting that cells can switch migration strategies plastically under the influence of the properties of the environment [137, 142], such as substrate stiffness [143, 144], geological confinement [137, 145], or adhesion complexes [137, 146].

To locate their target cells in vivo, NK cells have to infiltrate and patrol various of tissues. The 3D environments that NK cells pass through are mainly composed of extracellular matrix (ECM). The interaction between cells and ECM has been demonstrated plays critical roles in many vital cellular processes [147]. The major component of ECM is collagen which mainly presents as branch-like network of fibers [148]. Besides growth factors and chemical mediators diffusing inside, the physical characteristics of ECM such as dimensionality, stiffness, fibre thickness, and pore size between fibres also influences cellular functions [149-152]. By physically interacting with ECM, cell functions are mediated by mechanosensing and related signal cascades [153, 154]. On the other hand, cell migration is mediated by body reshaping due to guidance and confinement from ECM [155, 156]. CTLs are found to substantially reduced killing efficiency in high density of collagen due to an impaired migration. The nuclei deformation regulated by microtubules contributes to the velocity of a migrating CTL [157]. Cell-ECM interaction is also crucial in tumor research since significant structural changes in tumor-surrounding collagen tissues has been visualized [158, 159].

In mammals, type I collagen composes up to 90% of the protein content of connective tissues [158]. Therefore, reconstituted type I collagen matrices is often used to mimic an in vivo cellular environment for in vitro cell experiments [148].

2.4 Maximazation of NK killing efficiency

To defend our bodies from diseases, the innate and adaptive immune systems collaborate complementarily [3]. Theoretically, when exposed to invading microbes, the innate immune cells response almost immediately. Within minutes, phagocytes (e.g. neutrophils, macrophages, and dendritic cells) approach the corresponding site and remove pathogens or foreign particles via phagocytosis. Meanwhile NK cells are recruited to the battlefield to eliminate pathogen-infected cells. In between, dendritic cells and macrophages act as professional antigen-presenting cells (APCs). After having collected pathogen-derived antigens, these professional

APCs home to lymph nodes and present the antigens to naive T cells to initiate their activation and proliferation. T-lymphocytes population encompasses CD4^{+} T cells and CD8^{+} T cells. CD4^{+} T cells make up to 60-70% of the T cell population and are therefore the most abundant cell type [5, 160]. Once upon activation, most CD4^{+} T cells differentiate into T helper cells, which secrete an array of cytokines that can in turn shape functions of innate immune cells. For example, CD4^{+} Th cells can convert infected macrophages into more potent antimicrobial effector form via IFNγ [161], activate CD8^{+} T cells in killing infected cells, and help B cells in producing antibodies to mediate humoral immune responses[162]. Notably, emerging evidence indicates CD4^{+} T cells also crosstalk with NK cells and they do so very likely through their IL-2 production.

Among the cytokines secreted by CD4^{+} effector T cells, IL-2 is of great importance and has been well studied. Identified in 1976, IL-2 is the first type 1 cytokine that has been cloned [163]. IL-2 is a 15.5 kDa protein that bear a four α-helical bundle [164]. In human, IL-2 is mainly produced by CD4^{+} T cells upon activation by antigen. Three distinct IL-2 receptor chains have been described. IL-2 receptor α chain (IL-2Rα), also known as CD25, is uniquely expressed on activated lymphocytes. Though is ligand-specific, the bind between IL-2Rα and IL-2 is of low affinity; On NK cells and memory T cells, IL-2Rβ (CD122) and IL-2Rγ (CD132) combine with each other and form a complex that binds IL-2 with intermediate affinity; The highest affinity with IL-2 is achieved when the three receptor chains are expressed together on activated T cells [164]. When binds with a high affinity receptor, IL-2 is firstly captured by the IL-2Rα domain, following the recruitment of IL-2Rβ, the IL-2Rγ chain is the last to take part in [165]. Both the intermediate and the high affinity receptor can trigger functional IL-2 signals. IL-2Rβ domain is also shared by the IL-15 receptor as a key component. The IL-2Rγ chain is actually found a common chain shared by for the receptors of IL-2, IL-15, IL-7, IL-21, IL-9, and IL-4 [166]. It's therefore also known as the common cytokine receptor γ chain (γc). Nowadays, IL-2 is widely used to enhance the cytotoxic capacity of NK cells *in vitro* cultures [167]. IL-2 treatment significantly alters the surface receptor expression on NK cells. When exposed to IL-2, an upregulation of activating receptors, such as NKp44, DNAM-1 (CD226), and KLBR1 has been recorded while the expression of inhibitory receptors like KIR2DL2 and KIR3DL3 are found downregulated [168]. Adhesion molecules that play important roles in IS formation and cell migration are also upregulated on IL-2-stimulated NK cells, resulting in a tighter conjugate between individual cells than cells in the resting stage [169]. This promoted intercellular adhesion may partly contribute to the enhanced NK-mediated cytotoxicity upon IL-2 stimulation. Impacted by a low dose of IL-2 for a long time, NK cell population can be specifically expanded [170].

Evidence shows that T cell-derived IL-2 plays a central role in NK cell activation *in vivo*. IL-12/15/18–preactivated NK cells were demonstrated performed rapid proliferation when

exposed to IL-2 produced by CD4^{+} T cells in a mouse model [171]. In *Leishmania major*-infected mice, antigen-specific CD4^{+} T cells are found required to potentiate NK killing via IL-2 [172] . In presence of APCs and recombinant IL-12, endogenous IL-2 secreted by antigen-activated CD4^{+} T cells are able to stimulate CD56^{bright} NK cell IFN-γ production, which is related to NK cytotoxic functionality [173]. This T cell-mediated NK activation is abolished by neutralization of IL-2 [174, 175]. In human secondary lymph organs, CD56^{bright}CD16^{-} immature NK cells are enriched in close proximity to the T cell area. These NK cells can be converted into killing potent subsets upon IL-2 activation phenotypically similar to the peripheral blood NK cells [173, 176, 177]. Deficiency in CD4^{+} T cells leads to failure in NK activation in an infection mouse model [172]. Though the interaction between NK cells and IL-2-producing T cells has been defined *in vivo* which suggests a link between the innate and adaptive immune responses, the underlining mechanism of endogenous IL-2-mediated NK cell activation is still elusive [173, 178, 179].

2.4 Goals

As elaborated above, NK cells are crucial effector cells to eradicate tumorigenic or infected cells and CD4^{+} T helper cells are essential to potentiate NK killing capacity in an IL-2 dependent manner. Of note, IL-2 production by Th cells is transient [180] and administration of high doses of IL-2 in patients leads to severe side effects mainly from vascular leakage [181].

In this case, how exactly T cells potentiate NK killing function is still not fully understood. This thesis is aimed to address this question in the following aspects:

1) To determine how activated T cells impact NK cell cytotoxicity;
2) To reveal the mechanism of the T-boosted NK killing;
3) To analyze the intrinsic change in NK cells by T-boosting.
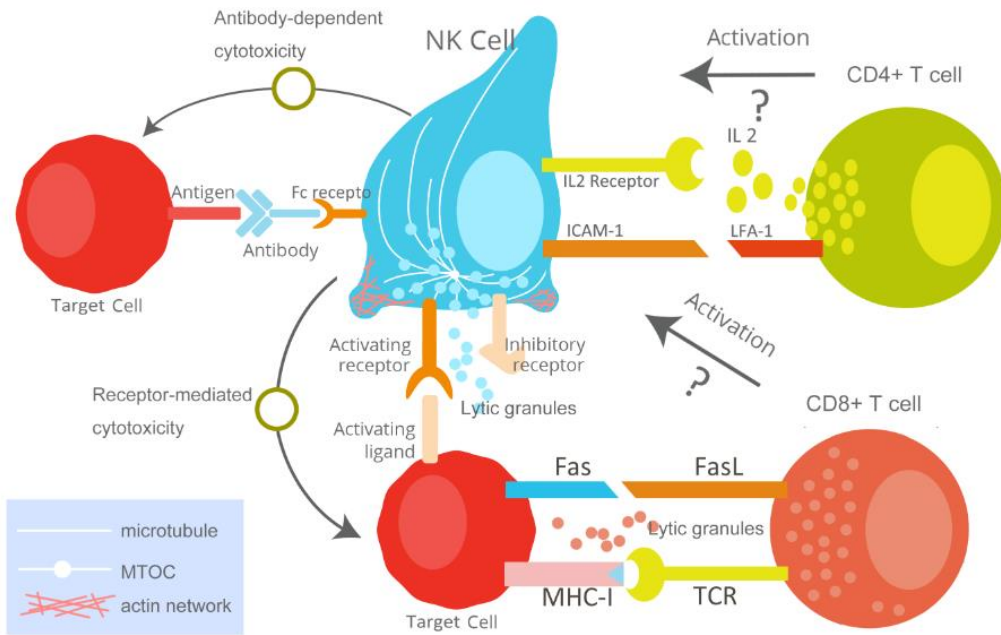
Figure 1. Schematic of the NK functions and NK-T crosstalk. NK cells can exert receptor-mediated cytotoxicity and antibody-dependent cytotoxicity against virus-infected cells or tumor cells. The NK killing functions are based on the synergy of activating/inhibitory receptors, IS formation, cytolytic protein release, and cell migration. The cytoskeleton plays important role in these aspects. It has been demonstrated that stimulated CD4$^+$ T helper cells can activate NK cells via cytokine, especially IL-2, secretion. How T cells impact NK functions needs to be further studied.

3. Materials and Methods

3.1 Reagents and antibodies

Reagents

Designation	Source	Reference
Calcein-AM	Thermo Fisher	C3100MP
CellTrace™ CFSE Cell Proliferation Kit	Thermo Fisher	C34554
Dynabeads® Human T-Activator CD3/CD28	ThermoFisher	11131D
NK Cell Isolation Kit, human	Miltenyi Biotec	130-092-657
CD4$^+$ T Cell Isolation Kit, human	Miltenyi Biotec	130-096-533
CD8$^+$ T Cell Isolation Kit, human	Miltenyi Biotec	130-096-495
CD56 Microbeads, human	Miltenyi Biotec	130-050-401
FibriCol® Type I Collagen Solution, 10 mg/ml (Bovine)	Advanced BioMatrix	#5133
LEGENDplex™ Human CD8/NK Panel	Biolegend	741065
NucleoSpin® RNA Plus	Macherey-Nagel	740984.50
ML7, myosin light chain kinase inhibitor	Abcam	ab120848
Y27632 dihydrochloride	Biomol	LKT-Y1000.1
Cell ID™ 127 IdU	Fluidigm	201127
penicillin/streptomycin	Sigma-Aldrich	P4333-100ML
Human Recombinant IL-2	VWR	PHC0023
Propidium iodide (PI)	VWR	BTIU40016
G418 Sulfate	Merck	345810-5GM
AIM V™ Medium, liquid (research grade)	Thermo Fisher	12055083
RPMI 1640 Medium	Thermo Fisher	21875034
MEM	Thermo Fisher	31095029
fetal calf serum (FCS)	Thermo Fisher	10270106
DPBS, no calcium, no magnesium	Thermo Fisher	14190094

All the other chemicals not mentioned in this table were purchased from Sigma-Aldrich (highest grade).

Antibodies

Designation	Clone	Source	Reference
Rituximab (biosimilar, Rixathon, Hexal Pharma)	-	local pharmacy	-
anti-Integrin alpha-L (ITGAL) antibody	Efalizumab /hu1124	Antibodies-online	ABIN5668045
IL2RA recombinant monoclonal antibody	Basiliximab	Abnora	RAB00048
PerCP anti-human CD3 Antibody	HIT3a	Biolegend	300326
Brilliant Violet 421™ anti-human CD3 Antibody	UCHT1	Biolegend	300434
APC/Cyanine7 anti-human CD3 Antibody	SK7	Biolegend	344818

Alexa Fluor® 488 anti-human CD16 Antibody	3G8	Biolegend	302019
PerCP anti-human CD16 Antibody	B73.1	Biolegend	360720
Alexa Fluor® 647 anti-human Perforin Antibody	dG9	Biolegend	308110
PE anti-human/mouse Granzyme B Recombinant Antibody	QA16A02	Biolegend	372207
Brilliant Violet 421™ anti-human CD107a (LAMP-1) Antibody	H4A3	Biolegend	328626
PE anti-human CD178 (Fas-L) Antibody	NOK-1	Biolegend	306407
Alexa Fluor® 647 anti-human IL-2 Antibody	MQ1-17H12	Biolegend	500315
Alexa Fluor® 488 anti-human CD3 Antibody	UCHT1	Biolegend	300415
APC Mouse Anti-Human CD56 (NCAM-1)	B159	BD Biosciences	555518

3.2 Cells

3.2.1 Cell lines

The cell line culture and separation were carried out by our technician team: Cora Hoxha , Kathrin Förderer, Sandra Janku, and Gertrud Schwär. K562 cells, Raji cells, K562 pCasper cells, OSU cells, MEC1 cells, SK-MEL 5 cells and SK-MEL 28 cells were cultured in RPMI 1640 medium supplemented with 10% of FCS and 1% of Penicillin-Streptomycin at $37°C$ with 5% CO_2. To culture K562 pCasper cells, 2.5 mg/ml of G418 was added in the culture medium.

3.2.2 Peripheral blood mononuclear cell (PBMC) preparation

The PBMC preparation was carried out by our technician: Carmen Hässig. Leukocyte reduction system (LRS) chambers from healthy donors were used to recover PBMCs. Cells in LRS chambers were carefully flushed out using Hanks' Balanced Salt Solution (Sigma-Aldrich) into a 50 ml tube prefilled with 16 ml of lymphocyte isolation medium (LSM). The tubes were centrifuged at 450 g (acceleration: 1, deacceleration: 0) for 30 min at 4°C, and the mononuclear cells desired were accumulated as a ring, which was carefully collected into another 50 ml tube and the tube was filled to 50 ml with HBSS for washing (300g, 15min, RT). The pellet was gently resuspended in 2-3 ml of erythrocyte lysis buffer (155 mM NH_4Cl, 10 mM $KHCO_3$ and 0.1 mM EDTA, pH 7.3) and kept at room temperature for 1-2 min to lyse the remaining red blood cells. Then the tube was filled with HBSS to 50 ml and centrifuged (250 g, 15 min, RT). The pellet was resuspended in PBS/0.5% BSA and kept on ice for subtype isolation. The research conducted in this study involving human materials has received approval from the local ethics committee.

3.2.3 NK cell negative isolation

The NK cell isolation was carried out by our technician: Carmen Hässig. Primary human NK cells were isolated negatively from PBMCs using NK Cell Isolation Kit human (Miltenyi Biotec, Cat. 130-092-657) according to the protocol provided by the manufacturer. The isolations were conducted manually or automatically with autoMACS® Pro Separator (Miltenyi). The steps for manual isolation are as follows (for 10 million PBMCs, each preparation maximum 200 million PBMCs):

Resuspend PBMCs in 40 µl of pre chilled (4℃) PBS/0.5% BSA

- Add 10 µl of NK Cell Biotin-Antibody Cocktail and incubate at 4℃ for 5 min
- Add 30 µl of PBS/0.5% BSA and 20 µl of NK Cell MicroBeads. Incubate at 4℃ for 10 min.
- Load the mix into a column attached to the magnetic separation system. Collect the elute and count the cells.

Isolated primary human NK cells were firstly resuspended in AIM V medium with 10% FCS at a density of 2×10^6 cells/ml for later treatment.

3.2.4 T cell negative isolation and stimulation

The T cell isolations were also carried out by our technician: Carmen Hässig. Primary human $CD4^+$ T cells and $CD8^+$ T cells were isolated from the autologous donors that provide the NK cells using $CD4^+$ T Cell Isolation Kit human (Miltenyi Biotec, Cat. 130-096-533) and $CD8^+$ T Cell Isolation Kit human (Miltenyi Biotec, Cat. 130-096-495) respectively according to the protocol provided by the manufacturer. The isolations were conducted manually or automatically with autoMACS® Pro Separator (Miltenyi Biotec). The steps for manual isolation are as follows (for 10 million PBMCs, each preparation maximum 200 million PBMCs):

Resuspend PBMCs in 40 µl of pre chilled (4℃) PBS/0.5% BSA

- Add 10 µl of $CD4^+$ /$CD8^+$ T Cell Biotin-Antibody Cocktail and incubate at 4℃ for 5 min
- Add 30 µl of PBS/0.5% PBS and 20 µl of $CD4^+$ /$CD8^+$ T Cell MicroBeads. Incubate at 4℃ for 10 min.
- Load the mix into a column attached to the magnetic separation system. Collect the elute and count the cells.

Isolated primary human $CD4^+$ /$CD8^+$ T cells were firstly resuspended in AIM V medium with 10% FCS at a density of 3×10^6 cells/ml for later treatment.

3.3 NK positive isolation from NK-T co-culture

NK cells from NK-T co-culture were positively isolated using Human CD56 MicroBeads (Miltenyi Biotec, Cat. 130-050-401) according to the manufacturer's instruction. The steps are as follows (maximum 10 million total cells for one isolation):

- Filter the cell mix with 30 µm nylon mesh (moistened with PBS/0.5% BSA before used) into a tube.
- Put the cells on centrifugation (300 g, 10 min, RT) and resuspend the pellet with 80 µl of PBS/0.5% BSA.
- Add 20 µl of CD56 MicroBeads. Mix well and rotate the tube at 4℃ for 15 min.
- Add 1 ml of PBS/0.5% BSA and put the tube on centrifugation (300 g, 10 min, RT)
- Resuspend the pellet with 500 µl of PBS/0.5% BSA and load the mix onto a MS column (pre-moistened with 500 µl PBS/0.5% BSA). Attach the column to the magnet for xx min.
- Wash the column three times using 500 µl of PBS/0.5% BSA.
- Remove the column from the magnet and collect the elute in a 1.5 ml tube.
- Centrifuge the tube (300 g, 10 min, RT) and resuspend the pellet in AIM V medium (with10% FCS) for counting.

3.4 Plate reader-based real time killing assay

The real-time killing assay was performed as reported previously [182]. The steps are as follows:

- Target cells (K562 for normal killing and Raji for ADCC) were loaded with 500 nM calcein-AM (in AIM V medium with 10 mM HEPES) at RT for 15 min on a tilter (slow speed). Density applied was 5×10^5 cells/ml.
- Centrifuge (200g, 5min, RT) and wash the pellet twice with AIM V/10 mM HEPES.
- Resuspend the pellet in AIM V/10 mM HEPES at a density of 1.25×10^5 cells/ml (For ADCC, add 1.25 µg/ml of Rituximab at this step).
- Transfer the cell suspension into a 96-well black with clear flat bottom plate (Corning) with a multi-channel pipette (200 µl/well). Resuspend the cells well in the reservoir before transfer.
- Fill the outer wells with sterilized ddH$_2$O and keep the plate in dark for 20 min at RT.
- Suspend the effector cells in AIM V/10 mM HEPES according to the desired E:T ratio. Carefully transfer the effector cells into the plate (50 µl/well).
- Put the plate into pre-warmed microplate reader (GENios Pro, TECAN). Measure the fluorescence every 10 minutes for 4 hours at 37°C with the following settings: the bottom read function (Ex 488/Em 520 nm), 3×3, 2 flashes per read.

- The following controls are included: Medium (AIM V/10 mM HEPES), live control, Medium+Triton (20 µl of 10% Triton-X100/well), total lysed control (20 µl of 10% Triton-X100/well)

- Index should be calculated to normalize the variation of pipetting:

$$Index = \frac{F_{live}(0)}{F_{exp}(0)}$$

- Killing efficiency is shown as the fraction of killed cells for each time point. The fraction is calculated by the following equation:

$$\%Killing(t) = \frac{F_{live}(t)\text{-}Index*F_{exp}(t)}{F_{live}(t)\text{-}F_{lysed}(t)}$$

(F_{live}: Fluorescence of target cells in live control; F_{exp}: Fluorescence of the experimental well; F_{lysed}: Fluorescence of lysed target cells in total lysed control; All fluorescence values are subtracted by the corresponding medium controls. All killing assays were done in duplicate).

3.5 Co-culture of NK and T cells

For the 3 day-co-culture, each 1×10^6 NK cells were co-cultured with 2×10^6 homologous T cells in 1-1.5 ml AIM V /10% FCS (scale up/down according to circumstances). To stimulate T cells, prewashed Dynabeads® Human T-Activator CD3/CD28 (Thermo Fisher Scientific) were added at a bead to T cell ratio of 0.8. After 2 days of stimulation, the beads were removed from the co-culture by magnet (2 min, RT).

For the 1 day-co-culture, NK cells (2×10^6/ml) were along cultured firstly while homologous T cells ($2\text{-}3\times10^6$/ml) were stimulated with prewashed Dynabeads® Human T-Activator CD3/CD28 (Thermo Fisher Scientific) at a bead to T cell ratio of 0.8. The beads were removed from the T cell culture by magnet (2 min, RT) after 2 days of stimulation. Subsequently, each 1×10^6 NK cells were co-cultured with 2×10^6 stimulated T cells in 1-1.5 ml fresh AIM V /10% FCS (scale up/down according to circumstances) for 24 h.

For experiments using transwell (Fig. 20), Corning® Transwell® polyester membrane cell culture inserts (pore size: 0.4 μm) were used. NK cell and CD4+ T cells cultured in the inserts (5×10^5 cells/250 μl) and the outer wells (1×10^6 cells/1.25 ml), respectively. To ensure the exchange of soluble factors between the inserts and the outer wells, 125 μl of supernatant in the inserts was carefully transferred into the outer wells. Then, 125 μl of supernatant in the outer wells was carefully transferred back into the inserts. The medium was manually exchanged every 24 hours for 3 days during co-culture.

3.6 NK proliferation assay

To determine the NK proliferation during co-culture with T cells, NK cells were loaded with CFSE (5 µM CFSE) prior to co-culture with autologous CD4^{+} T cells. According to the official protocol. After negative isolation, NK cells were loaded with CFSE (5 µM in PBS/5% FCS) in dark at room temperature for 15 min with gentle tilting. Wash one time with AIM V/10% FCS (200g, 5min, RT). The pellet was resuspended in AIM V/10% FCS and co-cultured with autologous CD4^{+} T cells for 3 days in a 48 Well plate (750 µl for each well: 5×10^5 NK cells, 1×10^6 T cells). The proliferation of NK cells was determined according to the data acquired with FACSVerse™ flow cytometer (BD Biosciences). The CFSE^{+} cells were gated as the NK cells. The detections were based on 10,000 sorted events. Data were analyzed with software FlowJo_V10 (FLOWJO, ICC). A discrete peak on a fluorescence histogram presents a generation in NK cell proliferation.

3.7 Determination of NK subsets

To determine the NK subsets, NK/ T co-culture cells were first washed with 500 µl of pre-chilled PBS/0.5% BSA (200g, 5 min, RT) twice, and were subsequently incubated with Alexa 488 anti-human CD16 antibody (1:50), APC mouse anti-human CD56 antibody (1:50), and PerCP anti-human CD3 (1:50) in PBS/0.5% BSA for 30 min at 4 °C in the dark. Then the cells were washed with 500 µl of pre-chilled PBS/0.5% BSA (200g, 5 min, RT) twice. The samples were measured with FACSVerse™ flow cytometer (BD Biosciences). The resulting data was analyzed with software FlowJo V10 (FLOWJO, ICC). Gates were set based on the FMO control. CD3^{-}CD16^{+}CD56^{+} in lymphocytes population were defined as NK cells.

3.8 Determination of cytotoxic protein expression

NK cells cultured alone or co-cultured with T cells were fixed in 500 µl of freshly prepared pre-chilled 4% PFA for 15 min at RT. After centrifugation (200g, 5 min at RT), the pellet was resuspended in 500 µl of 0.1% saponin in PBS/ 0.5% BSA/5% FCS for 1 hour at RT for permeabilization. After one time wash with 500 µl of PBS/0.5% BSA (200g, 5 min at RT), the cells were stained with the following panels: Alexa 647 anti-human Perforin (1:50) (Clone: dG9) / PerCP anti-human CD3 (1:50), PE anti-human Granzyme B (1:50) (Clone: QA16A02) / PerCP anti-human CD3 (1:50). The samples were measured with FACSVerse™ flow cytometer (BD Biosciences). The detections were based on 10,000 sorted events. The sesulting data was analyzed with software FlowJo_V10 (FLOWJO, ICC). Gates were set based on the FMO control. CD3^{-} populations in lymphocytes were gated as NK cells. The experiments were done by Wenjuan, Yang.

3.9 Degranulation assay

The degranulation level of NK cells was quantified according to the amount of exocytosed CD107a on the cell surface by FACs staining. In each well, effector cells (2.5×10^5) were seeded into a V-bottomed 96-well plate with or without target cells (1×10^5) in 25 µl of complete AIM V medium with 10% FCS. Brilliant Violet 421™ anti-human CD107a (LAMP1) antibody (1:25) and GolgiStop^{TM} (1:200) were added and mixed with the cells in the master tube. For ADCC, 1 µg/ml of Rituximab was presented in the medium. The plate was kept at 37°C with 5% CO_2 for 4 hours. Afterwards, the plate was centrifuged (200g, 5 min at RT) and washed twice with 100 µl of PBS/0.5% BSA for each well. Alexa 488 anti-human CD16 antibody (1:50), APC mouse anti-human CD56 antibody (1:50) and PerCP anti-human CD3 (1:50) were added into each well (50 µl of PBS/0.5% BSA) and kept for 30 min at 4°C in the dark. The samples were measured with a FACSVerse™ flow cytometer (BD Biosciences). The resulting data was analyzed with FlowJo v10 (FLOWJO, LLC). Gates were set based on the FMO control. CD3$^-$CD16$^+$CD56$^+$ in lymphocytes population were defined as NK cells. Wenjuan, Yang helped the experiments.

3.10 Determination of IL-2 concentration in culture supernatant

To test how much IL-2 was released by CD4$^+$ T cells, the culture supernatant of conditions to be tested was collected after the cells were spun down. To get rid of cell debris, the supernatant was centrifuged at 1000 g for 5 min and transferred into aliquot tubes (150 µl for each tube). Extra aliquots were kept at -80℃. The IL-2 concentration in culture supernatant was determined using LEGENDplex™ Human CD8/NK Panel (Biolegend) according to the manual provided by the manufacturer. Renping Zhao carried out the measurement. The assay was performed in a 96-well V-bottom plate. The data was acquired with FACSVerse™ flow cytometer (BD Biosciences) by reading the plate with autosampler. 4000 events were acquired for each sample. The data was finally processed and analyzed using LEGENDplexTM Data Analysis Software (Biolegend).

3.11 Preparation of collagen matrices

Type I Bovine collagen (Advanced BioMatrix) was stored at 4℃ with an origin density of 10 mg/ml. To make neutralized collagen solution (8 mg/ml), for each 400 µl 10 mg/ml collagen solution, 50 µl of pre-chilled 10×PBS solution was firstly added. After the collagen solution was fully homogenized by gently shaking the tube. Pre-chilled 1M NaOH solution (usually 41.6 µl) was then added and well mixed with the collagen solution. The pH value of the neutralized collagen solution was checked with pH stripes. The pH value was adjusted to approximate 7.4. All steps were carried out on ice. The neutralized collagen can be further

diluted to desired density (usually 2 mg/ml) with medium or PBS. Extra neutralized collagen can be kept at 4℃ for at least 2 weeks.

3.12 Live cell imaging

High content imaging was conducted on ImageXpress Micro XLS Widefield High-Content Imaging System (Molecular Devices) for 2D and 3D scenarios. K562 pCasper cells, K562 or Raji cells were used as target cells as indicated in the figure legend. K562 and Raji cells were loaded with 500 nM calcein-AM as elaborated in *Real-Time Killing Assay*. For ADCC, 1 μg/ml of Rituximab was added in the medium. For each well, 2.5×10^4 target cells and 6.25×10^4 NK cells were used.

For 2D killing, target cells were plated into a 96-well black with clear flat bottom plate (Corning) (200 μl of AIM V/10 mM HEPES each well) and settled for 20 min at RT in dark. Effector cells were subsequently added (50 μl of AIM V/10 mM HEPES each well). The killing process was visualized at 37℃ with 5% CO_2 for 4 hours with an interval of 10 min. The efficiency of 2D killing was is shown as the fraction of killed cells for each time point.

For 3D killing, target cells were resuspended in 2 mg/ml pre-chilled of neutralized collagen type I solution (Advanced Biomatrix) at a density of 6.25×10^5/mll and seeded in a 96-well black with clear flat bottom plate (Corning) (40 μl collagen solution/well). The plate was kept at 37℃ with 5% CO_2 for 40 min and then effector cells were added on top of the collagen at an E:T ratio of 2.5 : 1. The killing was visualized at 37℃ with 5% CO_2 for 24 h to 40 h with an interval of 10 to 20 min. Half well Falcon® 96-well black with clear flat bottom plates (Corning) were also used. In this case, volume and cell number were scaled down to half. The images were processed and analyzed using Image J (NIH Image). The efficiency of 3D killing was evaluated according to the total area of live cells for each time point.

For visualization of NK/CD4 contact, CFSE labeled NK cells and unlabeled stimulated CD4^{+} T cells awere used. 25 mm coverslips were coated with fibronectin (10 μg/ml in ddH_2O) at RT for 30 min in a humidity chamber (150 mm petri-dish with moisturized tissue paper). After removal of the fibronectin with a pump, the cell suspension (5×10^5 NK cells with 1×10^6 CD4^{+} T cells in 100 μl of AIM V without FCS) was settled on the coated area and kept in the humidity chamber at 37°C with 5% CO_2 for 20 min. Then the samples were washed gently with AIM V without FCS (1 ml/coverslip). The coverslips were mounted onto sample chamber and 1 ml of AIM V without FCS was added into the chamber. The samples were visualized at 37 °C with 5% CO_2 for 30-60 min with a time interval of 10 sec using Cell Observer (Zeiss) with a 40× or a 63× objective. The settings for each channel are as follows: bright field channel, voltage: 4.8 V, exposure time: 50 ms; GFP channel for CFSE (Ex 495/ Em 519 nm), laser intensity: 25%, exposure time: 100-150 ms. The images were processed and analyzed with Fiji (NIH Image).

3.13 NK migration

NK cell migration was visualized using light-sheet microscopy as described previously [183]. NK cells were stained with CellTrace™ CFSE as described in *3.6 NK proliferation assay*. The CFSE-labeled NK cells were either cultured alone or co-cultured with autologous CD4$^+$ T cells in AIM V medium with 10% FCS for 24 hours. The cells were resuspended in 2 mg/ml of pre-chilled neutralized collagen type I solution (Advanced Biomatrix) at a density of 3.125×10^6/ml (0.5×10^6 NK cells in 160 μl). The collagen-cell mix was sucked into a glass capillary (BRAND ™ Glass Transferpettor Caps, ref. 10303731) and kept at 37℃ with 5% CO_2 for 40 min. Afterwards, the samples were immersed in AIM V medium for 1 h for NK cell recovery. The samples were then visualized at 37℃ with 5% CO_2 for 30-60 min with an interval of 30 sec using the Z.1 light-sheet microscope (Zeiss). For the acquisition, Laser 488-30 was used, laser intensity: 0.2-1, laser block filter: LBF 405/488/561/640, beam spliter: SBS LP 490/BP 505-545, exposure time: 29.97-99.87 ms, acquisition mode: single illumination, objective: 20×. Z-stacks with a step-size of 1 µm for 201 slices were obtained for each sample. Cell trajectories were tracked with Imaris 9.0.2 (Bitplane). Translational drift correction was carried out for all the images and objects. Cell coordinates, track speed mean and track straightness data were exported and analyzed by Graphpad Prism 9. For comparison between alone cultured NK and T-boosted NK, the cells were visualized for 60 min and the tracks with a duration less than 30 min were excluded. For comparison between T-boosted NK and IL-2 receptor inhibitor treated T-boosted NK, the cells were visualized for 30 min and the tracks with a duration less than 10 min were excluded.

3.14 Immunocytochemistry (ICC) for endogenous IL-2 vesicles

13 mm coverslips were coated with fibronectin (100 µg/ml in ddH$_2$O) at RT for 30 min in a 24 well plate. After removal of the fibronectin with a pump. The cell suspension (5×10^5 unlabeled NK cells with 1×10^6 unlabeled CD4$^+$ T cells in 100 µl of AIM V/10% FCS) was settled on the coated area and kept at 37°C with 5% CO_2 for 20 min. Afterwards, the cells were washed gently with 500 µl of PBS to remove the floating cells and the medium. After removal of PBS using a pipette, freshly made pre-chilled 4% PFA (500 µl) was immediately added in the well and the plate was kept at RT for 20 min in a chemical hood. PFA was transferred to a special waste and PBS (500 µl/well) was used to wash the samples (5 min, three times). Then the permeabilization solution (PBS/0.3% Triton 100/ 5% FCS, 500 µl/well) was added and the plate was kept at RT for 1 hour. Alexa 488 anti-human CD3 Antibody and Alexa 647 anti-human IL-2 antibody in PBS/1% BSA (1:50, 50 µl/coverslip) was carefully added on the coverslip and kept at RT for 2 hours in dark. Then the samples were washed three times with PBS (500 µl/well, 5 min at

RT). Before mounting, the coverslip was quickly immersed into sterilized ddH_2O and the side without cells was dried with lens tissue and mounted on a glass slide with 20 µl of mounting medium (Thermo Fisher, ref. 9990402). ICC images were obtained with the Cell Observer using a 63× objective. The settings for each channel are as follows: bright field channel, voltage=4.8 V, exposure time: 50 ms; GFP channel for Alexa 488 (Ex 495/ Em 519 nm), laser intensity: 25%, exposure time: 50-150 ms; deep red channel for Alexa 647 (Ex 650/Em 668 nm), laser intensity: 25%, exposure time: 500-600ms. The images were processed and analyzed with Fiji (NIH Image).

3.15 NK infiltration

A Falcon® 96-well black with clear flat bottom plate (Corning) was coated with 2 mg/ml pre-chilled neutralized collagen type I solution (40 µl/well) and centrifuged at xx g for xx min at 4°C. Then the plate was kept at 37℃ with 5% CO_2 for 40 min. NK cells were labeled with CFSE after isolation (for details please refer to 3.x xxx) and cultured alone or with stimulated autologous $CD4^+$ T cells in AIM V medium with 10% FCS at 37℃ with 5% CO_2 for 24 h. To examine infiltration, $6.25×10^4$ NK cells (with or without $CD4^+$ T cells) in 250 µl of AIM V/10% FCS were added on top of the collagen. The plate was visualized for 24 h with an interval of 20 min at 37℃ with 5% CO_2 supply using ImageXpress Micro XLS Widefield High-Content Imaging System (Molecular Devices). The settings for each channel are as follows: bright field channel, intensity: 20%, exposure time: 50-100 ms; GFP channel (Ex 488/ Em 525 nm), laser intensity: 25%, exposure time: 50-100 ms. The number of NK cells recognized within the focus plane at each time point was analyzed automatically using Image J (NIH Image). Half well Falcon® 96-well black with clear flat bottom plates (Corning) were also used. In this case, all volume and cell number were scaled down to half.

3.16 Cytometry by time of flight (CyTOF)

The Cytometry by time of flight (CyTOF) tests were carried out and analyzed by Jérôme Paggetti, Etienne Moussay, and Anne Largeot in Luxembourg Institute of Health. Briefly, $1.5×10^6$ NK cells cultured alone and $3×10^6$ NK cells co-cultured with two times of $CD4^+$ T cells were stained for the mass cytometry analysis. All the antibodies used are listed in the table below (**Antibodies for CyTOF**). The cells were incubated with 50 µM of Cell-IDTM 127 IdU (Fluidigm) in 5 ml of complete RPMI media/10% FCS/1% P/S for 30 min at 37 °C with 5% CO_2 supply to stain the proliferating cells. The cells were then washed with PBS (no Ca^{2+} and Mg^{2+}) followed by a 500 g centrifugation at RT for 5 min. 5 µM Cell-ID cisplatin (Fluidigm) was then added into the cells. After a 5 min incubation, the cells were washed with PBS/10% FCS and spun down at 500 g for 10 min. The staining of extracellular surface was carried out

in 96-well plates. FC block Human TruStain FcX™ (Biolegend) was added at 5 μl/well for 10 min at RT. The cells were incubated with a cocktail of antibodies (No. 1-30) 30 min at RT. After the 30 min incubation with the antibodies, the cells were washed with PBS/10% FCS to get rid of the excess antibodies. Subsequently, a cocktail of the secondary labeling antibodies (No. 31-34) was added for 30 min incubation at RT followed by a washing step with PBS/ 10% FCS to remove the remaining antibodies. The cells were then fixed and permeabilized using the Fixation/Permeabilization kit (eBioscience) based on the manufacturer's instructions. To stain the intracellular molecules, the cells were incubated with a cocktail of pre-conjugated antibodies (No. 35-39) for 30 min at RT followed by a washing step with PBS/10% FCS to remove the excess antibodies. Afterwards, the cells were treated with 50 nM cell-ID Intercalator-Ir (Fluidigm) in Maxpar® Fix & Perm buffer (Fluidigm) overnight following the manufacturer's instructions. Before the acquisition, the fixed cells were washed twice with PBS and then twice with deionized water. The cells were diluted at a density of 1.5×10^6/ml in deionized water containing 10% EQ Four Element Calibration Beads (Fluidigm). The samples were analyzed with the Helios mass cytometer (Fluidigm) at a flow rate of 0.030 ml per minute. After acquisition, with the CyTOF software version 6.7, Normalization Passport EQ-P13H2302_ver2, the fcs files were normalized by utilizing EQ four elements calibration beads (Fluidigm) and randomized. Using FlowJo software, samples were pre-gated for cells including proliferating and non-proliferating (Idu +/-) cells, singlets and live cells. Respective .fcs files were exported and then uploaded to Cytosplore for advanced analysis.

Antibodies for CyTOF

No.	Designation	Clone	Source	Reference
1	Anti-Human CD11a (HI111)-142Nd	HI111	Fluidigm	3142006B
2	Anti-Human CD117/c-kit (104D2)-143Nd	104D2	Fluidigm	3143001B
3	Anti-Human CD69 (FN50)-144Nd	FN50	Fluidigm	3144018B
4	Anti-Human CD25 (2A3)-149Sm	2A3	Fluidigm	3149010B
5	Anti-Human CD2 (TS1/8)-151Eu	TS1/8	Fluidigm	3151003B
6	Anti-Human CD185/CXCR5 (RF8B2)-153Eu	RF8B2	Fluidigm	3153020B
7	Anti-Human TIGIT (MBSA43)-154Sm	MBSA43	Fluidigm	3154016B
8	Anti-Human CD56 (B159)-155Gd	B159	Fluidigm	3155008B
9	Anti-Human CD85j (GHI/75)-156Gd	GHI/75	Fluidigm	3156020B
10	Anti-Human CD337/NKp30 (Z25)-159Tb	Z25	Fluidigm	3159017B
11	Anti-Human CD186/CXCR6 (K041E5)-160Gd	K041E5	Fluidigm	3160016B
12	Anti-Human CD335/NKp46 (BAB281)-162Dy	BAB281	Fluidigm	3162021B
13	Anti-Human CD161 (HP-3G10)-164Dy	HP-3G10	Fluidigm	3164009B
14	Anti-Human CD314/NKG2D (ON72)-166Er	ON72	Fluidigm	3166016B

15	Anti-Human NKB1 (DX9)-167Er	DX9	Fluidigm	3167013B
16	Anti-Human CD127/IL-7Ra (A019D5)-168Er	A019D5	Fluidigm	3168017B
17	Anti-Human CD159a/NKG2A (Z199)-169Tm	Z199	Fluidigm	3169013B
18	Anti-Human CD122/IL-2Rb (Tu27)-170Er	Tu27	Fluidigm	3170004B
19	Anti-Human CX3CR1 (2A9-1)-172Yb	2A9-1	Fluidigm	3172017B
20	Anti-Human CD158b (DX27)-173Yb	DX27	Fluidigm	3173010B
21	Anti-Human CD57 (HCD57)-176Yb	HCD57	Fluidigm	3176019B
22	Anti-Human CD16 (3G8)-209Bi	3G8	Fluidigm	3209002B
23	Anti-Human CD132 (TUGh4)-148Nd	TUGh4	Fluidigm	3148014B
24	PE anti-human CD197 (CCR7)	G043H7	Biolegend	353203
25	FITC anti-human CD54 (ICAM-1)	HA58	Biolegend	353111
26	APC anti-human CD336 (NKp44)	P44-8	Biolegend	325109
27	Biotin anti-human CD126 (IL-6Rα)	UV4	Biolegend	352808
28	*Anti-Human CD3 (UCHT1)-141Pr	UCHT1	Biolegend	300402
29	*Anti-Human CD4 (RPA-T4)-145Nd	RPA-T4	Biolegend	300502
30	*Anti-Human CD8a (RPA-T8)-146Nd	RPA-T8	Biolegend	301002
31	Anti-PE (PE001)-165Ho	PE001	Fluidigm	3165015B
32	Anti-FITC (FIT-22)-174Yb	FIT-22	Fluidigm	3174006B
33	Anti-APC (APC003)-163Dy	APC003	Fluidigm	3163001B
34	Anti-Biotin (1D4-C5)-150Nd	1D4-C5	Fluidigm	3150008B
35	Anti-Human TNFa (Mab11)-152Sm	Mab11	Fluidigm	3152002B
36	Anti-Human IFNg (B27)-158Gd	B27	Fluidigm	3158017B
37	Anti-Human/Mouse Tbet (4B10)-161Dy	4B10	Fluidigm	3161014B
38	Anti-Human Granzyme B (GB11)-171Yb	GB11	Fluidigm	3171002B
39	Anti-Human Perforin (B-D48)-175Lu	B-D48	Fluidigm	3175004B

Antibodies marked with * were conjugated with heavy-metal in-house using the Maxpar® X8 Multimetal Labeling kit (Fluidigm, ref. 201300) according to the manufacturer's instructions.

3.17 RNA extraction and RNAseq

NK cells were positively isolated with CD56 microbeads from NK/T co-culture. The same procedure was also applied on NK alone condition. Isolated NK cells (1-2 $\times 10^6$) from each condition were harvested at 300 g for 10 min. After removal of the supernatant, the pellets were directly frozen with liquid nitrogen and kept at -80℃. RNA from all samples was extracted at the same time using commercial kit NucleoSpin® RNA Plus (Macherey-Nagel) according to the manufacturer's instruction. The RNA concentration was determined with NanoDrop™ OneC Microvolume UV-Vis Spectrophotometer (Thermo Fisher). Samples with A260/A280 ratio of 2.0-2.2 were regarded as pure. The quality of RNA samples was also checked with 1 % agarose gel. Samples with sharp, clear 28S and 18S rRNA bands were regarded as intact. The

RNA sequencing was carried out by Novogene using Illumina platforms, based on mechanism of SBS (sequencing by synthesis). The gene expression levels were estimated by Fragments Per Kilobase of exon model per Million mapped fragments (FPKM) which takes the effects into consideration of both sequencing depth and gene length on counting of fragments [184]. Readcount obtained from gene expression analysis is used for differential expression analysis. Differential expression analysis of the two groups (NK alone/T-boosted NK) was carried out using the DESeq2 R package [185]. This tool offers statistical routines for differential expression identification in digital gene expression data based on the negative binomial distribution model. The Benjamini and Hochberg's method was introduced to adjust the obtained P-values in order to control the false discovery rate. The adjusted P-values were presented as padj. Genes with padj<0.05 were defined as differentially expressed (DEGs) [186].

Functional annotation and enrichment analysis of the DEGs including Gene Ontology (GO) and Kyoto Encyclopedia of Genes and Genomes (KEGG) analysis were performed using a web-based functional annotation tool, DAVID database [187, 188]. For GO analysis, the GO Fat mappings were selected for each category to gain more specific terms.

3.18 Data analysis

Data were analyzed using GraphPad Prism 9 (GraphPad Software), ImageJ v1.53k, Fiji, Imaris 9.0.2 (Bitplane), ZEN black edition (Zeiss), AxioVision (Zeiss), Microsoft Excel (Microsoft), OriginPro (OriginLab), and R Studio. Heatmaps and enrichment plots were generated by http://www.bioinformatics.com.cn, an online platform for data analysis and visualization. Values were presented as mean ± S.E.M if not mentioned otherwise. Unpaired two-sided student's t-test was used to test the differences between two groups when data points were normally distributed. In cases the normality of data can't be determined, Mann-Whitney U test, a non-parametric test can be used to compare the distributions of two independent groups. P-values are stated in the figures.

4. Results

4.1 Killing efficiency of NK cells is significantly improved by activated T cells

To investigate whether T cells aid NK killing function, we firstly examined the impact of co-culture NK cells with T cells on NK killing efficiency. To this end, primary human CD4$^+$ T cells and NK cells were negatively isolated from the same healthy donors. Negative isolation minimizes pre-activation of these two cell types. NK cells were cultured either alone or with T cells in presence with anti-CD3/anti-CD28 antibody-coated beads (hereafter referred to as CD3/CD28 beads) for three days (Fig. 2A), as it takes three days for T cells to gain full effector function [189]. NK killing efficiency was determined using a plate-reader based real-time killing assay. In this assay, target cells were loaded with a green fluorescent dye calcein-AM and plated in a 96-well plate. When target cells were lysed by NK cells, the fluorescent dye is released into the supernatant, leading to a drop of fluorescence intensity at the bottom. The fluorescence intensity was measured using a micro-plate reader with the bottom-reading mode at 37°C every 10 min for 4 hours (Fig. 2B). K562 cells, a myelogenous leukemia cell line, were used as target cells as they don't express MHC-I molecules and can be therefore directly recognized by NK cells.
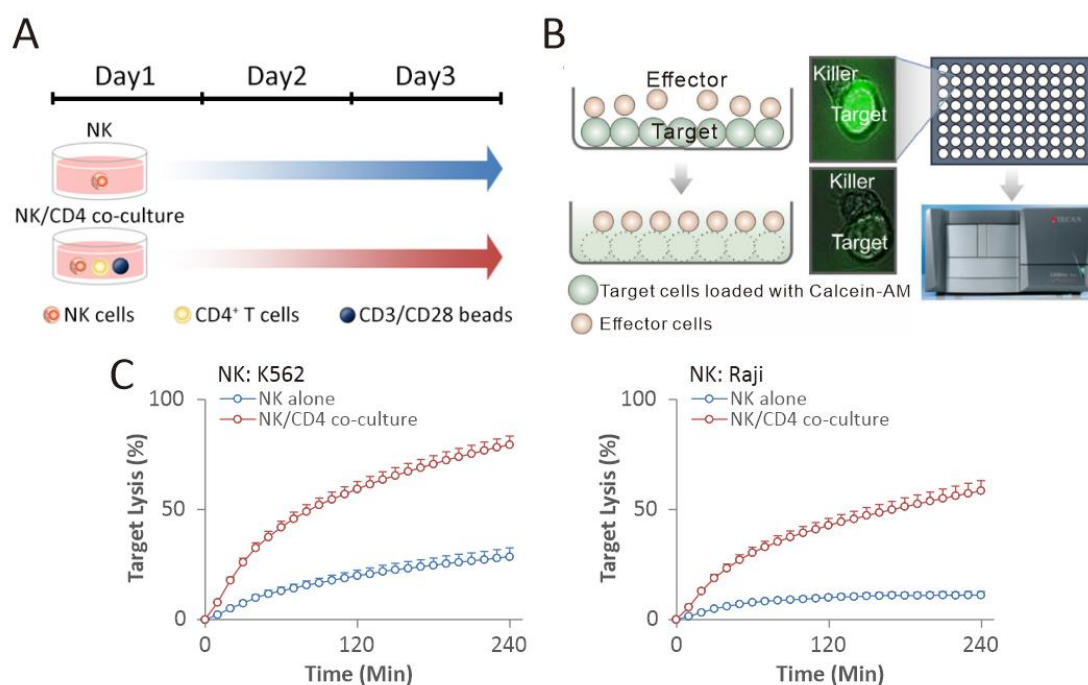
Figure 2. NK cells co-cultured with CD4$^+$ T cells exhibited significantly higher killing capacity. (A) Schematic diagram of cell culture. NK cells were cultured alone or co-cultured with CD4$^+$ T cells which were stimulated with CD3/CD28 beads for 3 days. (B) Sketch of real-time killing assay. The target cells were fluorescently labeled with Calcein-AM. The fluorescence loss due to effector mediated target cell lysis was recorded at 488/525 nm with plate reader. The sketch is adapted from Kummerow et al. 2014

[182]. (C) Real-time killing assay results reveal NK killing efficiency is boosted in both natural cytotoxicity (right panel) and ADCC (left panel). Calcein-loaded target cells were plated at 2.5×10^4 cells/well. The E:T ratio was 2.5:1. The plates were measured with plate reader at a time interval of 10 min for 4 h. n=20.

Using this real-time killing assay, we found that compared to NK cells cultured alone, the NK cells co-cultured with CD4$^+$ T cells exhibited substantially accelerated killing kinetics and overall enhanced killing efficiency against K562 cells (Fig. 2C, left panel).

Next, we examined NK killing capacity mediated by antibody-dependent cellular cytotoxicity (ADCC). To this purpose, we used Raji cells, a human B lymphoblastoid cell line original derived from a Burkitt lymphoma patient, as target cells. Raji cells cannot be directly recognized by NK cells due to their expression of MHC-I molecules (inhibitory KIR ligand) and lack of NK activating receptor ligands. To induce ADCC, Rituximab [190], an anti-CD20 antibody, clinically applied to treat non-Hodgkin B-cell lymphoma, was used to link Raji cells and NK cells as rituximab binds to CD20 on Raji cells and its Fc fragment can be engaged with Fc receptors on NK cells. Results of the real-time killing assay show that ADCC of NK cells was also drastically boosted by co-culture with CD4$^+$ T cells compared to NK cultured alone (Fig. 2C, right panel).

CD8$^+$ T cell, as another important subpopulation in T cells, are considered to primarily carry out antigen-specific killing as a complement to NK killing. Whether CD8$^+$ T cells could perform as helper cells to enhance NK killing is also of interest. To test this, NK cells were co-cultured with autologous CD8$^+$ T cells in the presence of CD3/CD28 beads. Both natural cytotoxicity (Fig. 3A) and ADCC (Fig. 3B) of the NK/CD8 co-culture cells were examined with real-time killing assay. Remarkably, a similar boosted NK killing as the case for NK/CD4 co-culture cells was verified.

Distinct from CD4$^+$ T cells, CD8$^+$ T cells are cytotoxic cells. Theoretically, the presence of CD8$^+$ T cells does not react efficiently to the target cells in this study, for K562 cells lack MHC class II molecules on their surface while Raji cells could only be recognized when pulsed with superantigen. To address the concern about a possible artificial effect from CD8$^+$ T cells, CD8$^+$ T cells were stimulated with CD3/CD28 beads for 3 days and applied to real-time killing assay. Compared to NK cell culture alone, CD8$^+$ T cells didn't mediate a higher killing efficiency which is far away from the level that NK/CD8 co-culture cells made (Fig. 3C, D). Thus, for the first time, CD8$^+$ T cells are discovered to 'help' NK killing capacity. Given the hypothesis that CD8$^+$ and CD4$^+$ T cells boost NK killing in a similar way, we used only CD4$^+$ T cells to conduct further investigation.
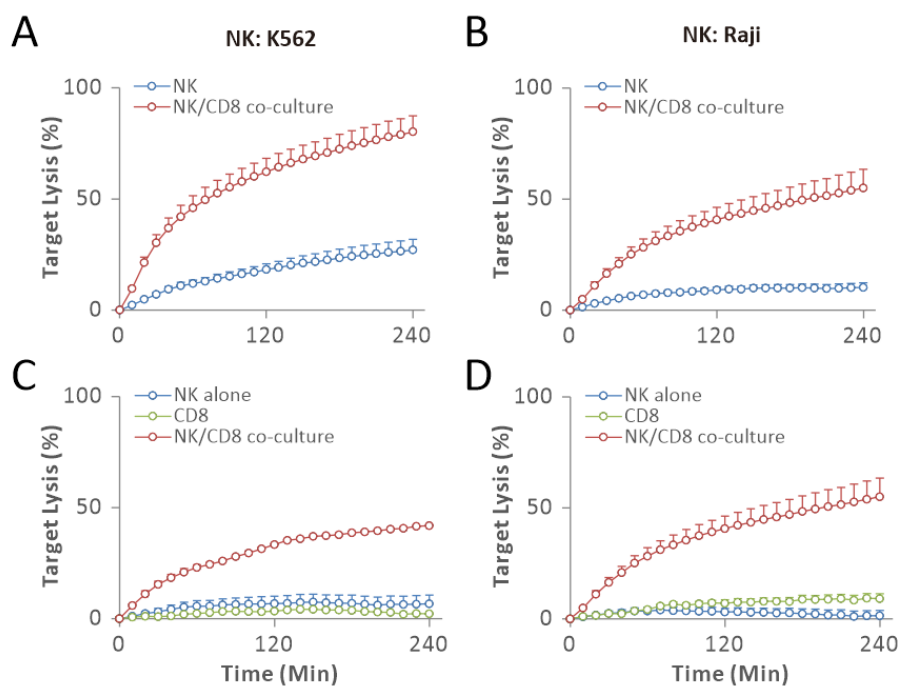
Figure 3. NK/CD8 co-culture also exhibited significantly higher killing capacity compared to NK alone. The killing efficiency of NK/CD8 co-culture cells was much higher than alone-cultured NK cells in both natural cytotoxicity (A) and ADCC (B). Stimulated CD8^{+} T cells were unable to mediate highly efficient killing against K562 (C) and Raji cells (D). Calcein-loaded target cells were plated at 2.5×10^4 cells/well. The E:T ratio was 2.5:1. The plates were measured with plate reader at a time interval of 10 min for 4 h. n=4.

To exclude possible artifacts from the real-time killing assay based on plate reader, this T cell-boosted NK killing was also determined with live-cell imaging using a high-content imaging system. Target cells were labeled with calcein-AM and killer cells were not labeled. Time lapse and quantification show that compared to NK cell cultured alone, NK/T cell co-culture exhibited faster killing kinetics and increased killing efficiency against K562 cells (natural cytotoxicity, Fig. 4A, B) and Raji cells (ADCC, Fig. 4C, D), which is in very good agreement with real-time killing assay based on plate reader.
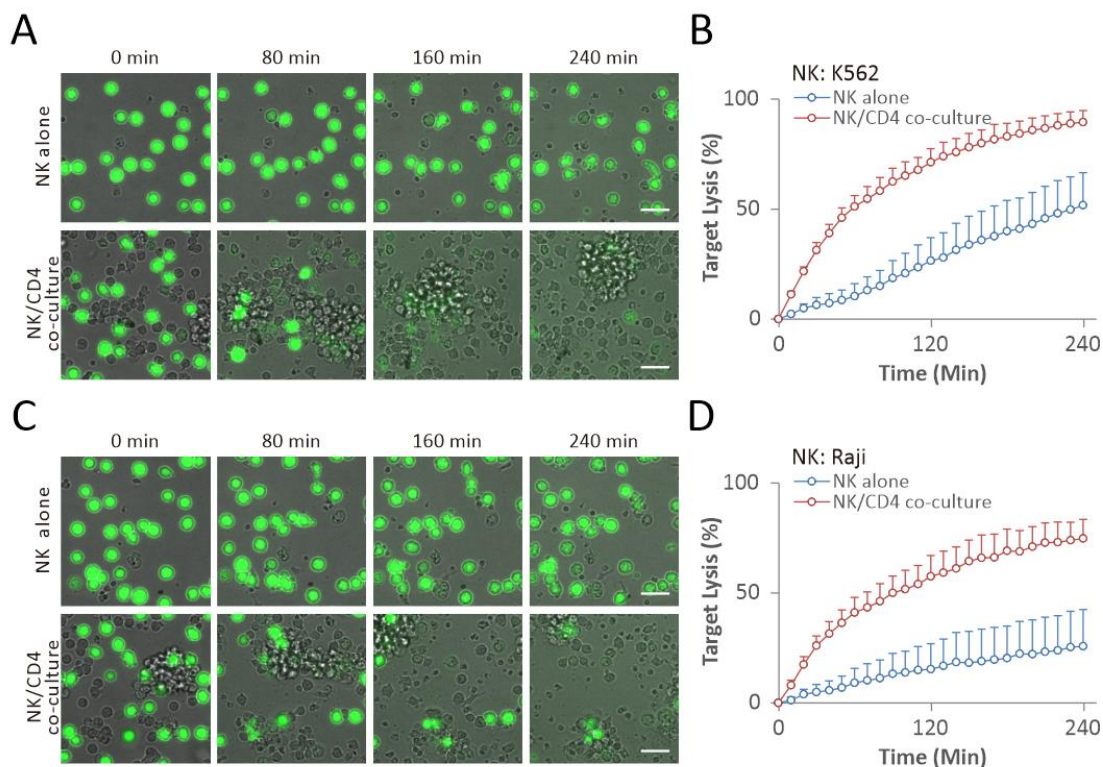
Figure 4. T cell-boosted NK killing is also verified with live-cell imaging on ImageXpress Micro XLS widefield high-content imaging system. (A) Time-lapse of a 4 h natural cytotoxicity test visualized with ImageXpress Micro XLS widefield high-content imaging system. A representative donor is shown as overlay of brightfield + GFP channels. Calcein-AM loaded K562 cells are of green color in GFP channel obtained at 488/525 nm. (B) Killing quantification from 4 donors. Live target cells were recognized with imageJ as detectable particles in GFP channel. The killing efficiency is evaluated according to the particle number change along the time series. (C) Time-lapse of a 4 h ADCC test visualized with ImageXpress Micro XLS widefield high-content imaging system. A representative donor is shown as overlay of brightfield + GFP channels. Calcein-AM loaded Raji cells are of green color in GFP channel obtained at 488/525 nm. (D) Killing quantification from 4 donors. Live target cells were recognized with imageJ as detectable particles in GFP channel. The killing efficiency is evaluated according to the particle number change along the time series. All target cells were plated at 2.5×10^4 cells/well. The E:T ratio maintains at 2.5:1. The plates were measured at a time interval of 10 min for 4 h. Scale bars are 40 μm.

To test whether different ratios of T cells over NK cells can influence the enhancement in NK killing efficiency, we examined three T:NK ratios 1:1, 2:1 and 4:1. Results from the real-time killing assay show that T:NK ratio of 1:1 was efficient to significantly enhance NK killing, which was only very moderately further increased by higher ratios (2:1 and 4:1) for natural cytotoxicity (Fig. 5A) and ADCC (Fig. 5B). Since the previous experiments were done with a T: NK ratio of 2:1, which showed stable enhancement in NK killing, this ratio was selected for further experiments.

31
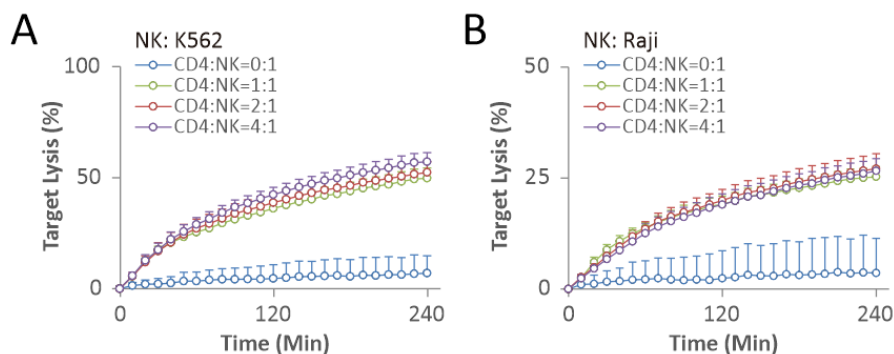
Figure 5. Increasing T to NK ratio did not further promote NK killing efficiency. NK cells that co-cultured with CD4+ T cells at T to NK ratios of 0:1, 1:1, 2:1, and 4:1 were tested with real-time killing assay against K562. In both natural cytotoxicity (A) and ADCC (B), T to NK ratio 2:1 gave outcoming good enough while 4:1 did not make it better. Calcein-loaded target cells were plated at 2.5×10^4 cells/well. The E:T ratio was 2.5:1. The plates were measured with plate reader at a time interval of 10 min for 4 h. n=4.

The period of NK/CD4 co-culture is therefore further explored and the same level of NK killing enhancement as the 3 days of co-culture is demonstrated can be achieved within 24 h. As shown in Fig. 6A, CD4+ T cells were activated with CD3/CD28 beads for 2 days. After the beads were removed on day 2, the activated CD4+ T cells were co-cultured with NK cells for 24 h. The NK killing in natural cytotoxicity (Fig. 6B, upper panel) and ADCC (Fig. 6B, lower panel) was elevated to a comparable level as the 3 day-co-culture. This 24 h-co-culture method was selected for further experiments if not otherwise mentioned.
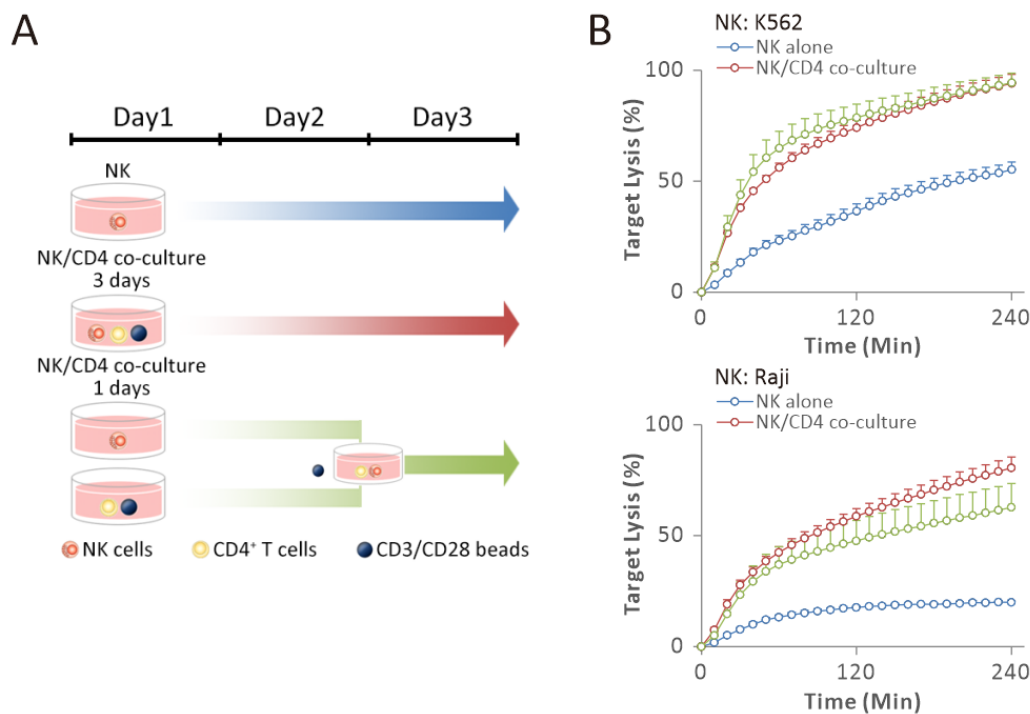
Figure 6. A duration of 24 h co-culture is sufficient to boost NK killing. (A) Schematic diagram of the 24 h-co-culture. CD3/CD28 beads were added to activate CD4+ T cells and were removed on day 2.

NK cells were then co-cultured with activated CD4$^+$ T cells for 24 h. (B) 24 h-co-culture is sufficient for fully established T-boosted NK killing. in both natural cytotoxicity (upper panel) and ADCC (lower panel). Calcein-loaded target cells were plated at 2.5×10^4 cells/well. The E:T ratio was 2.5:1. The plates were measured with plate reader at a time interval of 10 min for 4 h. n=5.

How long the boosted NK killing mediated by NK/CD4 co-culture lasts was also investigated. The NK/CD4 co-culture duration was elongated to 7 days from day 0. The NK killing was tested on day 3 (72 h) and day 7 (168 h). During the 7 day-co-culture, half of the culture supernatant was exchanged with fresh medium every 2 days. The results of real-time killing assay show that NK/CD4 co-culture result in a long-lasting NK function promotion. In both natural cytotoxicity (Fig. 7A) and ADCC (Fig. 7B), though the killing efficiency was reduced globally on Day 7 compared to that on Day 3, the NK/CD4 co-culture mediated much higher killing efficiency over the alone-cultured NK cells. The long-lasting NK killing enhancement indicates an intrinsic change in NK cells.
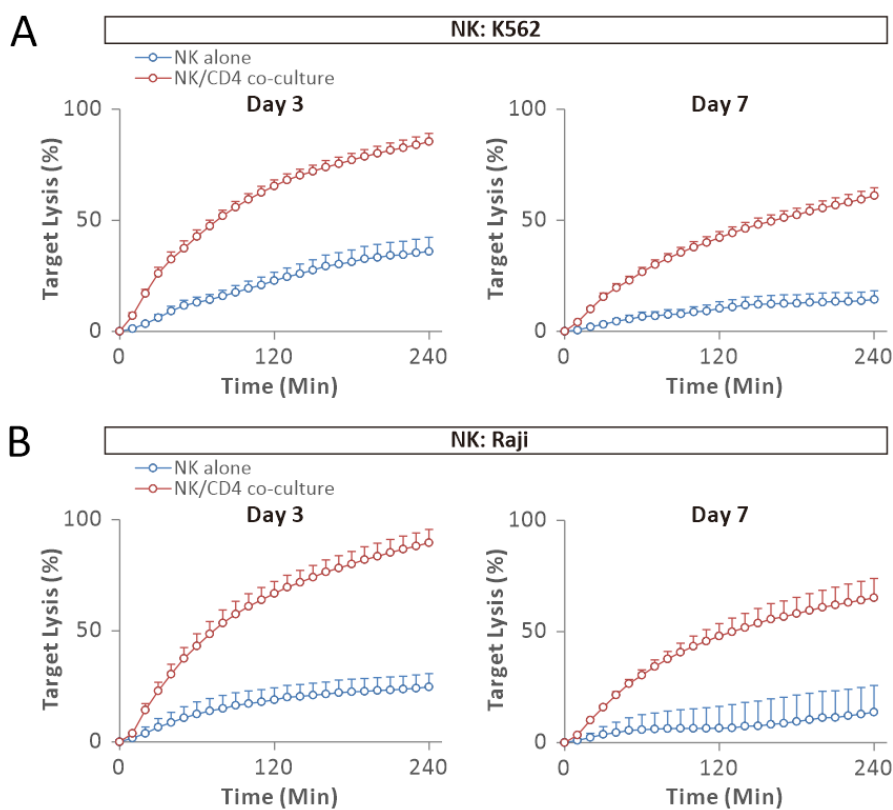
Figure 7. The NK/CD4 co-culture result in a long-lasting NK function promotion. The NK/CD4 co-culture duration was elongated to day 7 from day 0. NK killing was tested on day 3 (72 h) and day 7 (168 h). Real-time killing assay results reveal that T-boosted NK killing maintains for at least 4 days in both natural cytotoxicity (A) and ADCC (B). Calcein-loaded target cells were plated at 2.5×10^4 cells/well. The E:T ratio was 2.5:1. The plates were measured with plate reader at a time interval of 10 min for 4 h. n=20.

To prove that NK/CD4 co-culture leads to intrinsic enhancement in NK cell functions, NK cells were isolated from the NK/CD4 co-culture. In the previous experiments, T cells were always presented in the NK/CD4 co-culture conditions. Utilizing the Human CD56 Microbeads

(Miltenyi), the CD56^{+} NK cells were positively isolated from the one-day-co-culture. To determine apoptosis and necrosis of target cells, I used K562-pCasper cell line established by Christian S. Backes, etc. This is a stable K562 cell line expressing an apoptosis reporter pCasper, a GFP/RFP FRET pair linked by a caspase-3 recognition sequence [191]. A high-content imaging system was used to visualize the killing processes. Results show that it took isolated NK cells from NK/CD4 co-cultured considerably shorter time to initiate killing and they induced more apoptosis and necrosis compared to NK cells cultured alone (Fig. 8A, B). No significant difference in the apoptosis/necrosis ratio was found between the killing mediated by alone-cultured NK and T-boosted NK cells (Fig. 8C). Taken together, I conclude that the intrinsic killing capability of NK cells is significantly enhanced by co-culture with activated CD4^{+} T cells.
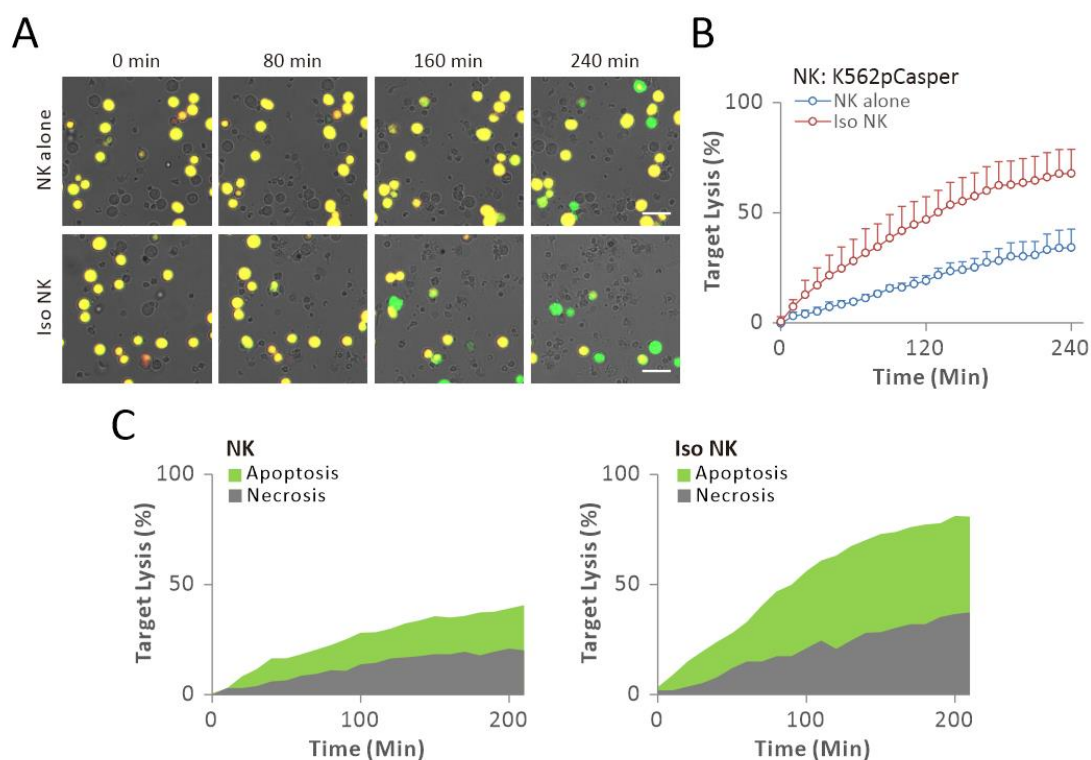
Figure 8. The intrinsic killing capability of NK cells is significantly enhanced by NK/CD4 co-culture. (A)After one day co-culture with stimulated CD4^{+} T cells, the NK cells were positively isolated with Human CD56 Microbeads (Miltenyi). Live-cell imaging shows that the isolated T cell-boosted NK cells (Iso NK) conducted higher target cells lysis ratio. A stable K562 cell line expressing an apoptosis reporter pCasper were used as the target cells and were plated at 2.5×10^4 cells/well. Cells were imaged with the ImageXpress Micro XLS widefield high-content imaging system at a time interval of 10 min for 4 h, and overlays of brightfield + GFP + FRET. Loss of signal in FRET channel and corresponding gain in GFP channel indicates the apoptosis of the target cell while signal reduction in both channels indicates necrosis of the target cells. The E:T ratio was 2.5:1.Scale bars are 40 μm. (B) Quantification from four donors is shown. n=4. (C) One representative out of four is shown, green and grey areas correspondingly represent the portion of apoptosis and necrosis. The ratio between apoptosis and necrosis was similar in the NK and Iso NK conditions.

Both K562 and Raji cells are derived from liquid tumors, can T-boosted NK cells also eliminate

solid tumor more efficiently? To this end, we used two melanoma cell lines, SK-MEL-5 and SK-MEL-28, which were established from patient-derived tumor samples. SK-MEL-5 cell line was obtained from a metastatic site (axillary lymph node) in a female patient with malignant melanoma in 1974. While SK-MEL-28 cell line was isolated from the skin tissue of a male malignant melanoma patient. Results from real-time killing assay reveal that killing efficiency of NK cells against both SK-MEL-5 and SK-MEL-28 cells was drastically enhanced after co-culture with $CD4^+$ T cells (Fig. 9A, B).

For a possible clinical application, to isolate sufficient quantity of primary T cells and NK cells requires large amount of peripheral blood from patients or donors, which is not feasible. We came up with a strategy to simulate T cells in PBMCs to enhance NK killing. We cultured PBMCs with or without the presence of CD3/CD28 beads for 3 days and conducted killing assay. Using K562 and Raji cells as targets, we found that CD3/CD28 bead-stimulated PBMCs exhibited a significantly enhanced killing efficiency (Fig. 9C, D). As proof of concept, we demonstrate that stimulating T cells in PBMCs can drastically boost NK killing activity.
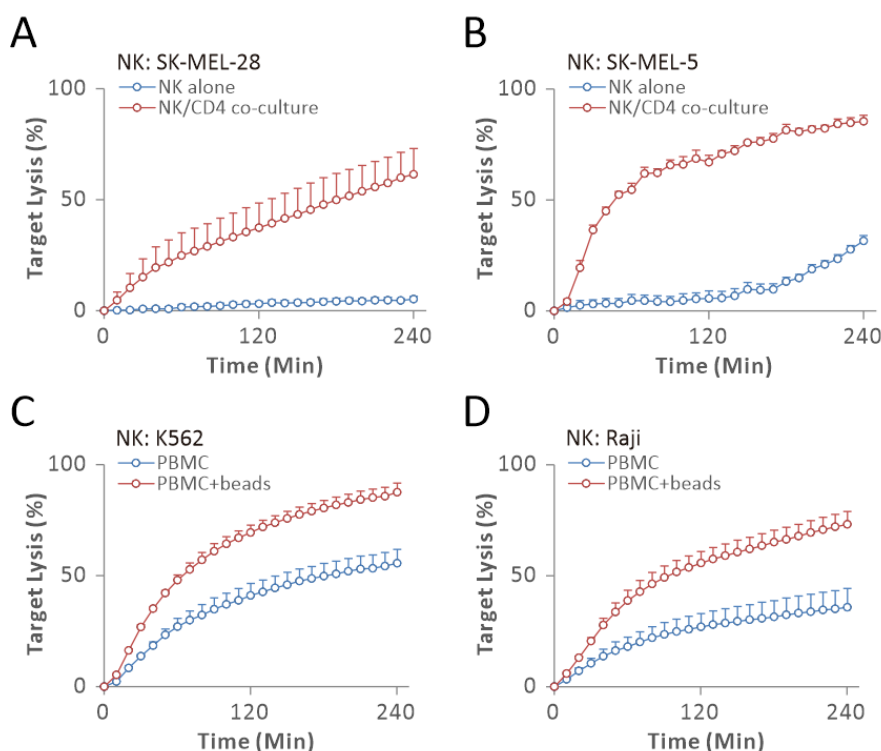
Figure 9. T cell-boosted NK cells destory tumor cells more efficiently. (A) NK cells against both SK-MEL-28 and SK-MEL-5 cells was drastically enhanced after CD4-boosting. Two melanoma cell lines, SK-MEL-28 and SK-MEL-5, were used as target cells and were plated at 25×10^3 cells/well. the E:T ratio was 5:1, n=4. (B) CD3/CD28 bead-stimulated PBMCs exhibited a significantly enhanced killing efficiency in both natural cytotoxicity and ADCC. For PBMC, PBMCs were cultured alone without any treatment. For PBMC+beads, PBMCs were activated with CD3/CD28 beads for 3 days. The E:T ratio was 20:1.

NK cells are surrounded in a 3D physiologic environment *in vivo*. I further verified th T-boosted NK killing in 3D scenario. NK cells were isolated from the NK/CD4 co-culture using the

Human CD56 Microbeads and the isolated NK cells were subsequently applied to 3D killing visualized using a high-content imaging system. As target cells, K562-pCasper cells were incorporated in 2 mg/ml collagen matrix. After collagen solidification, NK cells were added on the top of the matrix. In this setting, NK cells have to infiltrate and migrate in the 3D collagen matrix to locate and kill the target cells. Results show that the isolated T cell-boosted NK cells eliminated the target cells high efficiently while the alone-cultured NK cells failed to control the proliferation of the target cells (Fig. 10A, B). This result indicates that the T-boosted NK cells function the same in 3D matrix and further implies that the T cell-boosted NK killing may be highly relevant to a promoted NK migration.
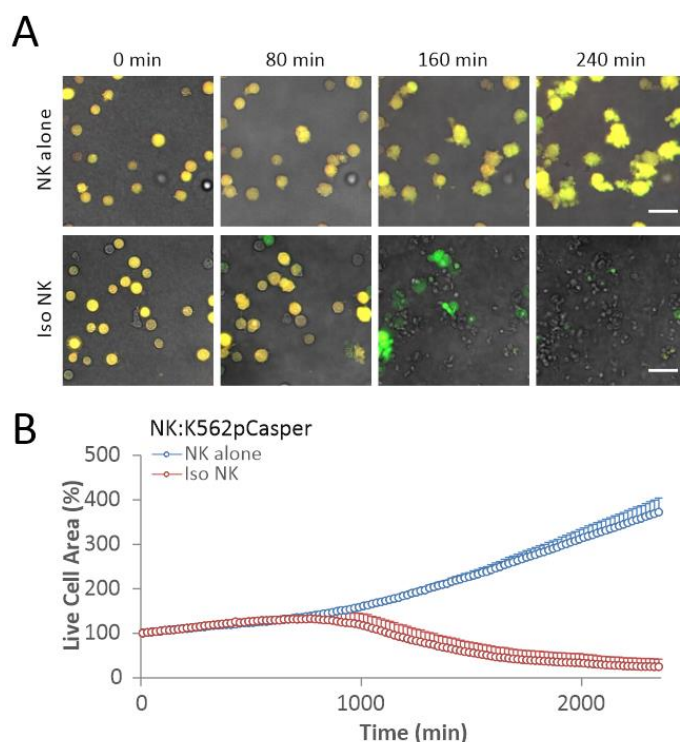
Figure 10. T-boosted NK cells can eliminate target cells high efficiently in 3D scenario. (A) NK cells were positively isolated with Human CD56 Microbeads (Miltenyi) from the NK+CD4 co-culture and applied to 3D killing against K562pCaper cells which were incorporated in 2 mg/ml collagen matrix. The killing processes were visualized with ImageXpress Micro XLS widefield high-content imaging system for 24 h and overlays of brightfield + GFP + FRET. Results show that the isolated T-boosted NK cells (labeled as Iso NK) conducted a much higher target cells lysis ratio while the alone-cultured NK cells failed to contain the target cell proliferation. Target cells were plated at 2.5×10^4 cells/well. Loss of signal in FRET channel and corresponding gain in GFP channel indicates the apoptosis of the target cell while signal reduction in both channels indicates necrosis of the target cells. The E:T ratio was 2.5:1. One representative out of four is shown. Scale bar is 40 μm. (B) Quantification of four donors is shown. The killing efficiencies were evaluated according to the live cell area. n=4.

To figure out whether the highly efficient killing mediated by NK/CD4 co-culture is indeed attributed to an enhancement of NK functions or actually a recovery of the original NK abilities, the killing efficiency of alone-cultured NK cells were tested on Day 0 (right after the isolation), Day 1, and Day 2. As shown in Fig 11, compared to Day 0, NK killing efficiency on Day 1 maintained at the same level while the killing efficiency on Day 2 was indeed reduced. However,

even the NK cells on Day 0 were not able to perform a high killing efficiency comparable to the NK/CD4 co-culture did. This fact indicates that the NK killing function *per se* was promoted by co-culture with CD4$^+$ T cells.
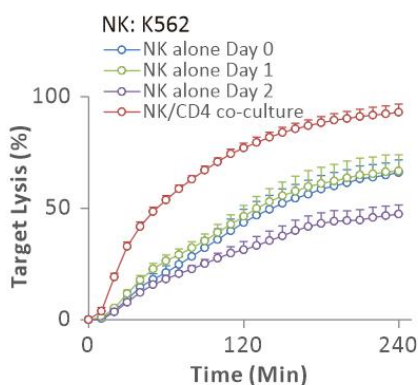
Figure 11. Co-culture with CD4$^+$ T cells indeed boosted NK killing efficiency. Though the killing efficiency of alone-cultured NK cells descended along culture time. The optimal killing efficiency mediated by NK cells cultured alone on Day 0 and Day 1 is still incomparable to the NK/CD4 co-culture did, which indicates a substantial enhancement on NK killing functions. Calcein-loaded K562 cells were plated at 2.5×10^4 cells/well as the target cells. The E:T ratio was 2.5:1. The plates were measured with plate reader at a time interval of 10 min for 4 h. n=4.

To rule out the possibilities that stimulated CD4$^+$ T cells alone could kill the target cells and CD3/CD28 beads also activated NK cells, NK cells stimulated by CD3/CD28 beads and activated CD4$^+$ T cells alone were tested with real-time killing assay. Theoretically, NK cells can't be activated by the CD3/CD28 activator beads as they lack CD3 and CD28 molecules on their surface. CD4$^+$ T cells, on the other hand, are mostly T helper cells that exhibit no cytotoxicity. As shown in Fig. 12, NK killing against K562 (Fig. 12A) and Raji (Fig. 12B) cells were not enhanced by co-culture with CD3/CD28 beads. While CD4$^+$ T cells alone could not mediate cytotoxicity against K562 (Fig. 12A) and Raji (Fig. 12B).
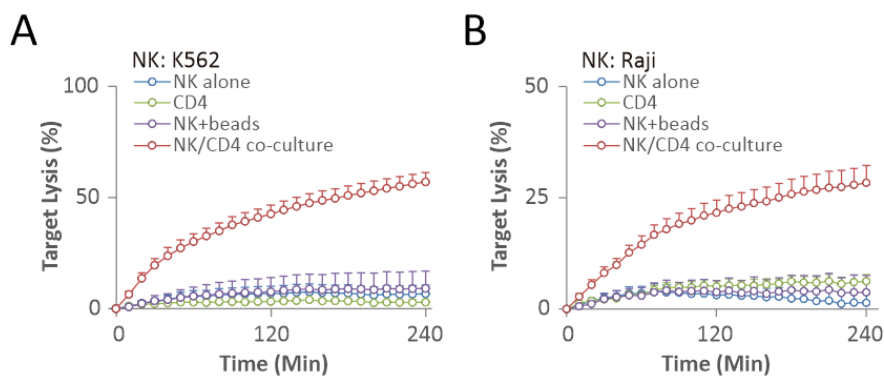
Figure 12. CD4$^+$ T cells mediate no cytotoxicity and CD3/CD28 beads don't affect NK killing. Neither CD3/CD28 stimulated NK cells nor stimulated CD4$^+$ T cells alone were able to mediate highly efficient killing against K562 (A) and Raji cells (B). Calcein-loaded target cells were plated at 2.5×10^4 cells/well. The E:T ratio was 2.5:1. The plates were measured with plate reader at a time interval of 10 min for 4 h. n=4.

To test whether the highly efficient killing mediated by NK/CD4 co-culture is attributed to

activated CD4$^+$ T cells. NK cells were co-cultured with unstimulated CD4$^+$ T cells for 3 days. Results of real-time killing assay against K562 cells (Fig. 13) suggest that unstimulated CD4$^+$ T cells are not capable of boosting NK killing, which indicates the stimulis that activate NK cells were from the stimulated CD4$^+$ T cells.
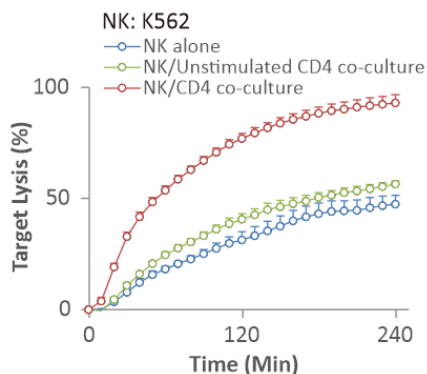
Figure 13. The highly efficient killing mediated by NK/CD4 co-culture is attributed to activated CD4$^+$ T cells. Co-culture with unstimulated CD4$^+$ T cells didn't promote NK killing efficiency at a comparable level as the activated CD4$^+$ T cells did. Calcein-loaded K562 cells were plated at 2.5×10^4 cells/well as the target cells. The E:T ratio was 2.5:1. The plates were measured with plate reader at a time interval of 10 min for 4 h. n=4.

A previous work from our group shows that the presence of non-target bystander cells can also enhanced NK cell killing efficiency [192]. Thus, I next examined whether T cells had this bystander effect to enhanced NK cell killing. To address this question, CD4$^+$ T cells stimulated for 3 days were mixed with NK cells cultured alone freshly before the killing assay started. In this scenario, NK killing was only marginally increased in a similar range as the bystander effect reported (Fig. 14A, B, green curve). These results suggests that bystander effect only contributed to a marginal, if not negligible, extend to the T cell-boosted NK killing.
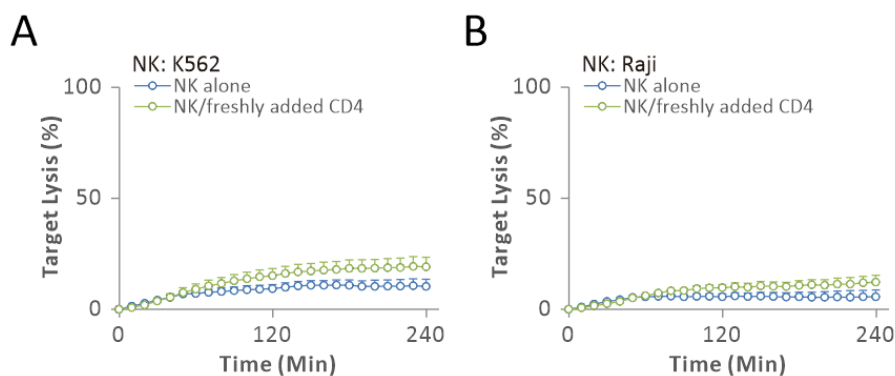
Figure 14. The bystander effect is ruled out from the T-boosted NK killing. Freshly added stimulated CD4$^+$ T cells just before the killing assay started could not enhance NK killing in natural cytotoxicity (A) and ADCC (B). Calcein-loaded target cells were plated at 2.5×10^4 cells/well. The E:T ratio was 2.5:1. The plates were measured with plate reader at a time interval of 10 min for 4 h. n=4.

4.2 NK motility is substantially enhanced by CD4⁺ T cells

4.2.1 NK viability, differentiation and lytic granule pathway are not altered by T cell co-culture

The next upcoming question is how NK cell killing efficiency was boosted by activated T cells. First, apoptosis of NK cells was examined using propidium iodide (PI) staining. PI is a small fluorescent molecule that binds to DNA but is unable to pass through intact cell plasma membrane. Dead cells can be distinguished by PI uptake. Flow cytometry results show that no significant PI-positive populations were detected in T cell-cocultured NK cells (Fig. 15 left panel). Next, NK cell proliferation was tested using CFSE. CFSE is a fluorescent dye that covalently binds inside cells to provide a stable, well-retained signal for long term. The cell proliferation generations can be traced by dye dilution with flow cytometry. NK cells did not exhibit detectable proliferation a lone or co-cultured with T cells (Fig. 15 right panel). Together, these results suggest that NK cell numbers are not changed by T cell co-culture.
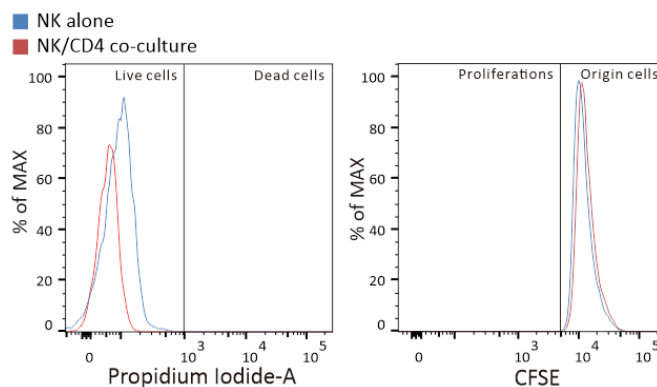
Figure 15. The NK cell number is not altered by T cell co-culture. NK cell viability (left panel) and proliferation (right panel) were demonstrated unaffected by co-culture with CD4⁺ T cells by flow cytometry. PI was excited with 488 nm laser and the emission was collected with 630/22 filter. CFSE was excited with 488 nm laser and the emission was collected with 527/32 filter. One representative donor is shown. n=4. The data acquisition and analysis were facilitated by Wenjuan Yang, and Denise Dolgener.

To determine which factor in the T-boosted NK cells plays central role in the promoted NK killing, the NK subpopulations and NK cytotoxic protein expressions were firstly checked. NK cells consist of two distinct subpopulations: the cytokine-releasing CD56^{bright} subset and the more killing competent CD16^{bright}CD56^{dim} subset. We compared the subpopulation distribution of the T-boosted NK cells with alone-cultured NK cells based on flow cytometry. No difference was determined in the fractions of the subpopulations (Fig. 16A, B).
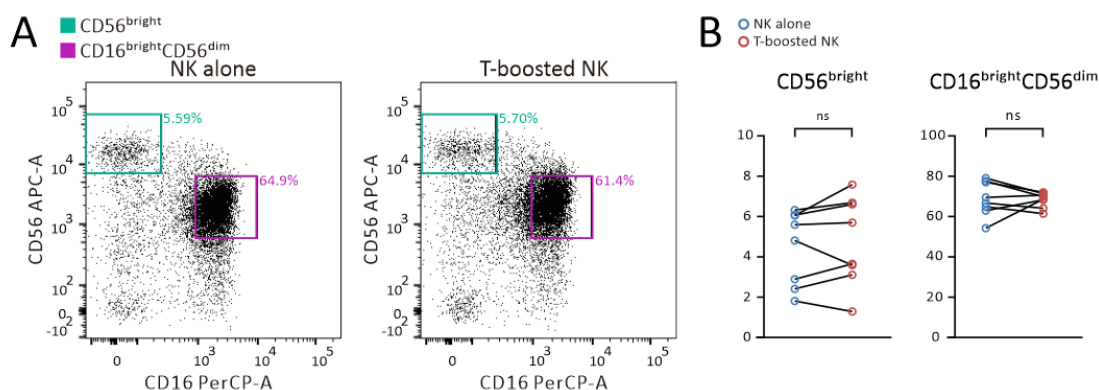
Figure 16. Co-culture with CD4+ T cells didn't affect NK subpopulation distribution. (A) The distribution of the two major NK subpopulations of one representative donor. Cytokine-releasing CD56bright subset and the more cytotoxic CD16brightCD56dim subset were not affected by the co-culture with activated CD4+ T cells. The subpopulation was analyzed via flow cytometry. (B) Quantification of all 8 donors. The data acquisition and analysis were facilitated by Wenjuan Yang, and Archana Yanamandra.

The major killing machinery employed by NK cells is the lytic granules (LGs). The expressions of corresponding cytolytic proteins, such as granzyme B, perforin, and pro-apoptotic molecule FasL, are therefore analyzed with flow cytometry. Surprisingly, cytolytic proteins were not upregulated in the T-boosted NK cells compared to the alone-cultured NK cells and (Fig. 17A-C). The T-boosted NK cells expressed less granzyme B while perforin and FasL were also slightly downregulated.

Besides the expression of cytolytic proteins, the delivery of the LGs could also affect the NK killing efficiency. The target recognition-induced LG release was subsequently quantified utilizing CD107a degranulation assay. CD107a is also referred to as LAMP1 (lysosome-associated membrane protein-1), which would be integrated into the plasma membrane after LG release [193]. Though a significant increase in CD107a expression upon encountering target cells was observed which indicates a functional NK LG release, there was no alternation identified in the T-boosted NK cases. (Fig 17D).

Apparently, co-culture with activated CD4+ T cells doesn't alter the NK subpopulation distribution. Furthermore, neither the NK LG protein expression nor the NK degranulation can explain the T-boosted NK killing. There must be some other factor is responsible for the drastically enhanced NK killing capacity.
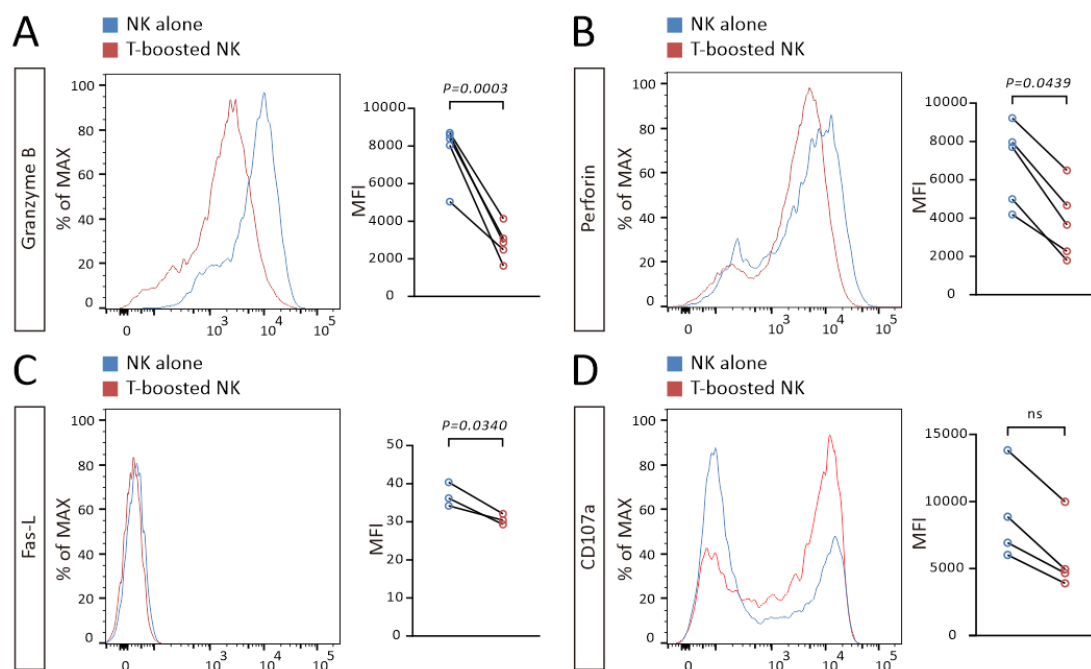
Figure 17. The LG protein expressions and LG release can't explain the T-boosted NK killing. The expressions of LG proteins were analyzed via flow cytometry. Granzyme B (A), perforin (B) and FasL (C) expressions were all reduced in T-boosted NK cells. (D) CD107a degranulation assay was introduced to test the LG release in NK cells via flow cytometry. A significantly increased CD107a expression in encountering with target cells was observed indicating a functional LG release machinery in NK cells, but it was not altered by co-culture with CD4+ T cells. For all results, the left panel displays the results from one representative donor out of four, while the right panel shows the quantification from all four donors. The data acquisition and analysis were facilitated by Wenjuan Yang, and Renping Zhao.
.

4.2.2 Co-culture with CD4+ T cells enhances NK cell motility

Since NK cells locate and afterward kill their targets depending on intact migration ability, and we've verified T-boosted NK killing in 3D scenario (Fig. 9), we turned our focus to the motility of NK cells. To mimic a physiologically relevant scenario, NK cells were incorporated into a 3D collagen matrix. The migration of NK cells was thereafter visualized, tracked, and quantified using light-sheet microscopy. We found that trajectories of T-boosted NK cells were much longer compared to alone-cultured NK cells (Fig. 18A, B).

The migration velocity of NK cells was substantially increased by the co-culture with activated CD4+ T cells (Fig. 18C left panel). Concerning the fast-migrating fraction (speed above 0.05 µm/s), only less than 10% of alone-cultured NK cells was in this range, whereas 60% of the T-boosted NK cells fell in this category. In addition, The NK migration persistence, indicating how directed the cells move, was also slightly enhanced by CD4+ T cells (Fig. 18C right panel). These data suggest that NK cell motility is enhanced by T cell co-culture.
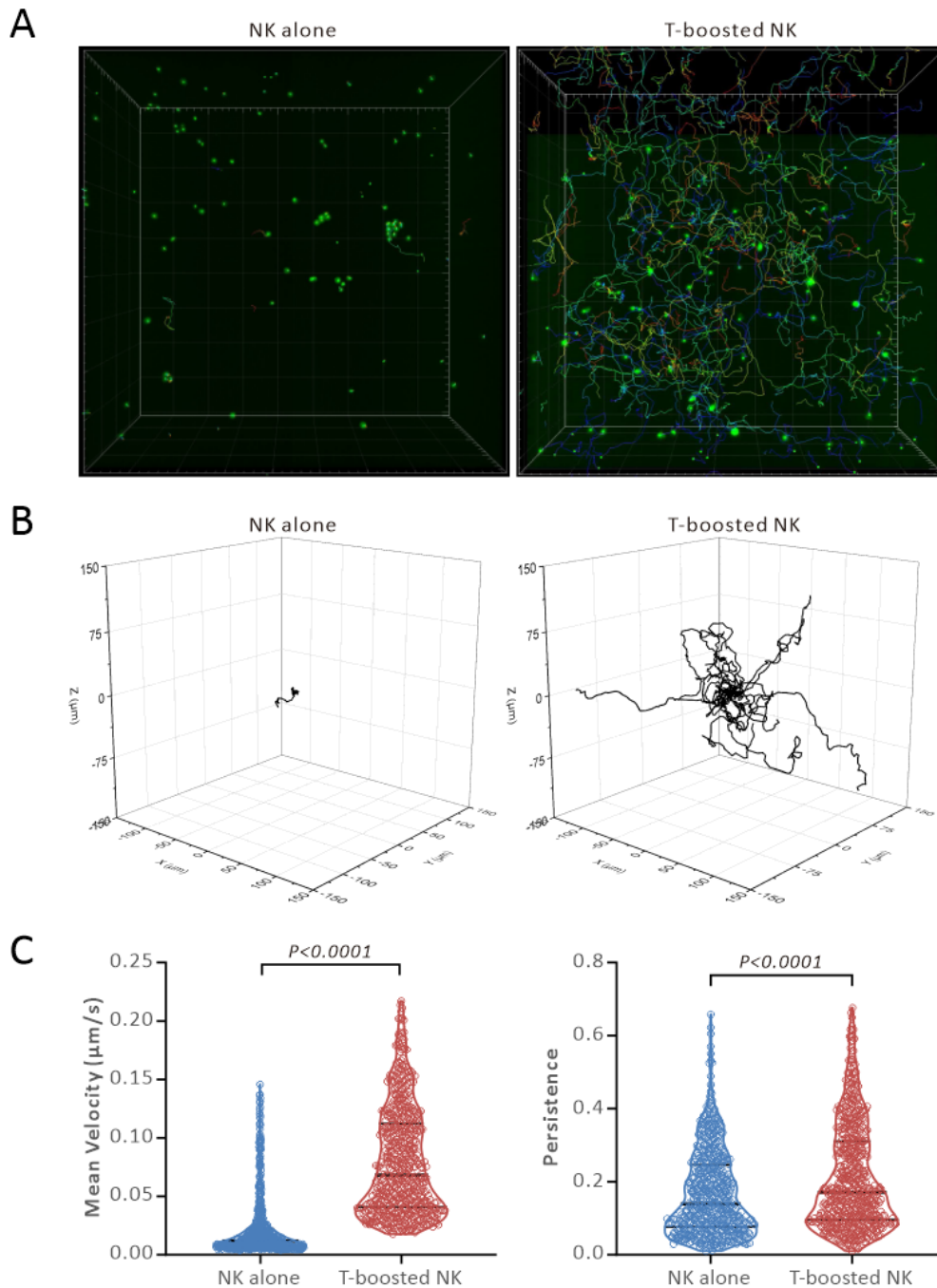
Figure 18. Co-culture with CD4+ T cells substantially boosts motility of NK cells. (A) NK cells were labelled with CFSE (GFP) after 2 days culture. CFSE labelled NK cells were then cultured alone or co-cultured with stimulated autologous CD4+ T cells for 24 h. For both conditions, 0.5×10^6 NK cells were incorporated into 100 μL 2 mg/ml Type 1 bovine collagen. Samples were observed with light-sheet microscopy for 60 min at 37 °C with 5% CO_2. The cell migration was tracked and visualized with software Imaris. Green dots are NK cells and lines are cell migration tracks. Result show that T-boosted NK cells were much more mobile than NK cells alone. (B) Trajectory plots show the T-boosted NK cells searched a much larger area in 30 min than the alone-cultured NK cells which suggest that T-boosted NK cells tend to move longer distances in a more directed way. One representative donor is shown. 30 cells were randomly chosen for each condition. **(C left panel)** Both the mean velocity of NK cell migration and the fraction of highly mobile NK cells were significantly enhanced by co-culture with activated CD4+ T cells. (**C right panel**) NK migration persistence was also slightly enhanced by T cells. 574 cells for NK alone and 597 cells for T-boosted NK with a track duration longer than 30 min were included. n=4. The data acquisition and analysis were facilitated by Renping Zhao, Rouven Schoppmeyer.

4.2.3 Myosin II activity is essential for the T-boosted NK migration

Myosin II, as a major cytoskeleton component expressed in lymphocytes, is reported essential for generating contractile forces that facilitate cell migration. The Myosin II activity is based on the myosin light chain (MLC) phosphorylation. Since the Myosin light chain kinases (MLCK) and the Rho-associated protein kinase (ROCK) are the two major types of enzymes that regulate the MLC phosphorylation, MLC inhibitor ML7 and ROCK inhibitor Y27632 were introduced to analyze how Myosin II takes effect in the T-boosted NK migration. To test the NK migration ability in different conditions, CFSE-labeled NK cells were loaded on the top of prepared 2 mg/ml Type 1 bovine collagen. The NK cell infiltration was observed with ImageXpress Micro XLS widefield high-content imaging system for 24 h. NK cells that infiltrated into the collagen and reached the focus plane were recorded. Based on the cell numbers recorded, the NK infiltration efficiency, indicating the migration ability of NK cells, was evaluated (Fig. 19A). For the inhibitor-treated T-boosted NK cells, inhibitors were presented in the medium at desired concentration throughout the whole acquisitions. As shown in Fig 19B, T-boosted NK cells exhibited much higher infiltrating ability than the alone-culture NK cells, in accordance with the results of migration analysis shown in Fig. 18. Treatment of Myosin II-related kinase inhibitors significantly affected the T-boosted NK infiltration. As shown in Fig 19C, MLC inhibitor ML7 suppressed the T-boosted NK infiltration in a dose dependent manner. 5 μM of ML7 slightly reduced the infiltration, 15 μM of ML7 suppressed the infiltration significantly, and 30 μM of ML7 almost eliminated the infiltration. Rock inhibitor Y27632, on the other hand, abolished the T-boosted NK infiltration at a concentration of 10 μM. The depletion of MLC phosphorylation kinase activities leads to NK migration failure indicating Myosin II an indispensable factor for the T-boosted NK motility.
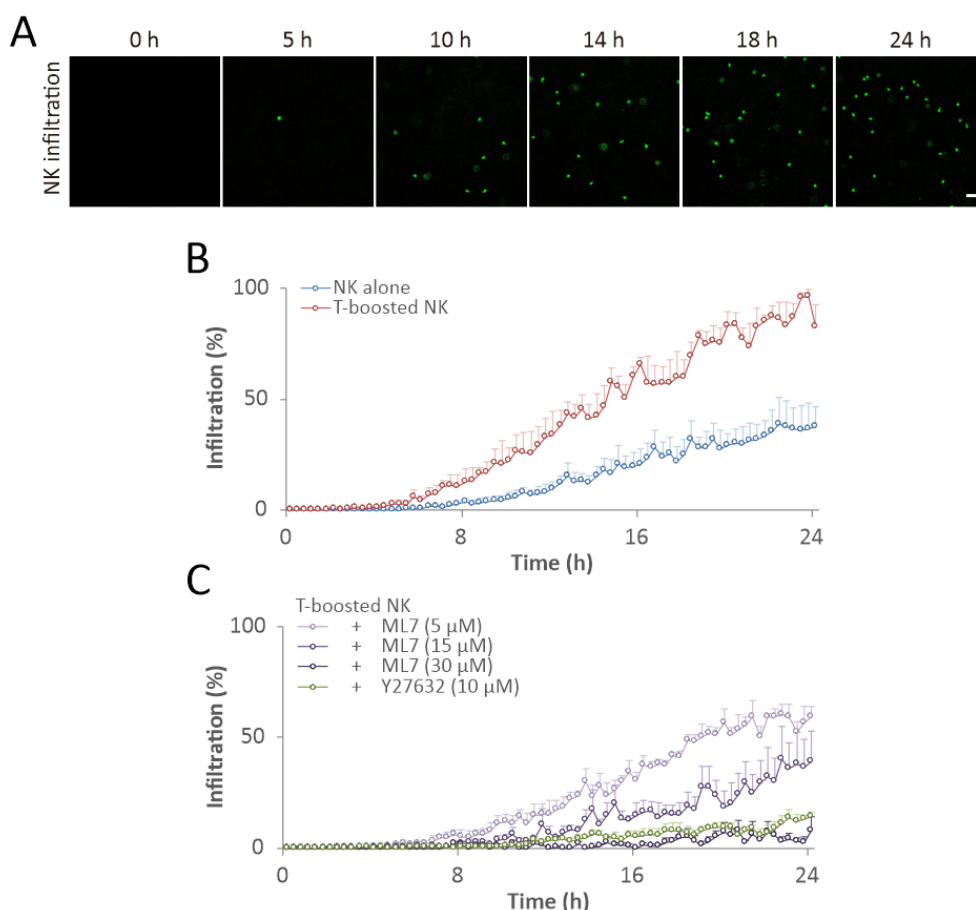
Figure 19. A depleted MLC phosphorylation kinase activity leads to vanished T-boosted NK migration. (A) One representative sample is shown to illustrate how NK cells infiltrated the collagen. NK cells were labelled with CFSE (GFP) after 2 days culture. CFSE labelled NK cells were then cultured alone or co-cultured with stimulated autologous CD4$^+$ T cells for 24 hours. For all the conditions, same quantity of NK cells was loaded on top of 2 mg/ml Type 1 bovine collagen. Samples were observed with ImageXpress Micro XLS widefield high-content imaging system for 24 h at 37 °C with 5% CO_2. The NK cells which infiltrated the collagen and migrated to the focus plane in GFP channel (green dots with clear edge) were recorded. The NK infiltration efficiency was evaluated according to the recorded cell numbers in time serials. Scale bar is 40 μm. (B, C) T-boosted NK cells infiltrated the collagen with much higher efficiency compared to the alone-cultured NK cells. This T-boosted NK infiltration was eliminated in the presence of MLCK inhibitor ML7 and ROCK inhibitor Y27632. Quantification of four donors is shown. All conditions for one donor were tested in the same independent experiment. The infiltration percentages were calculated based on the maximum cell number recorded in the independent experiment.

4.3 Physical contact between NK cells and T cells are essential for the T-boosted NK killing

4.3.1 Physical contact is indispensable for the T-boosted NK killing

To test how CD4$^+$ T cells boosted NK functions, the necessity of cytokine secretion by Th cells was first examined since it is believed to be the primary mediator to facilitate activation of other immune cells including NK cells [194]. For the NK/CD4 co-culture, NK cells not only have access to the CD4-released cytokines but also physical contact with the CD4$^+$ T cells. To test whether the CD4-release cytokines *per se* independent of the physical contact between NK and

CD4$^+$ T cells is sufficient to boost NK killing efficiency, a transwell system was introduced to avoid the NK-CD4 physical contact without affecting the accessibility of NK cells to the CD4-release cytokines. With transwells, NK cells were cultured in the inserts with porous bottom that only permit permeation of molecules like cytokines while the CD4$^+$ T cells were cultured in the outer wells. The reverse way, namely NK cells were in the outer wells while CD4$^+$ T cells were in the inserts, was also tested (data not shown). Interestingly, the presence of CD4$^+$ T cells (no matter in inserts or in outer wells) activated with beads for 3 days could only slightly elevate the NK killing efficiency, incomparable to the NK/CD4 co-culture with physical contact (Fig. 20A). This fact indicates that NK-CD4 physical contact plays a critical role in the T-boosted NK killing.

To fully demonstrate the importance of the NK-CD4 physical contact, two artificial possibilities were ruled out. First, concerning that NK cells might not have complete accessibility to the CD4-release cytokines, the supernatant in the insert and the outer well was manually mixed during the 3 day-cultures, which are found did not boost NK killing efficiency (Fig. 20B). Second, to exclude the possibility that NK or T cells were in a suboptimal status in the inserts, NK cells were also cultured with the medium from 3-day activated CD4$^+$ T cells for 1 day. In this scenario, the NK killing efficiency was still not boosted (Fig. 20C). Thus, the physical contact between T cells and NK cells is demonstrated essential for the T-boosted NK killing.
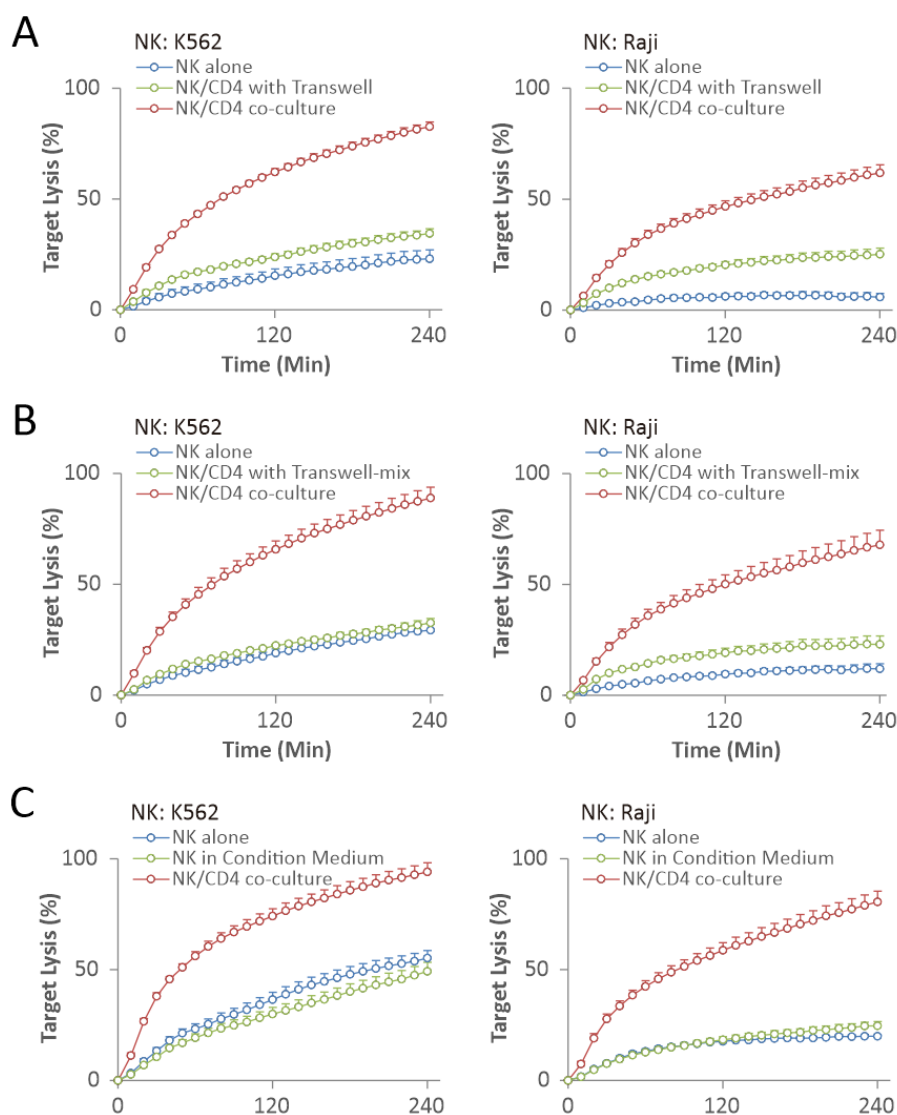
Figure 20. Evidence for the necessity of the NK-CD4 physical contact in the T-boosted NK killing. (A) To test how physical contact takes effect in the T-boosted NK killing, transwell system was introduced. NK cells were cultured in the transwell insert while the activated CD4⁺ T cells were cultured in the transwell outer well to avoid the NK-CD4 physical contact without affecting the accessibility of NK cells to the CD4-release cytokines. NK killing can't be boosted without physical contact between NK cells and T cells. (B) The supernatant between the insert and the outer well was manually mixed to guarantee that NK cells have complete accessibility to the CD4-release cytokines, which did not ameliorate NK killing efficiency. (C) To rule out the possibility that NK or T cells were in a suboptimal condition in the inserts, the medium from 3-day activated CD4⁺ T cells (CM) was taken to culture NK cells for 1 day. The killing efficiency of the NK cells cultured in CM was no better than alone-cultured NK cells. K562 cells were used as target cells for natural cytotoxicity. Raji cells were used as target cells for ADCC. The E:T ratio was 2.5:1. n=4.

4.3.2 Characterization of the physical contact between NK and T cells

We utilized live-cell imaging to visualize the NK/CD4 contact to have a better insight of the NK/CD4 physical interaction. Activated CD4⁺ T cells were unlabelled and NK cells were labelled with CFSE. The NK/CD4 interaction was visualized using Zeiss Cell Observer with GFP channel (for CFSE labeled NK cells) and brightfield channel. As one representative shown in Fig. 21A, the CD4⁺ T cell formed dynamic leading edge when migrating and touch the NK

cell actively. The contact between the NK and the CD4+ T cell is tight but mobile which slid from the leading edge to the rear part of the CD4+ T cell. The two cells departed from each other after a dynamic contact last around 240 s.

The duration of the contact between NK and T cells was quantified (Fig. 21B). The result reveals that the interaction between NK and T cells was in general very transient, lasting 470.54 s on average, which is much shorter than the contact between T cells and their target cells that last range from tens of minutes to hours [195].
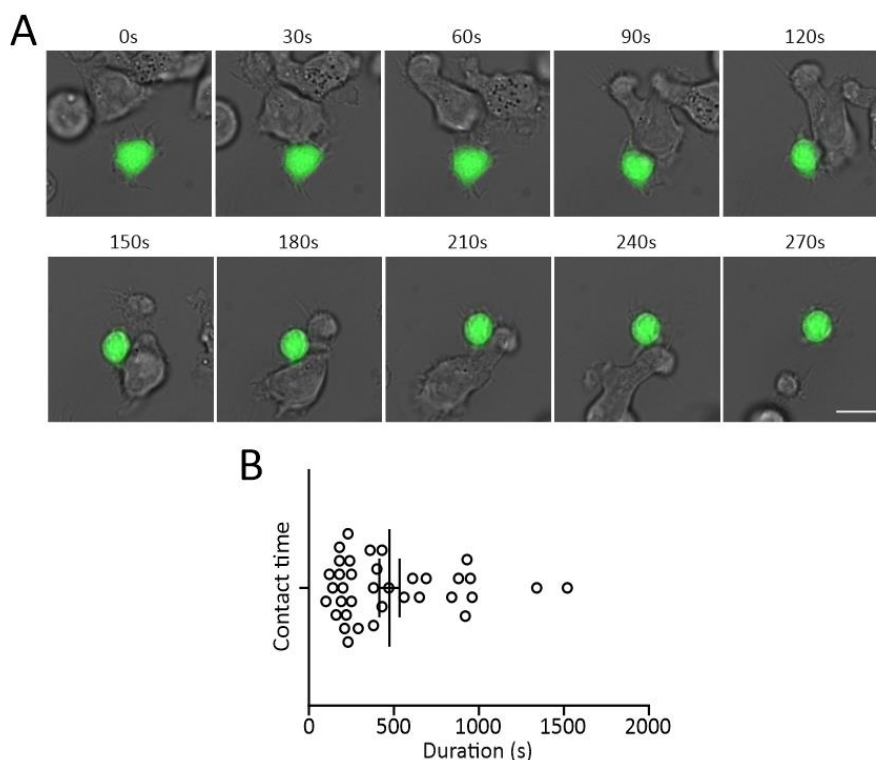
Figure 21. The visualization of the physical contact between NK cells and T cells. The interaction between NK and CD4+ T cells was visualized using live-cell imaging with Zeiss Cell Observer. NK cells were labelled with CFSE (detectable in GFP channel). CD4+ T cells were unlabelled. (A) One representative of NK/CD4 interaction is shown. The CD4+ T cell migrated fast and actively approached the NK cell. Transient but close contact was formed between the T cell and the NK cell. Scale bar is 10 μm. (B) The contact between NK and T cells was in general very transient, lasting 470.54 s on average. 36 cells from 4 independent experiments were analysed. The data acquisition and analysis were facilitated by Renping Zhao.

4.4 T cells boost NK cell killing function via locally released IL-2

Do the CD4+ T cells activate NK cells only by physical contact or by a synergy of physical contact and other factors? It has been reported previously that NK cells can be activated by IL-2 which is a major cytokine released by activated CD4+ T cells [196]. Moreover, the results of CyTOF and RNAseq reveal that subunits of IL-2 receptor on NK cells were upregulated upon co-culture with CD4+ T cells. However, our previous data has shown that conditional medium from activated CD4+ T cells were unable to promote NK killing efficiency (Fig. 20E, F). To examine whether the physical contact-dependent T-boosted NK killing is IL-2 independent, the

function of IL-2 receptor on NK cells were blocked using Basiliximab, a neutralizing antibody against IL-2 receptor alpha chain (CD25), during the 24 h-co-culture. Unexpectedly, in this case, T-boosted NK killing against K562 cells was abolished to the basal level as NK cells cultured alone (Fig. 22A). On the other hand, for ADCC mediated by NK cells treated with Basiliximab, the fast-killing phase was suppressed to the basal level as alone-cultured NK cells, whereas the slow killing phase seemed not to be affected (Fig. 22B). Moreover, though co-culture with CD4$^+$ T cells doesn't affect the NK subsets distribution, a treatment of 5 µg/ml Basiliximab for 24 h drastically reduced the high killing competent CD16^{bright}CD56^{dim} subset in NK/CD4 co-culture (Fig. 22C) while the CD56^{bright} subset was left unaffected (data not shown). These results indicate that, besides the NK-CD4 physical contact, IL-2 receptor-mediated signaling is essential for the T-boosted NK killing function, especially for the natural cytotoxicity.
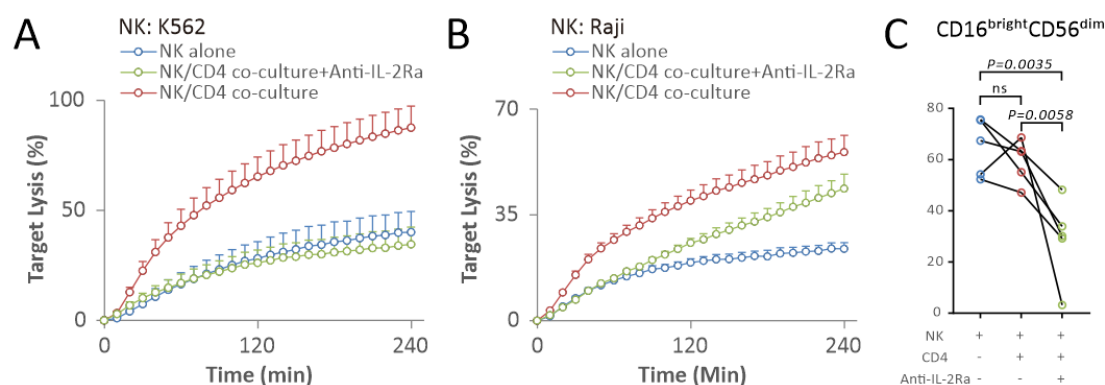
Figure 22. IL-2 receptor-mediated signaling is essential for the T-boosted NK killing function. (A) T-boosted NK killing against K562 cells was abolished to the basal level as NK cells cultured alone by blocking IL-2 receptor using Basiliximab. Basiliximab is a neutralizing antibody against IL-2 receptor alpha chain (CD25). For +Bas condition, autologous primary human CD4$^+$ T cells and NK cells were first cultured separately and T cells were activated with activating beads for 2 days. After the removal of the beads from T cells, the NK cells, and the activated T cells were mixed and co-cultured in freshly prepared AIMV medium with 5 µg/ml Basiliximab for 24 h. Real-time killing results show that NK cells killing efficiency can't be boosted by co-culture with stimulated T cells without IL-2 receptor functionality. (B) In the presence of Basiliximab, the fast-killing phase of ADCC mediated by NK cells was suppressed to the basal level as NK cells cultured alone, whereas the slow killing phase seemed not to be affected. n=4. (C) Flow cytometry results show that the distribution proportion of the more cytotoxic CD16^{bright}CD56^{dim} subset was significantly reduced by the Basiliximab-treated NK/CD4 co-culture. Quantification of 5 donors is shown. The acquisition and analysis of the FACS data were facilitated by Wenjuan Yang.

Since previous data has shown that the T-boosted NK killing is due to a promoted NK motility and IL-2 receptor-mediated signaling plays key roles in the T-induced NK activation. Whether the absence of IL-2 receptor function abolish the T-boosted NK migration was tested (Fig. 23). 5 µg/ml Basiliximab was presented in the 24- NK/CD4 co-culture to block the IL-2 receptor-mediated signaling. The NK migration was visualized with light-sheet microscopy. Trajectory plots (Fig. 23A) show that blocking IL-2 receptor eliminates the T-boosted NK motility. The velocity as well as straightness of NK cell migration were not enhanced by activated CD4$^+$ T

cells in the presence of Basiliximab (Fig. 23B, C). Thus, the T-boosted NK migration is highly associated with intact IL-2 receptor-mediated signaling.
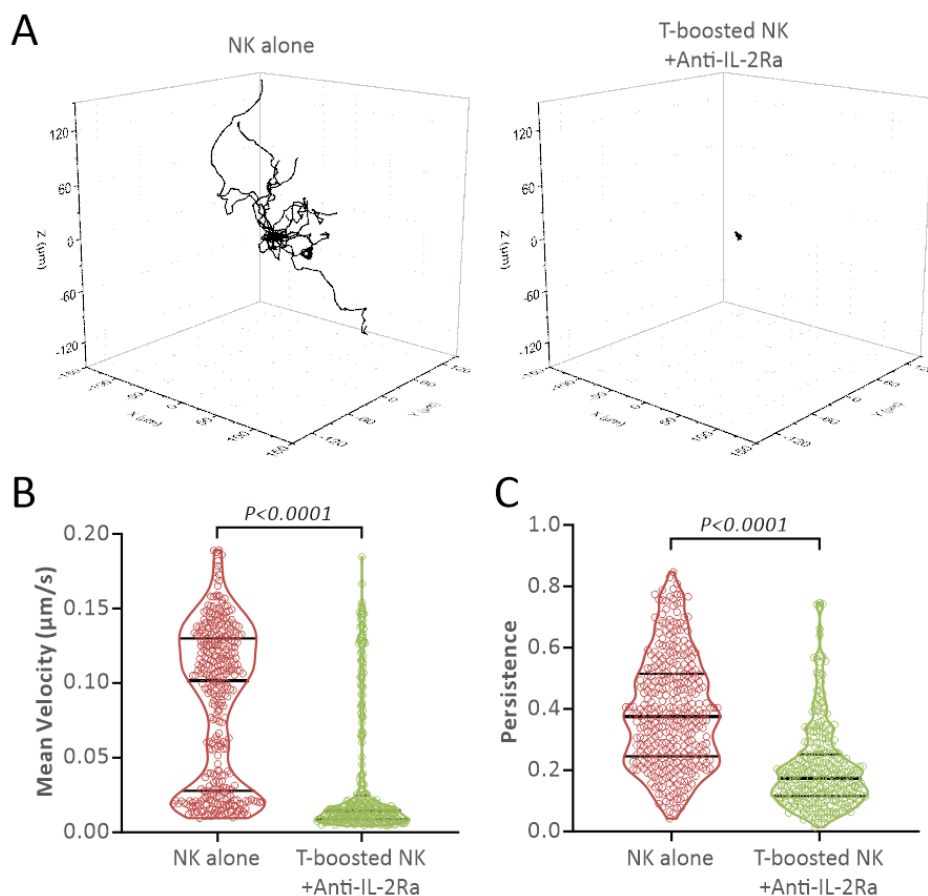
Figure 23. Neutralization of IL-2 receptor abolishes the T-boosted NK motility. (A) NK cells were labelled with CFSE (GFP) after 2 days culture. CFSE labelled NK cells were then co-cultured with stimulated autologous CD4^{+} T cells for 24 h. For the Basiliximab-treated condition, the co-culture was carried out in AIMV medium with 5 μg/ml Basiliximab. For both conditions, 0.5×10^6 NK cells were incorporated into 100 μL 2 mg/ml Type 1 bovine collagen. Samples were observed with light-sheet microscopy for 30 min at 37 °C with 5% CO_2. Black lines are cell migration tracks. Results show that NK cells killing migration can't be boosted by co-culture with stimulated CD4^{+} T cells without IL-2 receptor functionality. One representative donor is shown. 30 cells were randomly chosen for each condition. (B) Both the migration velocity of NK cells and the fraction of highly mobile NK cells were significantly reduced by blocking IL-2 receptor with Basiliximab. (C) NK migration persistence was also significantly reduced by the treatment of Basiliximab. n=2. The data acquisition and analysis were facilitated by Renping Zhao.

Since the presence of IL-2 is essential for the T-boosted NK killing function, the next question is how much IL-2 is required? To test this, supernatant of cell cultures under different conditions was collected. The concentration of IL-2 in the supernatant released by activated CD4^{+} T cells was determined using a flow cytometry-based multiplex cytokine assay. The quantification shows that the IL-2 in the supernatant from 3 day-co-culture of NK and CD4^{+} T cells was at a comparable level as the 3-day-stimulated CD4^{+} T cells; IL-2 released by NK cells alone (NK) was very low and close to the low detection limit (Fig. 24A right panel). From the 1 day-NK/CD4 co-culture however, a low dose of IL-2 close to the low detection limit was also

determined (Fig. 24A right panel). To determine the corresponding concentration for recombinant human IL-2, we also cultured NK cells with different concentrations of recombinant human IL-2 (rhIL-2, 0.5 ng/ml, 5 ng/ml, and 50 ng/ml) for 3 days and harvested the supernatant. We found that 50 ng/ml and 0.5 ng/ml of rhIL-2 is close to IL-2 concentration in the supernatant from 3 day-co-culture and 1 day-co-culture, respectively (Fig. 24A). Therefore, to mimic 1 day-co-culture boosting effect, NK cells were cultured in presence of 0.5 ng/ml of rhIL-2 for 1 day. NK killing was not enhanced (data not shown). The culture time was even extended to 3 days, no NK killing enhancement was detected (Fig. 24B). Since has been demonstrated that CM of 3-day-activated CD4$^+$ T cells was incapable of boosting NK killing in 24 h (Fig. 20E, F). We then used 50 ng/ml of rhIL-2 to boost NK cells for 3 days. We found that 3 day-boosting reached the level of CD4-boosting in three-fifths of the cases (6 out of 10). These results suggest that NK killing is not boosted by IL-2 released into the supernatant. Combined with the fact that physical contact is also essential for the CD4-mediated NK activation. It's reasonable to hypothesize that CD4$^+$ T cells boost NK function by IL-2 released into the cleft of contact site, where a very high local concentration can be reached.
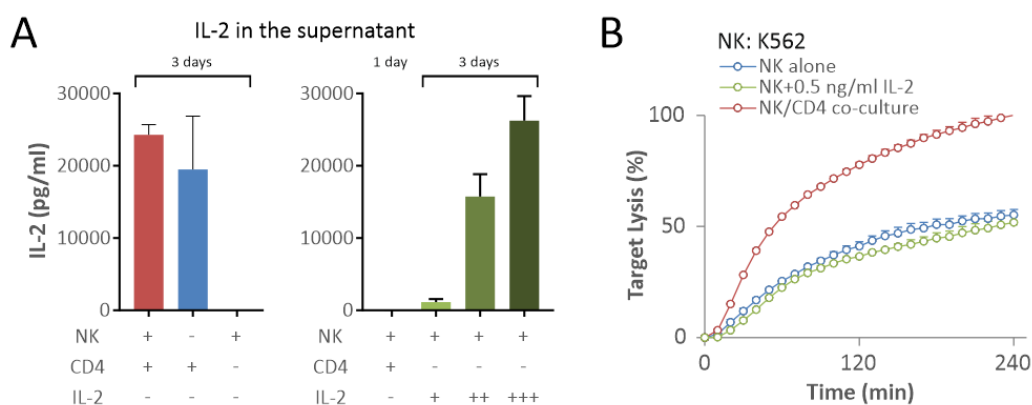
Figure 24. T-boosted NK killing is not attributed to the IL-2 distributed in the culture supernatant. (A) A flow cytometry-based multiplex cytokine assay was used to determine the IL-2 concentration in the supernatant of the cell cultures. The results of 3 day-NK/CD4 co-culture, 3 day-stimulated CD4$^+$ T cells, and 3 day-NK alone are shown in the left panel. The results of 1 day-NK/CD4 co-culture, and NK cells cultured in presence of 0.5 ng/ml of rhIL-2 (+), 5 ng/ml of rhIL-2 (++), and 50 ng/ml of rhIL-2 (+++) are shown in the right panel. 3 day-NK/CD4 co-culture and 3 day-stimulated CD4$^+$ T cells secreted IL-2 into supernatant in a comparable level whereas 3 day-NK alone and 1 day-NK/CD4 co-culture both released much less IL-2 very close to the detection limit. n=4. Error bars, S.D. (B) NK cells were cultured in AIMV with 0.5 ng/ml of rhIL-2 (Which is demonstrated close to IL-2 concentration in the supernatant from 1 day-NK/CD4 co-culture) to mimic 1 day-co-culture boosting effect. No enhancement in NK killing was detected in such case. n=4. The acquisition and analysis of the multiplex cytokine assay data were contributed by Renping Zhao.

To examine the hypothesis that IL-2 is released at the NK/CD4 contact site, immunostaining was carried out to localize the IL-2-containing vesicles in CD4$^+$ T cells upon contact with NK cells. NK cells and activated CD4$^+$ T cells were co-cultured for 30 min and fixed subsequently. CD4 cells were labeled with Alexa Fluor® 488 anti-human CD3 Antibody. The endogenous IL-2 in CD4$^+$ T cells was labeled with Alexa Fluor® 647 anti-human IL-2 Antibody. With a

brightfield channel, unlabeled NK cells, labeled CD4$^+$ T cells and IL-2-containing vesicles are therefore distinguished (Fig. 25A, left panel). To quantified the localization of the IL-2-containing vesicular structures in CD4$^+$ T cells, as shown in Fig. 25A (right panel), the CD4$^+$ T cells were divided evenly in diameter into 3 regions and the region closest to the NK/CD4 contact site was defined as *vicinity of the contact site* (V). The CD4$^+$T cells with an approximate sphere shape were analyzed. If the vesicular structures containing endogenous IL-2 tend to accumulate at the NK/CD4 contact site, the mean fluorescence intensity (MFI) of Alexa 647 of the V region should be higher than that of the rest part of the cell body. Results show that the MFI of the Alexa 647 channel in the V region was significantly higher than that in the resting region (Fig. 25B). Among the 65 cells examined, 5 cells presented higher MFI in the V regions. IL-2-containing vesicles were enriched in the vicinity of the NK/CD4 contact site in 92.3% of the CD4$^+$ T cells. This data supports the hypothesis that IL-2 is released locally at the NK/CD4 contact site.
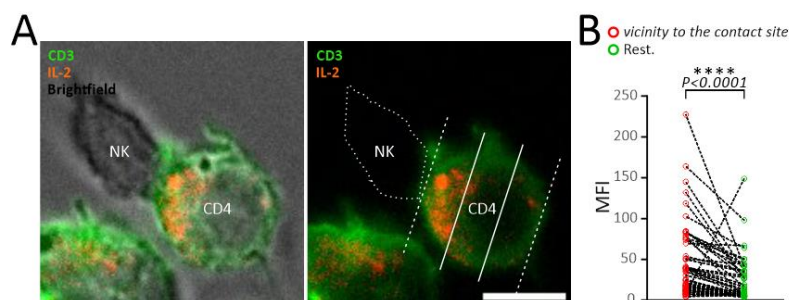
Figure 25. The IL-2-containing vesicular structures in CD4$^+$ T cells tend to accumulate at the NK/CD4 contact site. (A) The location of IL-2-containing vesicular in CD4$^+$ T cells upon contact with NK cells was analyzed. CD4$^+$ T cells were labeled with Alexa Fluor® 488 anti-human CD3 Antibody (GFP). IL-2-containing vesicular was labeled with Alexa Fluor® 647 anti-human IL-2 Antibody. NK cells were unlabeled. Cells were imaged with Cell Observer (Zeiss). One representative is shown. The body of the CD4$^+$ T cell was separated evenly in diameter into 3 areas as displayed in the right panel. The area closest to the NK/CD4 contact site was defined as *"vicinity to the contact site"* (the area from the left dashed line to the left solid line). The rest areas of the CD4$^+$ T cell was defined as "Rest.". (B) The MFI of the Alexa 647 channel in the *vicinity to the contact site* region and the Rest. region of 65 cells from 4 donors were analysed. CD4$^+$ T cells with roundish shape, significant IL-2 expression, and contact with a single NK cell were selected. Scale bar is 5 μm. The data acquisition was facilitated by Renping Zhao.

4.5 Functionality of LFA-1 is essential for the T-boosted NK killing

Physical contact is mainly initiated/mediated by adhesion molecules, among which LFA-1/ICAM-1 interaction plays a critical role in IS formation [48] [197]. To examine the impact of LFA-1 on T-boosted NK killing, the functionality of LFA-1 was blocked using Efalizumab during the 24 h-NK/CD4 co-culture. Efalizumab is an antibody binding to the alpha-like I domain/subunit of LFA-1 (CD11a), which blocks LFA-1/ICAM-1 interaction and is once used to psoriasis treatment [198]. Results show that in presence of Efalizumab, stimulated CD4$^+$ T cells were not able to boost NK killing against K562 cells any more (Fig. 26A). Given the fact

that Efalizumab can block LFA-1/ICAM-1 interaction, the remaining Efalizumab on NK cell surface might reduce killing by interfering the IS formation. To rule out this possibility, the T-boosted NK cells were pre-incubated with Efalizumab for 15 minutes and the antibody was washed away before the killing assay started. In this scenario, T-boosted NK killing against K562 was not affected at all (Fig. 26B). Furthermore, though co-culture with CD4+ T cells doesn't affect the NK subsets distribution, a treatment of 5 µg/ml Efalizumab for 24 h sigfinicantly reduced the high killing competent CD16^{bright}CD56^{dim} subset in NK/CD4 co-culture (Fig. 26C) while the CD56^{bright} subset was left unaffected (data not shown). Together, these results suggest that functionality of LFA-1 plays a critical role in the T-boosted NK killing.
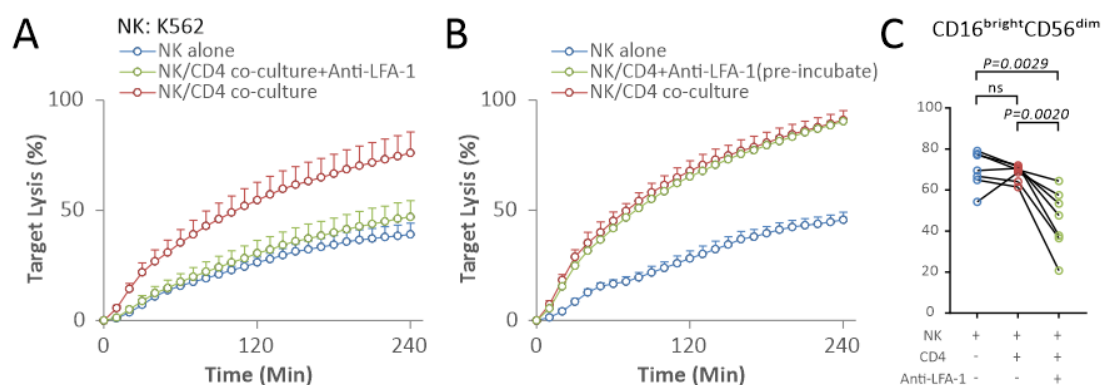
Figure 26. Functionality of LFA-1 is essential for natural cytotoxicity of the T-boosted NK cells.
(A) CD4+ T cells were not able to boost NK killing against K562 cells any more once the functionality of LFA-1 was blocked by Efalizumab during the 24 h-NK/CD4 co-culture. Efalizumab is an antibody binding to the alpha-like I domain/subunit of LFA-1 (CD11a), which blocks LFA-1/ICAM-1 interaction. For the Efalizumab-treated condition, autologous primary human CD4+ T cells and NK cells were cultured separately for the first 2 days. During this period, CD4+ T cells were activated with CD3/CD28 activating beads. After the first 2 days, the beads were removed from T cells. NK cells and activated CD4+ T cells were then co-cultured in freshly prepared AIMV medium with 5 µg/ml Efalizumab for 24 h before he real-time killing assay started. NK killing can't be boosted by co-culture with CD4+ T cells without the LFA-1/ICAM-1 interaction. (B) The possibility that the remaining Efalizumab on NK cell surface could reduce killing was excluded. For the condition with pre-incubate of Efalizumab, no Efalizumab was used during the 24 h-NK/CD4 co-culture. T-boosted NK cells were only pre-incubated with 5 µg/ml Efalizumab for 15 min before the real-time killing assay. In this case, T-boosted NK killing against K562 was not affected at all. (C) Addition of Efalizumab during 3 day-culture substantially reduced IL-2-boosted NK killing to a level even lower than NK cells alone. For the IL-2-activated NK cells, 50 ng/ml rhIL-2 was presented in the culture medium for 3 days. For the Efalizumab-treated condition, 5 µg/ml Efalizumab was presented to the IL-2-activated NK cells for 3 days. The presence of Efalizumab during culture fully suppressed the IL-2 induced elevation on NK killing. n=4. The acquisition and analysis of the FACS data were facilitated by Wenjuan Yang.

The next question is whether LFA-1 is equally important for NK-mediated ADCC. To surprise, the presence of Efalizumab during 24-h-NK/CD4 co-culture rather slightly enhanced ADCC mediated by T-boosted NK cells instead of impairing (Fig. 27A). Efalizumab bears Fc framework. It is considered that monoclonal antibody aggregates have potential risk for activating Fcγ receptor series (FcγRI, FcγRIIA, FcγRIIB, and FcγRIIIA) on immune cells [199]. Thus, we postulated that the remaining Efalizumab on NK surface was responsible for this further enhancement. Similar as above, we mimicked this situation by pre-incubated T-boosted

NK cells with Efalizumab for 15 minutes and wash the antibody away. Indeed, in this case, a further enhancement in ADCC mediated by T-boosted NK cells was observed (Fig. 27B). It implicates that the LFA-1 function influence the NK killing in a more complicated way. Instead of impacting the killing machinery in NK cells *per se*, it rather impacts the NK recognition of MHC-I negative target cells, presumably inhibitory and/or activating receptor pathway.
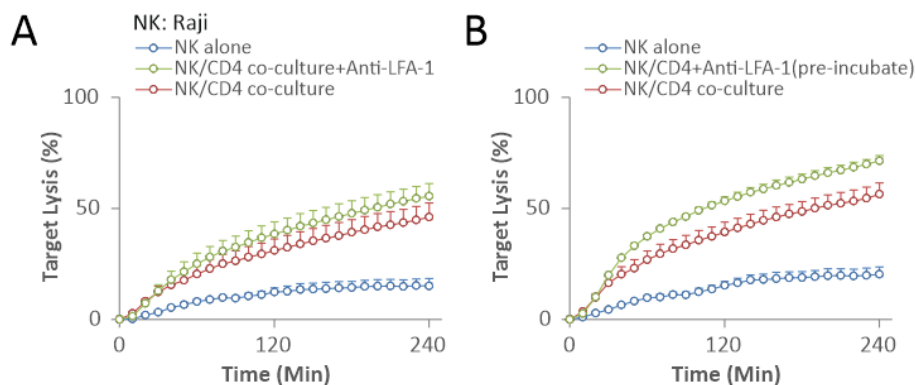
Figure 27. 24 h-Efalizumab treatment didn't impair the ADCC mediated by T-boosted NK cells. (A) The presence of Efalizumab during 24-h-NK/CD4 co-culture slightly enhanced ADCC mediated by T-boosted NK cells instead of impairing. Cells were treated in the same way as (Fig. 32A). (B) Remaining Efalizumab on NK surface was responsible for this further enhancement for ADCC. Cells were treated in the same way as (Fig. 32B). n=4.

Concerning Efalizumab blocks LFA-1 on both T cells and NK cells, to distinguish LFA-1 on which cell type is decisive, we replaced CD4$^+$ T cells with IL-2 to boost NK killing in presence of Efalizumab for 3 days. We found that although IL-2 could efficiently elevate NK killing to a similar level as CD4$^+$ T cells, killing of IL-2-boosted NK cells was substantially reduced to the level even lower than NK cells alone with addition of Efalizumab (Fig. 28A, B), which suggest that the LFA-1 on NK cells is responsible for the T-boosted NK function.

Interestingly, although it seemed like functionality of LFA-1 was not crucial for ADCC, at least for 24 h-NK/CD4 co-culture (Fig. 28A, B), the NK-mediated ADCC was also abolished even with 3 day-IL-2-stimulation (Fig. 28B). The long-term absence of LFA-1 signaling results in a loss of NK killing activity indicating that intact LFA-1 function is indispensable for NK-mediated cytotoxicity. Combining the results shown above, the functionality of LFA-1 on NK cells is suggested essential for the T-boosted NK killing.
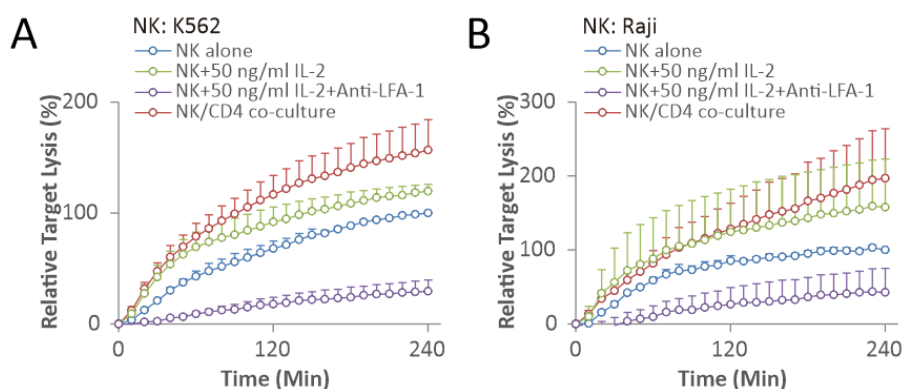
Figure 28. The long-term absence of LFA-1 signalling results in a loss of NK killing activity. Incubated with Efalizumab for 3 days abolished NK natural cytotoxicity (A) NK-mediated ADCC (B) even with 50 ng/ml IL-2 stimulation at the same time. Cells were treated the same way as (Fig. 32C). The data was show as relative target lysis (%) for clarity. n=4.

4.6 Surface molecule profiling of T cell-boosted NK cells

To define the immune signatures of the T-boosted NK cells, 36 molecules including surface markers, cytotoxic proteins, activating/inhibitory receptors, adhesion molecules, transcription factors, and chemokine receptors on/in NK cells are examined using cytometry by time-of-flight (CyTOF, also referred to as mass cytometry) by our collaborators, Jérôme Paggetti, Etienne Moussay, and Anne Largeot in Luxembourg Institute of Health. CyTOF is a powerful tool that allows simultaneous analysis of more than 30 cellular markers of samples consisting of millions of cells. The data was analyzed with software Cytosplore [200] and Cytofast [201]. 0.5×10^5 NK alone cells and 1.5×10^5 NK/CD4 co-culture cells from 5 donors were analyzed. Based on the expression patterns of the CD-markers, perforin, and IdU, the NK and CD4^{+} T cells were identified. IdU was a cell cycle marker that was introduced to facilitate the single cell gating. IdU marks the S phase of the cell cycle by inserting into the DNA of proliferating cells. In presence of IdU, a proper single cell gating can be performed without excluding the single cells in late S [202]. The T-boosted NK cells have distinct maker profile from the NK alone cells. The NK cells (NK alone and T-boosted NK) were selected and explored in higher resolution embedding of the hierarchy and finally embedded at the full single-cell data level. The distribution of the landmarks at the data level reveals 21 clusters within the NK cells. According to the heatmap based on all of the 36 marker expressions and all the identified 21 clusters shown in Fig. 29A. interesting clusters with unique immune signature can be identified in the T-boosted NK cells which express high level of CD3, CD4, CD69, CD2, CD25, CD126, CD127, and perforin (highlighted in Fig. 29A). CD3 and CD4 are T cell receptors and usually absent on NK cells. In human, NK cells are typically defined as CD3^{-}CD56^{+} cells [203]. Up-regulation of CD69, CD2, and CD25 is corelated to NK cell activation [204, 205]. CD127 expression on NK cells is associated with a low level of GzmB (in accordance with the result) and of a high potential for self-renewal and increased TNF and IFN-γ production upon

stimulation with IL-12 and IL-18 [206]. CD126, also known as interleukin-6 receptor subunit beta (IL-6Rβ), is a component of the IL-6 receptor complex. Previous studies, however, have shown a low expression or an absence of CD126 on human NK cells [207]. How the expression of CD126 affects NK function is still elusive. Meanwhile, these cells are CD16^{bright}CD56^{dim}, indicating they are highly killing competent. Half of these cells express high amount of CD57, which identifies a final maturation of the CD56^{dim} cells with optimal cytotoxic activities [208]. The interesting T-boosted NK subtypes mainly belong to cluster 19 and 21. Cluster 19 is the CD57^{high} one. The heatmap of relative abundance for each cluster in each individual sample is shown in Fig. 29B. Cluster 19 and 21 are particularly enriched in sample 2. Whether they are in responsible for the T-boosted NK killing requires further analysis.
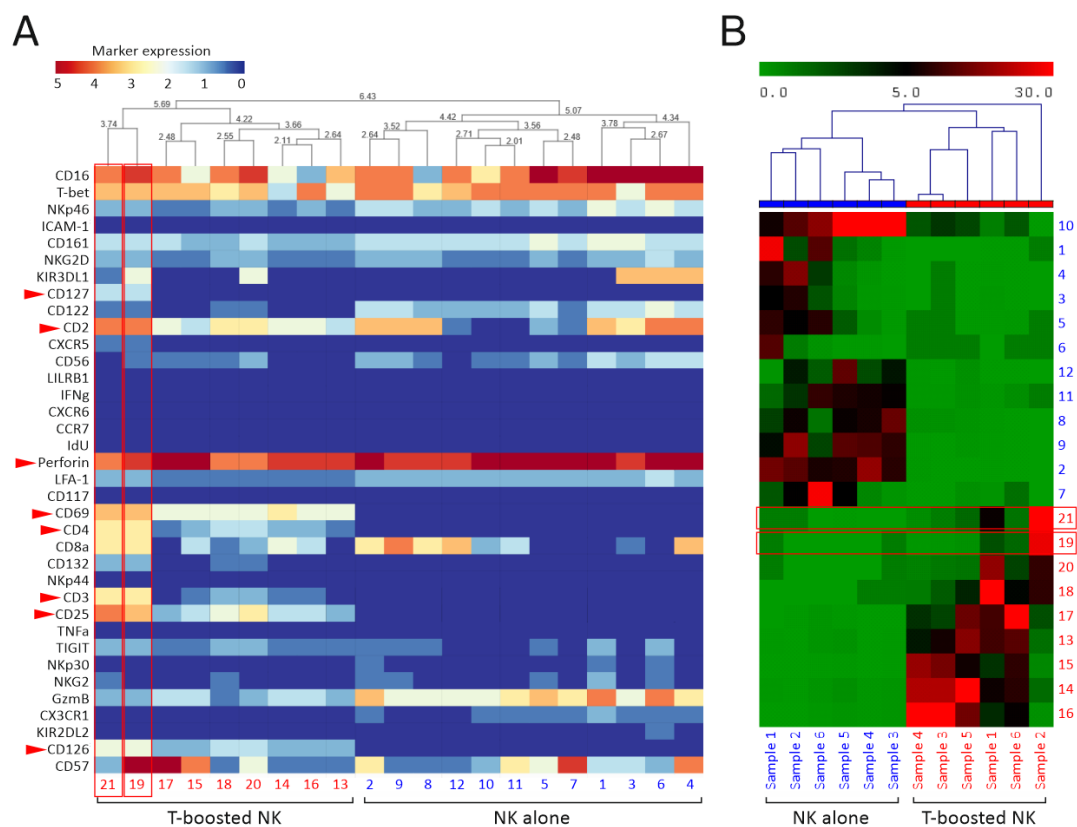
by Jérôme Paggetti, Etienne Moussay, and Anne Largeot in Luxembourg Institute of Health

Figure 29. CyTOF-based analysis reveals that NK cells were polarized into distinct subtypes upon co-culture with CD4$^+$ T cells. (A) Heat map representing the expression patterns in the identified 21 NK clusters. A single column corresponds to the expression data of a single cluster, and a single row corresponds to a single maker. The color ranging from red to blue indicates marker expressions from large to small. Cluster 21 and 19 are highlighted with red frames; The highly expressed markers in Cluster 21 and 19 are highlighted with red arrows. (D) Heat map representing the cluster distribution in the NK and T-boosted NK samples. A single column corresponds to the cluster distribution of a single sample, and a single row corresponds to a single cluster. The color ranging from green to red indicates cluster distribution from low to high. Cluster 21 and 19 are highlighted with red frames. This figure was contributed by Jérôme Paggetti, Etienne Moussay, and Anne Largeot in Luxembourg Institute of Health.

The NK proliferation, subpopulation distribution, cytotoxic protein expression, and degranulation were examined using flow cytometry above (Fig. 15-17). These results are

further verified with data from CyTOF. Results show that the expression of CD16 and CD56 on NK cells were not affected by the co-culture with CD4+ T cells (Fig. 30A), indicating there was no subpopulation shift. CD57, as a hallmark indicates the final maturation of NK cells, was also left unaffected (Fig. 30A).

From the overview level of the CyTOF data, IdU expression was only visualized in a cluster of CD4+ T cells (Fig. 29A). The mean signal intensity if IdU in all the 5 donors shows no difference between the NK alone cells and T-boosted NK cells (Fig. 30B), further verified that the proliferation of NK cells is not affected by co-culture with CD4+ T cells.

The expression of cytotoxic proteins and the cytokine release of NK cells were then examined. CyTOF data shows down-regulated GzmB and unaffected perforin (Fig. 30C). No difference of TNFa and IFNg production were determined (Fig. 30D).
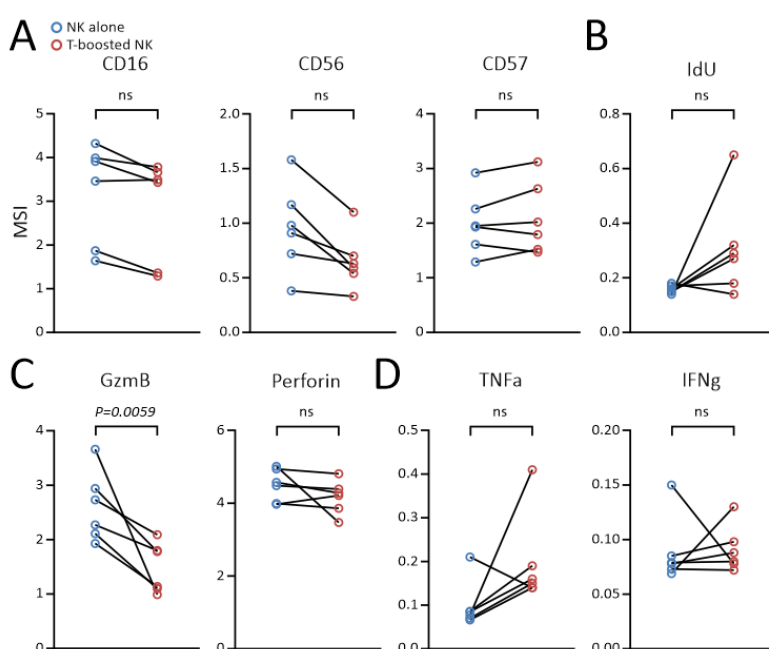
Figure 30. NK cell subpopulation, maturation, proliferation, cytotoxic protein, and cytokine release were not affected by co-culture with CD4+ T cells. (A) CD16, CD56 and CD57 expression on NK cells were not affected by co-culture with CD4+ T cells. (B) The unaffected IdU expression indicates co-culture with CD4+ T cells doesn't affect NK proliferation. (C) In T-boosted NK cells, GzmB expression was down-regulated while the perforin expression was intact. (D) The TNFa and IFNg production were not affected by the co-culture with CD4+ T cells.

The NK recognition is regulated by serial of activating and inhibitory receptors [24]. The expressions of these receptors were analyzed using CyTOF. The results are shown in Fig. 31. For activating receptors, NKp46, NKp44, NKp30, and NKG2D were examined. NKp46 and NKp44 expressions were significantly reduced in the T-boosted NK cells while NKp30 and NKG2D expressions were left unaffected (Fig. 31A). On the other hand, among inhibitor receptors including NKG2A, KIR2DL2_L3, KIR3DL1, LILRB1, CD161, and TIGIT, only the expression of TIGIT was slightly enhanced. No difference was determined in the expressions of the other inhibitory receptors (Fig. 31B). The balance of the activating/inhibitory receptors

is unlikely to be the reason of the T-boosted NK killing.
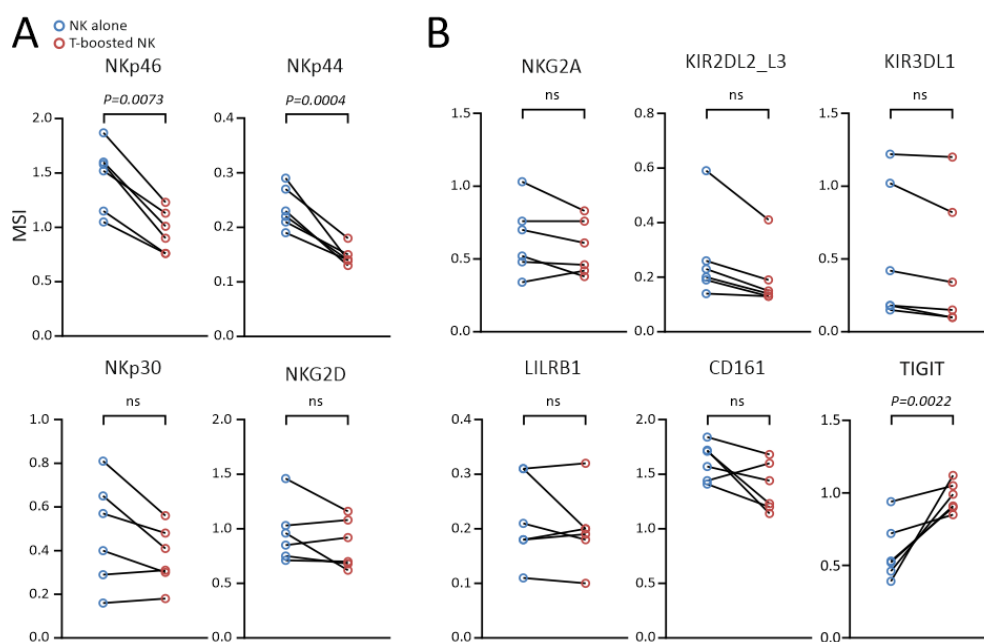
Figure 31. CyTOF data reveals how the co-culture with CD4+ T cells affected the expression of activating/inhibitory receptors on NK cells. (A) The expressions of the activating receptors. (B) The expressions of the inhibitory receptors.

It has been reported that the NK activation is associated with up-regulation of IL-2 receptor, chemokine receptors, CD69, and adhesion molecules [169, 204, 209, 210]. We therefore examined the expressions of these molecules. As shown in Fig. 32A, IL-2 receptor subunit CD25 expression was significantly enhanced on T-boosted NK cells, which indicates activation of the NK cells. The expression of CD132 was also up-regulated. However, the expression of CD122 was down-regulated.

Chemokine receptor expressions on NK cells were also altered due to the co-culture with CD4+ T cells (Fig. 32B). CXCR5 and CCR7 expression were enhanced while the CX3CR1 expression was reduced. The acquisition of CCR7 indicates a fully activating stage of NK cells [204]. CXCR5 and CX3CR1 expressions are responsible for the recruitment of the CD56dim NK cells to inflamed tissues [209, 210].

Notable, the CD69 expression on NK cells was significantly promoted (Fig. 32B). CD69 is an early activation marker expressed on many cell types in the human immune system human. The up-regulation suggests activation of NK cells both *in-vitro* and *in-vivo* [204].

Moreover, the CyTOF data reveals how the co-culture with CD4+ T cells affected the expressions of adhesion molecules on NK cells. Adhesion molecules play important roles in cell migration and IS formation [211, 212]. As shown in Fig. 32C, interestingly, the expression of LFA-1 was down-regulated while the ICAM-1 expression was up-regulated. CD2 expression, on the other hand, was left unaffected.
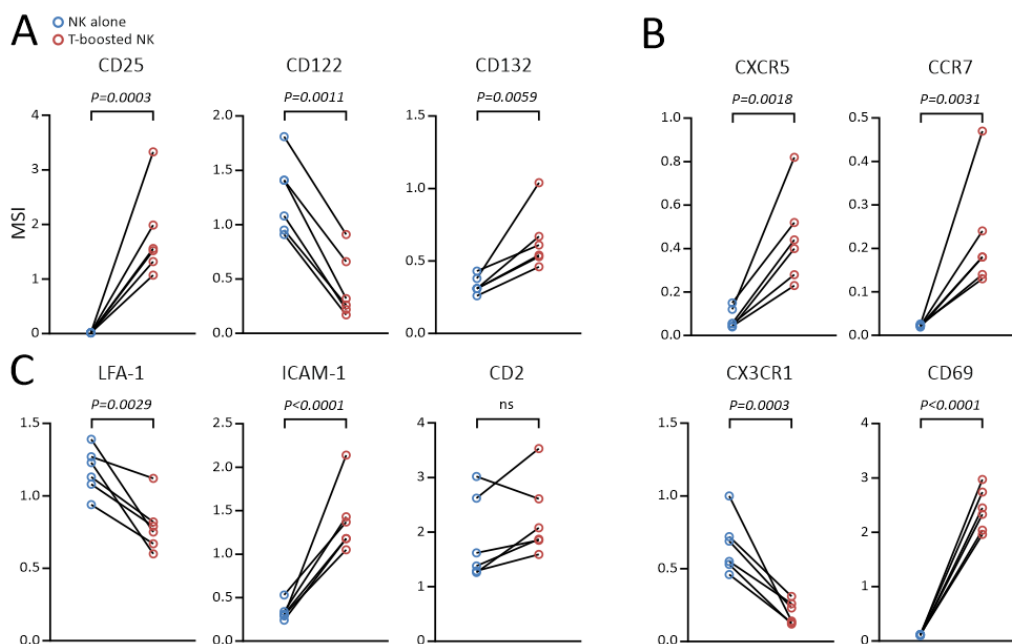
Figure 32. Expressions of IL-2 receptor subunits, chemokine receptors, CD69, and adhesion molecules on NK cells are altered upon co-culture with CD4+ T cells. (A) The expressions of the IL-2 receptor subunits. (B) The expressions of the chemokine receptors and CD69. (C) The expressions of the adhesion molecules.

Together, all these results indicate that the T-boosted NK cells are in a higher activating statue compared to the alone-culture NK cells. And it has been further supported that the proliferation, subpopulation distribution, cytotoxic protein expression, and activating/inhibitory receptors are not the reason for the enhanced NK killing, which indirectly highlights the importance of the NK migration.

4.7 Analysis of gene expression in T-boosted NK cells

4.7.1 An overview of changed pathways and cellular functions

To examine how the co-culture with CD4+ T cells affected the gene expressions of NK cells on transcriptional level, we generated RNA-sequencing libraries of the alone-cultured NK cells and the T-boosted NK cells. 6130 differentially expressed genes (DEGs) with corrected P value (padj)<0.05 were identified. Compared to the alone-cultured NK cells, 3689 genes were upregulated while 2441 genes were downregulated in T-boosted NK cells (Fig. 33).
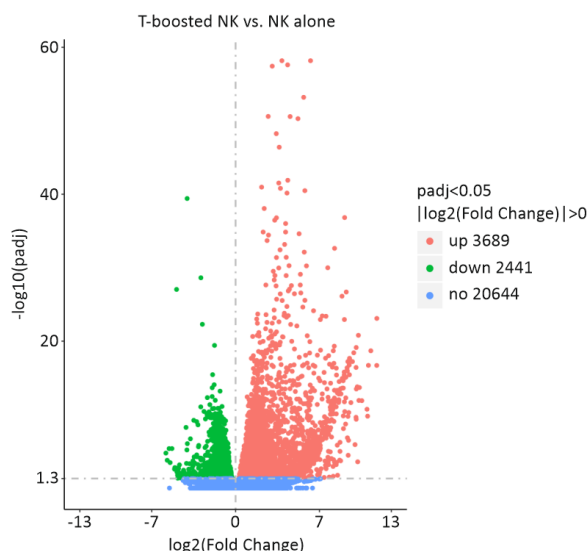
Figure 33. Volcano map of the differentially expressed genes (DEGs) in T-boosted NK cells compared to NK alone. The horizontal axis represents the fold change of genes in in T-boosted NK cells compared to NK alone, while the vertical axis shows the degree of statistically significant changes in gene expression. The Benjamini and Hochberg's method was introduced to adjust he obtained P-values in order to control the false discovery rate. The adjusted P-values are displayed as padj. A lower padj value indicates a more significant difference. Up-regulated genes are denoted by red dots, down-regulated genes by green dots, and blue dots indicate no significant difference in gene expression.

The expression patterns of the DEGs were presented in the clustering heat map (Figure 34). Hierarchical clustering analysis was carried out of log2(FPKM+1) of union DEGs, within the two comparison groups of T-boosted NK and NK alone cells. FPKM stands for Fragments Per Kilobase of transcript per Million mapped reads, a commonly used unit for measuring gene expression levels in RNA sequencing data, represents the number of fragments or reads that are mapped to a gene, normalized by the length of the gene and the total number of fragments in the sample. FPKM values are proportional to the abundance of the gene in the sample, and can be used to compare gene expression levels across different samples [184, 213].

Functional enrichment analysis was carried out to further study the DEGs. Gene Ontology (GO) enrichment analysis were performed using a web-based functional annotation tool, DAVID database [187, 188]. Three categories, biological process (BP), cellular component (CC) and molecular function (MF) were detected. The 20 most significantly enriched terms (padj<0.05) in each category are presented in Fig. 35. For BP category, DEGs were particularly enriched in cellular response to stress/DNA damage stimulus, cell cycle related process, cellular protein modifications, positive regulation of metabolic process, and cellular component organization; For CC category, in cytosol, ribosome, mitochondrion, nuclear, envelop, and notably, in T cell receptor complex, MTOC, and anchoring/adherens junction. For MF category, in enzyme/Kinase binding, nucleotide/RNA binding, nucleoside phosphate/ATP binding, ion/anion binding, organic cyclic compound binding, and structural constituent of ribosome.
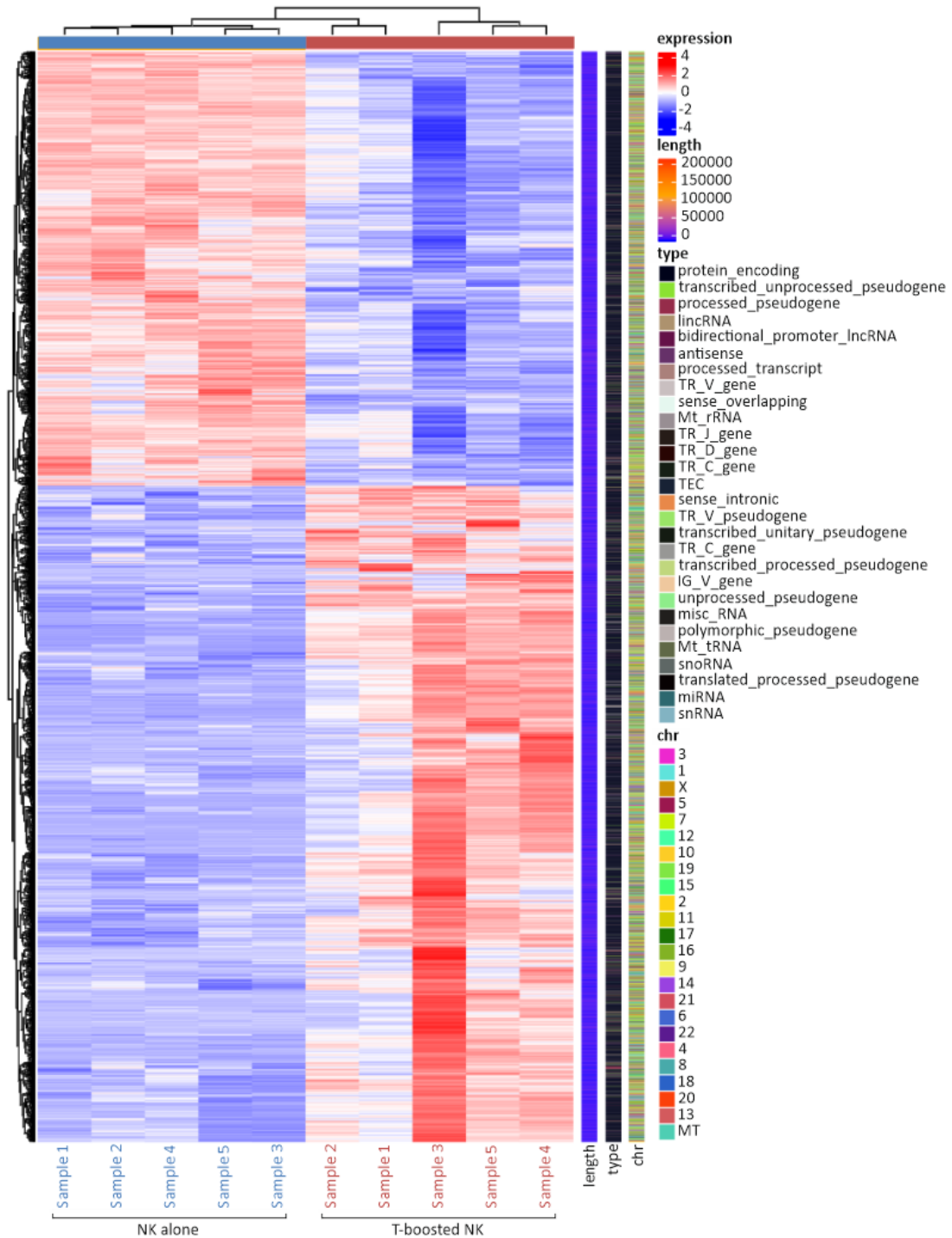
Figure 34. The clustering heat map of DEG expression profiles for T-boosted NK cells. Heat map representing the expression patterns of all the 6130 DEGs across T-boosted NK and NK alone datasets. The data was clustered using the log2(FPKM+1) value. A single column corresponds to the genetic data of a single sample, and a single row corresponds to a single gene. The gene expressions were indicated by the color of each cell, red is upregulated and blue is downregulated in the corresponding sample. The log2(FPKM+1) values (from large to small) were represented as color gradients from red to blue. The references to expression levels, gene length, gene types, and chromosome locations are displayed in different colors and on the figure's right side.
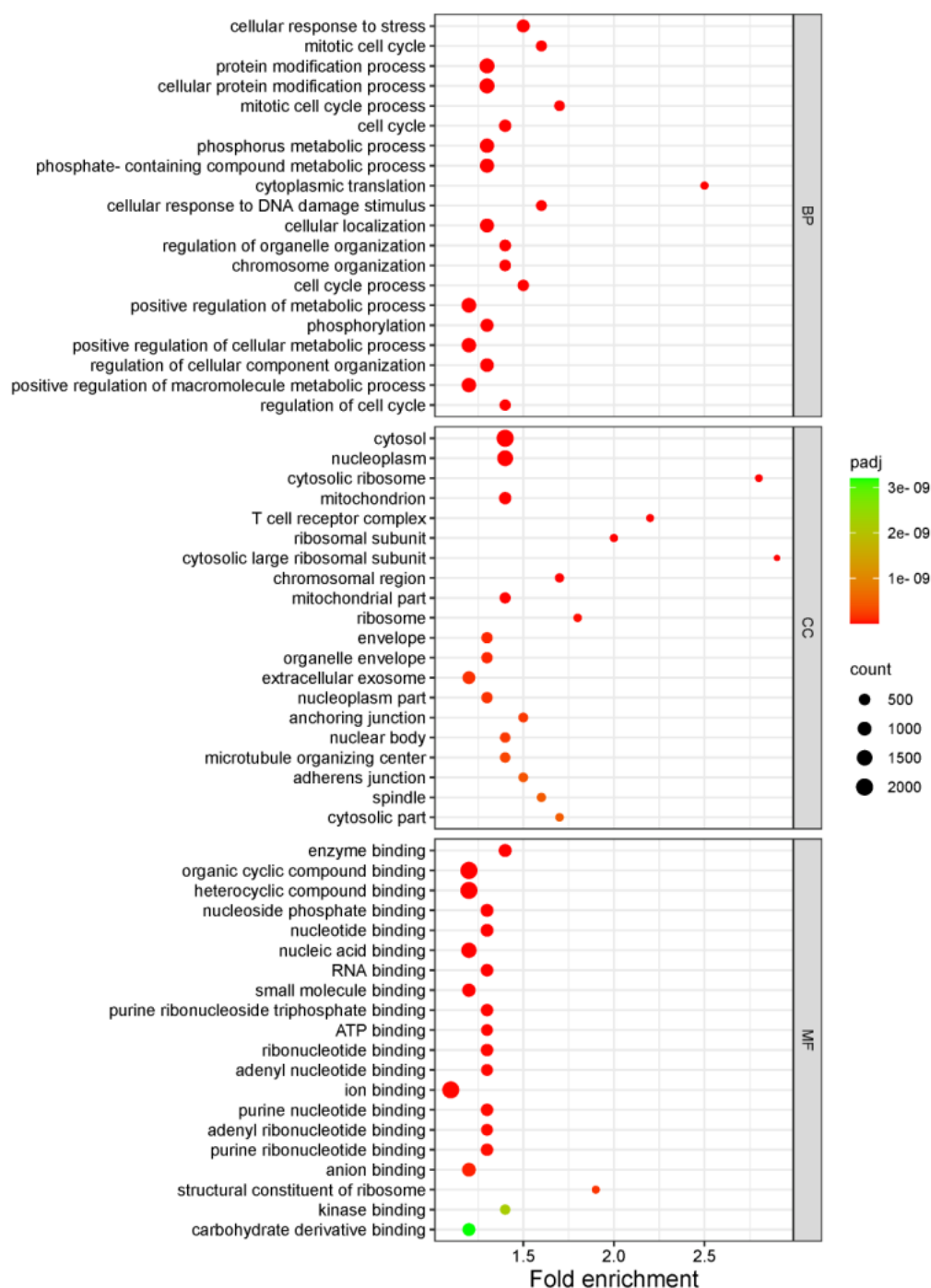
Figure 35. GO terms enrichment analysis of the DEGs. GO enrichment analysis of DEGs was conducted using DAVID. The top 20 significantly enriched (padj<0.05) GO terms in biological process (BP), cellular component (CC), and molecular function (MF) are displayed.

Kyoto Encyclopedia of Genes and Genomes (KEGG) pathway analysis was further investigated. The 20 most significantly enriched pathways (padj<0.05) are presented in Fig. 36. Notably, in Metabolism pathways, there were 510 DEGs enriched in Metabolic pathways while 39 DEGs in Biosynthesis of amino acids and 21 DEGs in Fructose and mannose metabolism. In Genetic information processing pathways, 86 DEGs were enriched in Ribosome, 23 DEGs in DNA replication and 21 DEGs in Base excision repair. In Cellular processing, 64 DEGs were

enriched in Apoptosis, besides DEGs were enriched in Cell cycle/Oocyte meiosis, p53 signaling pathway, and Cellular senescence. DEGs were also enriched in terms under the pathways of Environmental information processing, Organismal systems, and Human diseases.
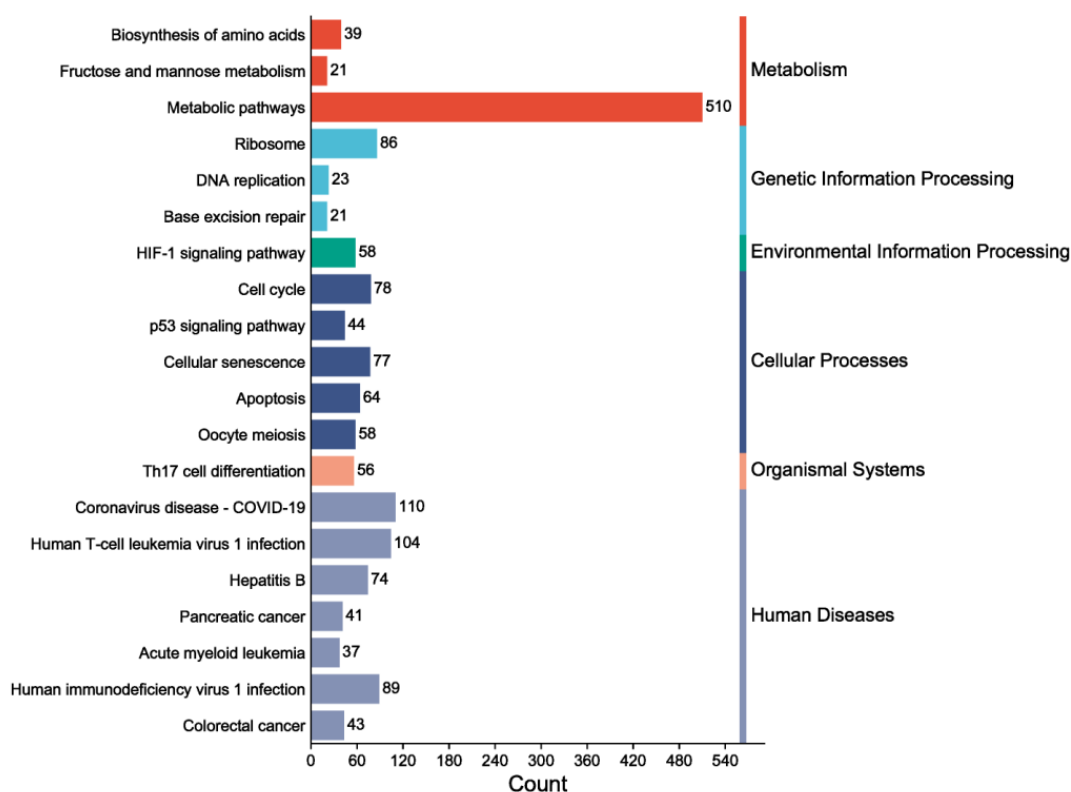
Figure 36. The 20 most enriched pathways in KEGG pathway analysis. KEGG pathway enrichment analysis of DEGs was conducted using DAVID. The top 20 significantly enriched (padj<0.05) pathway terms in Metabolism, Genetic inforamtion processing, Environment information processing, Cellular processes, Organismal systmens, Human diseases categories are displayed.

4.7.2 Cytoskeletal elements in NK cells were altered by the co-culture with T cells

Cytoskeleton play central roles in cell migration [214]. To examine how the co-culture with CD4$^+$ T cells affected cytoskeleton protein expressions on transcriptional level, we performed GO enrichment analysis to explored the DEGs enrichment in cell migration, cytoskeleton, and cell adhesion related terms using DAVID (Fig. 37). In biological processes (BP), gene changes were significantly (padj<0.05) enriched in 11 terms related to organization and regulations of cytoskeleton organization, and 7 terms associated with Leukocyte and T cell migration. In cell component (CC), DEGs were mainly enriched in cytoskeleton including microtubule, actin and kinesin complex, focal adhesion, and cell-cell/cell-substrate junctions. In molecular function (MF), gene changes were enriched in cell adhesion molecule binding, cytoskeletal protein binding, and myosin phosphatase activity.
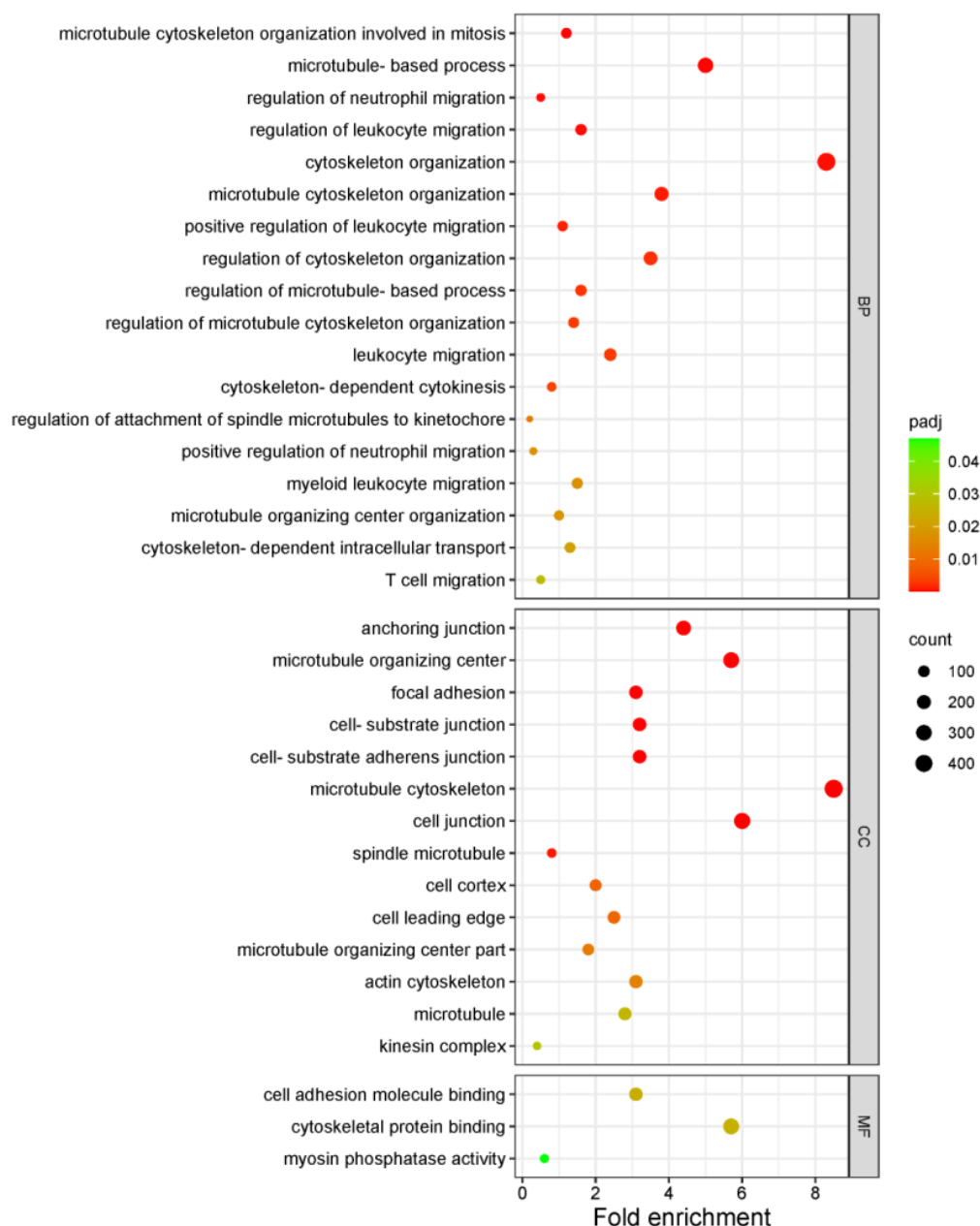
Figure 37. GO enrichment analysis shows DEGs enriched in cytoskeleton and cell migration related terms. The significantly enriched (padj<0.05) cytoskeleton and cell migration related GO terms in biological process (BP), cellular component (CC), and molecular function (MF) are displayed.

The expressions of single genes related to cytoskeleton and cell migration were further examined. As the major component of NK cell skeleton, actin, actin nucleating factors, as well as actin nucleation promoting factors were firstly analyzed. As shown in Fig. 38A, ACTA2 (encoding actin alpha 2), ACTB (encoding actin beta), ACTG1 (encoding actin gamma 1) were expressed in NK cells with FPKM values >1 in at least one experimental group. Among these genes, ACTB and ACTG1 were highly expressed with FPKM values >1000 in at least one group. Notably, the expression of ACTG1 was greatly enhanced (>1 fold). The two main classes of actin nucleating factors, Arp2/3 complex and formins family, were checked (Fig.

38B, C). The Arp2/3 complex is involved in the formation of branched actin networks, while formins are involved in the formation of unbranched actin filaments [215]. In the T-boosted NK cells, 3 Arp2/3 subunit genes were found differently expressed. ARPC5L (encoding actin related protein 2/3 complex subunit 5 like) was significantly upregulated while in contrast, ARPC4 (encoding actin related protein 2/3 complex subunit 4) and ARPC5 (encoding actin related protein 2/3 complex subunit 5) were slightly downregulated (Fig. 38B). Among the formin family, 3 members were found expressed differently in T-boosted NK cells. The expression of INF2 (encoding inverted formin, FH2 and WH2 domain containing) was significantly enhanced. DIAPH1 (encoding diaphanous related formin 1) and FHOD1 (encoding formin homology 2 domain containing 1) were also upregulated but expressed at relatively low level (Fig. 38C). Moreover, expressions of 7 actin nucleation promoting factors and 1 formin binding proteins were revealed altered in T-boosted NK cells (Fig. 38D). For actin nucleation promoting factors, the expressions of WASF2 (encoding WAS protein family member 2), WASHC2A/ WASHC2C/ WASHC3/ WASHC4/ WASHC5 (encoding WASH complex subunit 2A/2C/3/4/5), and BRK1 (encoding BRICK1, SCAR/WAVE actin nucleating complex subunit) were changed. WASF2, WASHC3, and BRK1 were upregulated while WASHC2A, WASHC2C, WASHC4, and WASHC5 were downregulated in T-boosted NK cells. Formin binding protein, FNBP1 (encoding formin binding protein 1) was significantly upregulated. Notably, WASF2, BRK1, and FNBP1 were highly expressed in NK cells.
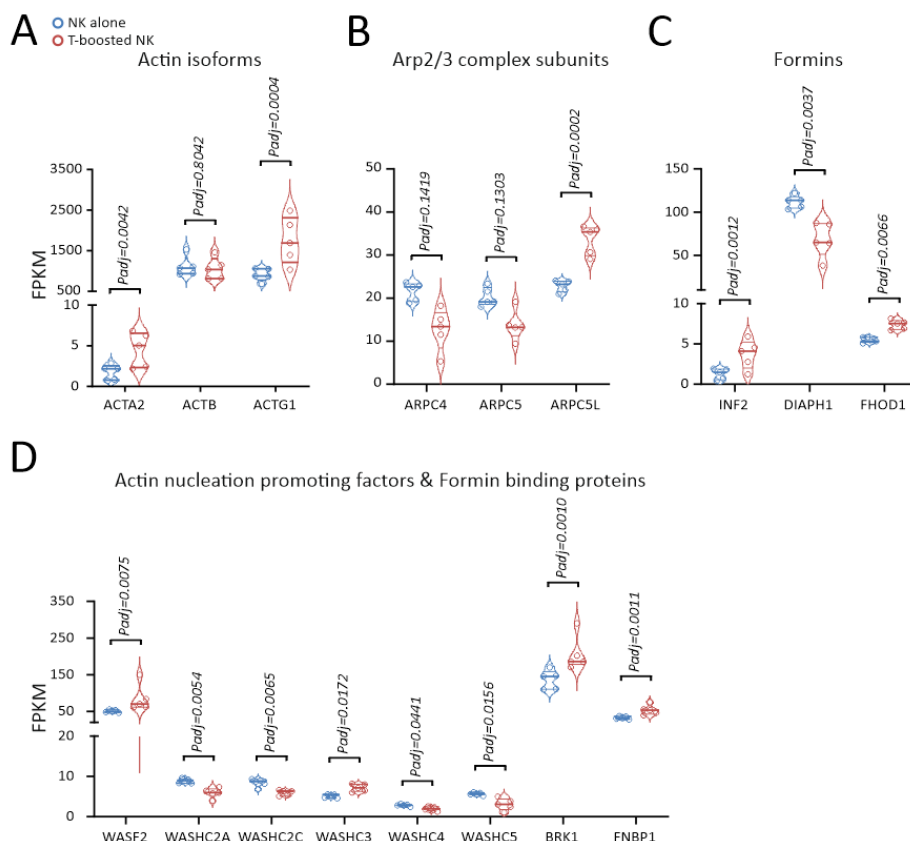
Figure 38. Expressions of actin related genes. Gene expressions are presented as FPKM. Genes with

FPKM values >1 in at least one experimental group are shown. (A) Gene expressions of actin subunits. (B) Gene expressions of Arp2/3 complex subunits. (C) Gene expressions of formins. (D) Gene expressions of actin nucleation promoting factors and formin binding proteins. padj values are indicated in plots.

In our study, we've demonstrated Myosin II and corresponding MLC phosphorylation kinase activities indispensable factors for the T-boosted NK motility (**4.2.3**, Fig. 19). The expressions of Myosin molecules as well as enzymes regulating MLC phosphorylation, MLCK and ROCK, were checked. Myosin subunit genes MYL6B (encoding myosin light chain 6B), and MYO1G (encoding myosin IG) were significantly upregulated while MYL12A (encoding myosin light chain 12A), and MYO1F (encoding myosin IF) were downregulated (Fig. 39A). Surprisingly, the 4 MYLK genes in NK cells, MYLK, MYLK2, MYLK3, and MYLK4, were all found unexpressed or expressed at very low levels (Fig. 39B). The expressions of ROCK genes showed no significant difference, though ROCK1 was expressed at a relative higher level (Fig. 39C).
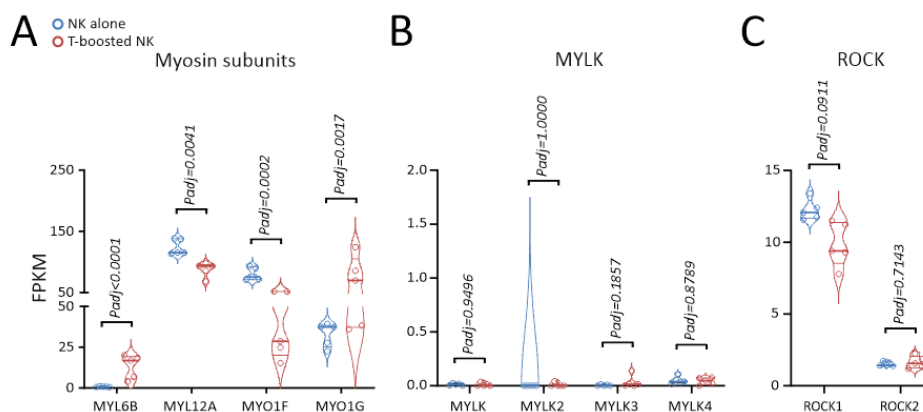
Figure 39. Expressions of myosin subunits, MYLK and ROCK. Gene expressions are presented as FPKM. (A) Gene expressions of Myosin subunits. (B) Gene expressions of MYLK. (C) Gene expressions of ROCK. padj values are indicated in plots.

Another major cytoskeleton component is Microtubule. Since microtubules are cylinder-shaped molecules made up of α and β-tubulin heterodimers. The expressions of tubulin subunits were checked (Fig. 40). TUBA1B (encoding tubulin alpha 1b), TUBA4A (encoding tubulin alpha 4a), and TUBB (encoding tubulin beta class I) were significantly upregulated. Notably, TUBA1B and TUBB were highly expressed (with FPKM value >100 in at least one experimental group) and enhanced by more than 2 folds.
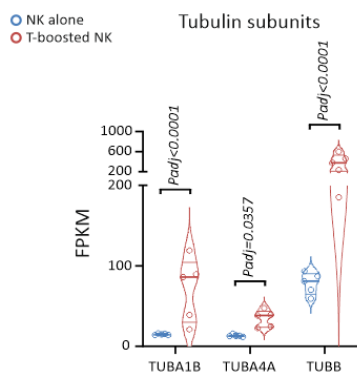
Figure 40. Expressions of tubulin subunits. Gene expressions of tubulin subunits are presented as FPKM. padj values are indicated in plot.

A wide variety of microtubule-associated proteins (MAPs) regulate the dynamics of microtubules. We further defined 38 MAPs genes that expressed (with FPKM values >1 in at least one experimental group) and significantly (padj<0.05) changed in NK cells (Fig. 41A). Compared to NK alone, the T-boosted NK cells presented distinguish MAPs expression patterns. 13 differentially expressed MAPs (FPKM value>10 in least one experimental group) are listed in Fig. 41B. Among the typical microtubule stabilizers, MAP4 (encoding microtubule associated protein 4) and TPX2 (encoding TPX2, microtubule nucleation factor) were upregulated. A typical microtubule destabilizer, STMN1 (encoding stathmin 1) was also upregulated. On the other hand, a serial of Kinesin super family members, including KIF2A, KIF2C, KIF21B, KIF22, KIFC1, and KIFC3 (encoding kinesin family member 2A, 2C, 21B, 22, C1, and C3) were altered in T-boosted NK cells. Among these Kinesin members, only KIF21B was slightly downregulated while others were upregulated. MAPs that interact with Dynein, DCTN2 (encoding dynactin subunit 2) and MAPRE1 (microtubule associated protein RP/EB family member 1) were upregulated. Notably, elongation factor 1 alpha, EEF1A1 and EEF1A2 (encoding eukaryotic translation elongation factor 1 alpha 1 and 2), were significantly upregulated. EEF1A1 was expressed in T-boosted NK cells at very high level (FPKM>4000).
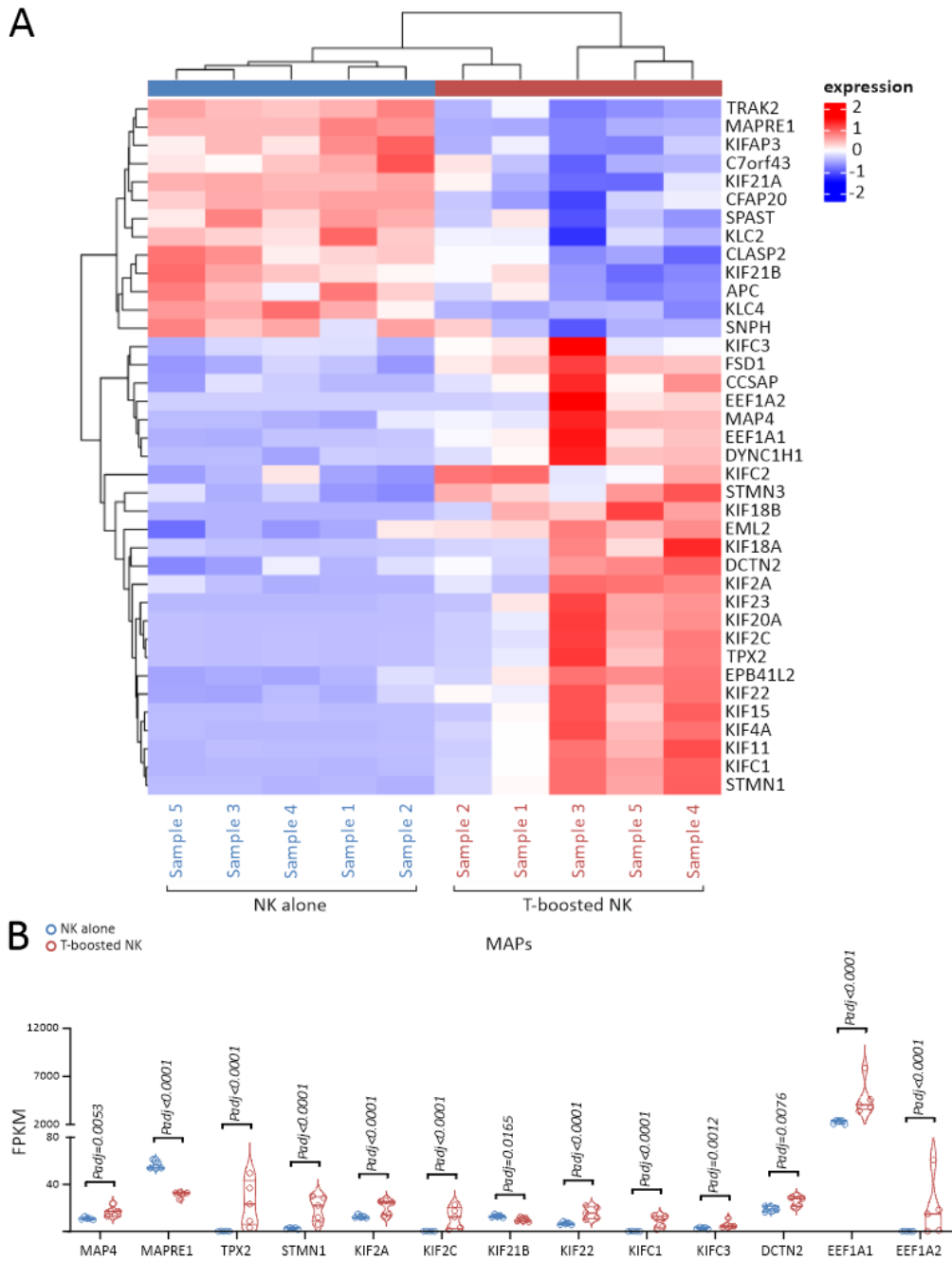
Figure 41. Expressions of MAPs genes were altered in T-boosted NK cells. (A) Heat map representing the expression patterns of 38 differentially expressed MAPs. The data was clustered using the log2(FPKM+1) value. A single column corresponds to the genetic data of a single sample, and a single row corresponds to a single gene. The gene expressions were indicated by the color of each cell, red is upregulated and blue is downregulated in the corresponding sample. The log2(FPKM+1) values (from large to small) were represented as color gradients from red to blue. The references to the gene expression levels are on the figure's right side. (B) Gene expressions of 13 highly expressed MAPs are presented as FPKM. padj values are indicated in plot.

Last but not the least important, the expressions of intermediate filaments in NK cells were checked (Fig. 42). Interestingly, the expression of VIM (encoding vimentin) was highly expressed (FPKM>100) and significantly enhanced by more than 2 folds. In lamin family, LMNB1 (encoding lamin B1) and LMNA (encoding lamin A/C) were upregulated. We also

defined a downregulated expression of KRT10 (encoding keratin 10) in T-boosted NK cells which is considered primarily expressed in epithelial cells.
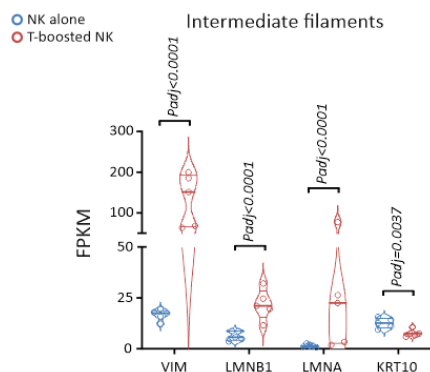
Figure 42. Expressions of intermediate filaments. Gene expressions of intermediate filaments are presented as FPKM. padj values are indicated in plot.

4.7.3 T-boosted NK cells expressed TCR and related molecules

Through the CyTOF data analysis, we found significantly upregulated expressions of CD3 and CD4 molecules on T-boosted NK cells while these molecules were absent on NK alone cells (Fig. 29, Fig. 43A). On mRNA level, the RNAseq data also revealed that a serial of T cell receptor molecules were differentially expressed on T-boosted NK cells (Fig. 43B). CD3D (encoding CD3d molecule) and CD4 (encoding CD4 molecule) mRNA expressions were highly upregulated (FPKM>100) in agreement with the corresponding surface molecule expressions revealed by the CyTOF data. Besides, 7 TCR variable region genes, including TRAV13-1, TRAV12-2, TRAV12-3 (encoding T cell receptor alpha variable 13-1, 12-2, and 12-3), TRBV7-2, TRBV2, TRBV6-1, and TRBV6-2 (encoding T cell receptor beta variable 7-2, 2, 6-1, and 6-2) were significantly upregulated on T-boosted NK samples while these molecules were absolutely absent on NK alone samples (Fig. 43B).
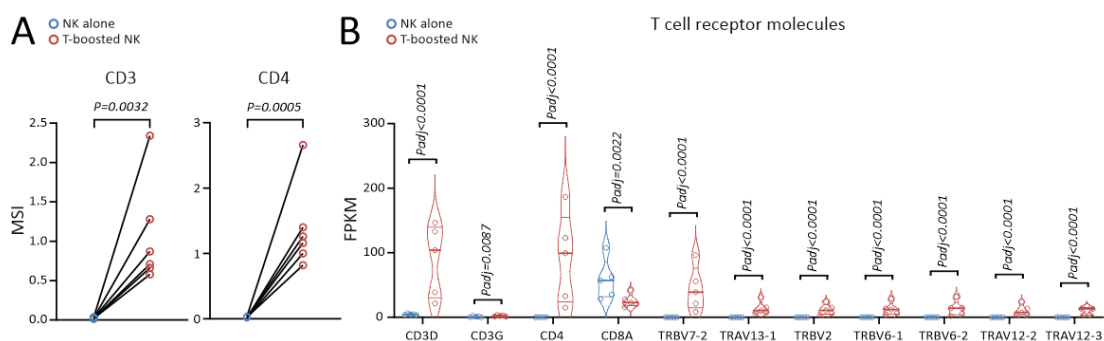
Figure 43. Upregulated TCR molecule expressions on T-boosted NK cells. (A) CyFOF data revealed upregulated CD3 and CD4 expression on the surface of the T-boosted NK cells. Molecule expressions are presented as mean signal intensity (MSI) (B) RNAseq data revealed upregulated mRNA expressions of TCR molecules in T-boosted NK cells. Gene expressions are presented as FPKM. padj values are indicated in plots.

5. Discussion

This study demonstrated that the killing capacity of NK cells can be substantially boosted by co-culture with activated T cells *in-vitro*. The T-boosted NK cells are in an activated state and possess high mobility, enabling them to infiltrate bio-matrix and destroy target cells more efficiently. Expressions of many cytoskeleton molecules associated with cell migration are found modulated in the T-boosted NK cells. CD4$^+$ T cells are demonstrated to achieve this via their IL-2 release and transient but close contacts with NK cells. Evidence shows that CD4$^+$ T cells release IL-2 locally at the NK/CD4 contact site. Signaling of adhesion molecules, LFA-1 and ICAM-1, is also revealed to play roles in this CD4-induced NK activation.

5.1 Significance of the T-boosted NK killing

NK cells and CD4$^+$ T cells are both major "pillars" of the immune system. NK cells play vital roles in innate immunity to be responsible for eliminating tumorigenic and pathogen-infected cells without prior activation while CD4$^+$ T cells are the central players of adaptive immunity that facilitate other immune cell functions via their cytokine secretion based on antigenic activation [216]. Evidence *in-vivo* has been reported that NK cells can be found in the vicinity of the T cell area in the secondary lymph organs and be potentiated by T cell-derived IL-2 [173]. Based on the knowledge up now on, the CD4$^+$ T cell-mediated NK activation in secondary lymph organs is briefed as a sequential model: First, the APCs such as dendritic cells present antigenic peptides to CD4$^+$ T cells which leads to the priming of T cells. The T cell priming then results in T cell activation followed by the IL-2 secretion. The stimulated CD4$^+$ T cells enhance the expression of CD25 to gain a more efficient response to IL-2. The IL-2 derived by T cells directly activates NK functions and leads to the upregulation of high-affinity IL-2 receptors in NK cells which eventually amplifies the IL-2-induced NK activation. According to this model, NK activation due to memory CD4$^+$ T cell-derived endogenous IL-2 upon a secondary challenge is predictable [217]. An enhanced NK cell response by CD4$^+$ T cells has been determined in PBMCs from vaccinated individuals re-exposed to the inactivated rabies virus [218]. However, beside the input, the output and the mediator (IL-2) of the NK/CD4 interaction, the underlying mechanism of how exactly CD4$^+$ T cells potentiate NK killing function is still not fully understood.

We examined the T-boosted NK cells in multiple aspects *in-vitro* which provides evidence to depict the CD4$^+$ T cell-mediated NK activation in more detail. We demonstrated that the T-boosted NK cells perform highly efficient killing capacity against different types of tumor cell lines. By analyzing serial marker expressions in NK cells using flow cytometry-based methods, we further prove that the T-boosted NK cells are at activated state, but the enhanced NK killing

function is closely associated with a drastically promoted NK migration instead of cytotoxic protein expressions. T-boosted NK cells are highly motile and capable of infiltrating ECM like collagen matrix and migrate at higher speed and straightness. IL-2 release and close physical intercellular contact are demonstrated essential for the CD4$^+$ T cells to boost NK function. CD4$^+$ T cells and NK cells form transient but close contact when encountering each other. The endogenous IL-2-containing vesicles in CD4$^+$ T cells are enriched towards the NK/CD4 contact site, indicating IL-2 is locally released at the contact site. Thus, a high local concentration of IL-2 may be formed at the NK/CD4 contact site which enables NK activation without creating a high global IL-2 concentration that induces side effects. Intact adhesion molecule LFA-1/ICAM-1 interaction is required for a complete CD4-induced NK activation, especially in long-term cases.

These results provide us with more detailed insight into the CD4-induced NK activation and the underlying mechanism. By connecting two important players in both innate and adaptive immunity, our work underlies the importance of interaction between CD4 and NK cells, shedding light on developing new strategies to enhance efficacy of NK-based adoptive immunotherapy.

5.2 Greatly enhanced NK migration and killing capacity by T cells

With the name of "killer", NK cells exert their function by eliminating the tumorigenic or pathogen-infected cells. To arrest "criminals", the "policeman", NK cells, have to patrol the host body to locate the targets. An intact migrating ability that enables NK cells to infiltrate tissues and biomatrix from the blood vessels is therefore a critical part of their core functions [19, 21-23]. In this study, we tested the killing efficiency of the T-boosted NK cells against human leukemia cell line K562, human B lymphocyte cell line Raji (ADCC), and human melanoma cell line SK-MEL-5, SK-MEL-28. The T-boosted NK cells showed greatly enhanced killing capacity against these tumor cell lines. We further revealed that the T-boosted NK cells neither recognized target cells more efficiently nor released more cytotoxic protein to destroy the target cells, but migrate much faster and more directly. The enhanced migration and killing capacity of the T-boosted NK cells suggest their potential value in immunotherapy. To overcome tumors, immunotherapy including immune checkpoint inhibitors and Chimeric antigen receptor (CAR) T-cell that enlist and strengthen the power of a patient's immune system to attack tumor cells, has been rapidly developed over the past decade [219]. CAR T therapy utilizes activated T cells and also possesses an IL-2 secretion. Given the fact that T cell-boosted NK cells show potential anti-tumor activities (both liquid and solid tumor cell lines) and optimized migration ability in this study, combining NK cells with CAR T cells may lead to positive outcomes. Tumor cells generate immunosuppressive microenvironment that leads to NK dysfunction in order to escape

from immunity. The NK infiltration and surveillance are found impaired when exposed to the inhibitory molecules released by tumor cells [220]. T-boosted NK cells, with optimized migration ability, may located and infiltrate tumors more efficiently. To test this, further experiments have to be carried out in future. For instance, to test the killing efficiency of the T-boosted NK cells against tumor cell spheroid *in-vitro*. The anti-tumor efficiency of T-boosted NK cells can be further examined in in-vivo experiments in animal models.

Our RNAseq data reveals expression changes on many cell migration-related genes and provides hints about the key factors that are responsible for the enhanced NK migration due to T cells. Go enrichment analysis revealed DEG enrichment in a serial of terms associated with actin, myosin, microtubule, and intermediate filaments. For actins, the RNAseq data revealed highly upregulated expressions of actin subunits ACTA2 and ACTG1, as well as expressions of actin nucleating factors and nucleation promoting factors in T-boosted NK cells. These changes could lead to an acceleration in generation rate of actin and therefore influence the consequent migration. For microtubules, Go enrichment analysis shows enrichment in microtubule organizing center in CC category, and gene expressions of tubulin subunits, TUBA1B, TUBA4A, and TUBB were significantly upregulated. Besides, 38 MAP genes including microtubule stabilizers/destabilizers, motor proteins, and elongation factors were found differentially expressed in T-boosted NK cells. These results may indicate a promoted microtubule dynamic. Our RNAseq data also identified upregulation of IFs including vimentin, lamin B1, and lamin A/C genes. The major function of vimentin is to preserve the structural integrity of cells, stabilize interactions within the cytoskeleton, and provide resistance to prevent cells from damage [221]. On the other hand, lamin A/C is primarily responsible for the mechanical stiffness of nuclei while lamin B1 functions to maintain the integrity of nuclear instead of stiffness [222]. The upregulated vimentin, lamin A/C, and lamin B1 may result in better cell resistance and protect the nuclear from damage which helps the NK cells to survive during the boosted migration. Besides, according to KEGG pathway analysis and GO enrichment analysis, DEGs were enriched in many metabolism-related terms. Moreover, GO enrichment analysis also shows DEGs were highly enriched in terms related to ribosome functions. Ribosomes are in responsible for protein synthesis[223]. Since the T-boosted NK cells acquire high motility, they naturally need more energy and cytoskeleton dynamic to fuel their movement. A promoted metabolism and ribosome activity is therefore predictable.

However, the mRNA expression is not necessarily correlated to the protein expression level and cell behavior outcomes [224]. For example, though we demonstrated in our research that Myosin II and corresponding MLCK activities are indispensable factors for the T-boosted NK motility (4.2.3, Fig. 19), RNAseq data revealed upregulation of some Myosin subunit genes but no changes in MYLK and ROCK expressions. In further, the interested gene expression results might be further tested on protein level using real-time PCR. Whether T-boosted NK cells

generate larger contractile force during their migration can be measured using traction force microscopy (TFM), micropillar arrays, or atomic force microscopy (AFM). Oxygen consumption rate (OCR) and extracellular acidification rate (ECAR) of the NK cells could also be measured using metabolic analyzers such as Seahorse XF Analyzer. OCR reflects mitochondrial respiration and ATP production, while ECAR indicates glycolytic activity [225]. Changes in OCR and ECAR can provide insights into the metabolic state of the T-boosted cells. We may further examine the cell migration outcomes using computational models with the inputs including more actin subunits, upregulated nucleation factors/nucleation promoting factors, altered microtubules/MAPs, enhanced IFs, and enhanced energy metabolism, to test whether these factors finally result in enhanced NK migration.

5.3 Locally released IL-2

In this study, we demonstrated that IL-2 and NK/CD4 physical contact play pivotal roles for the CD4-boosed NK killing. On one hand, blockage of IL-2 receptor function completely abolishes the T-boosted NK killing indicating IL-2 is indispensable. On the other hand, transwell experiments and NK cells cultured in CD4$^+$ T cell culture supernatant revealed that IL-2 alone is not sufficient for CD4$^+$ T cells to boost NK killing which highlights the necessity of the physical contact between NK and CD4$^+$ T cells. Combining the IL-2 and the physical contact, CD4$^+$ T cells can boost NK killing within 24 hours at very low global concentration of IL-2 in the culture supernatant (<0.5ng/ml). Presenting NK cells with global IL-2 concentration of 0.5 ng/ml for one day cannot elevate NK killing at all. These data suggest the hypothesis that IL-2 is locally released at the NK/CD4 contact site, where a high concentration of IL-2 may be generated. Evidence that supports this hypothesis was revealed with ICC staining, IL-2-containing vesicles in CD4$^+$ T cells were found accumulated in the vicinity of the NK/CD4 contact site.

IL-2 has been long approved for the treatment of tumors [226]. However, high dose of IL-2 (600-720 IU/ml) will induce many side effects in vivo including vascular leak syndrome (VLS), which is observed in cancer patients treated by IL-2 as an immunotherapeutic reagent to stimulate effector function of T cells and NK cells [227]. We also tried to stimulate NK cells using IL-2 with 50 ng/ml, a concentration reached only in cytokine storm in vivo [228], for 3 days. Two-thirds of cases (4 out of 6) reached the level of T-boosted NK killing. In our study, we demonstrated that the NK/CD4 physical contact can provide an optimal venue to activate NK cells at a high dose of local-secreted IL-2 without a high global IL-2 affecting the other cells in vicinity. However, the local concentration of IL-2 at the contact site, presumably exceeding 50 ng/ml, still needs to be determined.

In this study, the expression of IL-2 receptor components on NK cells were examined using

CyTOF and RNAseq. Our data shows that, upon co-culture with CD4^{+} T cells, the IL-2Rα (CD25) and the IL-2Rγ (CD132) expressions on NK cells were significantly up-regulated while the IL-2Rβ (CD122) expression was down-regulated. On transcriptional level, however, all three domains were significantly up-regulated. CD25, CD122, and CD132 are the three identified distinct chains of IL-2 receptor. CD132 is also known as the common γ chain (γc) for it's being shared by serial cytokine receptors including IL-2, IL-15, IL-7, IL-21, IL-9, and IL-4 [166]. CD122, on the other hand, is shared by IL-2 and IL-15 receptors. Only CD122 and CD132 are involved in the signal transduction due to their large intracellular domains. There are two functional IL-2 receptor forms have been identified, the dimeric low-affinity receptor comprised of only CD122 and CD132, and the trimeric high-affinity receptor involves all three domains [229]. On NK cells, the low-affinity IL-2 receptor is revealed at a high level while only a low level of CD25 is identified [230]. To form a high-affinity receptor, IL-2 is believed to bind CD25 initially, CD122 and CD132 are then recruited subsequently and finally come into a stable quaternary structure. After a rapid internalization of the final quaternary structure, CD122, CD132 as well as IL-2 are degraded promptly in the lysosome while CD25 is recycled back to the cell surface [231]. With this model, the up-regulated CD25 expression in T-boosted NK cells indicates the presence of high-affinity IL-2 receptor form. The down-regulation of surface CD122 and the up-regulation of CD122 mRNA may be due to the rapid internalization of the high-affinity receptor. In our study, we utilized Basiliximab to competes with IL-2 to bind to CD25 in order to neutralize IL-2 receptor function. However, we can't block the IL-2 receptor on NK cells specifically with the antibody. IL-2 receptor on CD4^{+} T cells may also play roles in the NK/CD4 interaction. To further confirm on which side (NK or CD4) the IL-2 receptor is responsible for the T-boosted NK function, we plan to use siRNA to silence IL-2 receptor expression in cells. Considering the primary human NK cells are technically difficult to be transfected, transfecting CD4^{+} T cells with IL-2 receptor siRNA may provide indirect evidence to address this issue.

Our results also implicate a potential directional IL-2 release of the CD4^{+} T cells. CD4^{+} T cells are known to release cytokines in a multidirectional manner. IL-4, TNF, and CCL3 are found secreted through this multidirectional pathway which seems to tend to influence bystander cells by the molecule gradients [232]. However, it has been observed in both in vivo and in vitro immunocytochemistry staining that some critical cytokines accumulate towards the IS site inside CD4^{+} T cells stimulated by APCs. Evidence suggests that activated CD4^{+} T cells release cytokines at the synapse which explain the target specificity of cytokine secretion [233-236]. Cytokines such as IL-2, IFN-γ, and IL-10 are found delivered via this antigen-specific pathway. How the CD4^{+} T helper cells deliver their cytokine secretion specifically to the effector cells without affecting bystander cells in the surrounding environment is not so clear. The NK/CD4 interaction is different from conventional IS. Whether CD4^{+} T cells deliver IL-2 to NK cells in

a similar pathway is left to be further explored.

Imaging technology with high resolution like Total internal reflection fluorescence microscopy (TIRFM) or Scanning electron microscope (SEM) may provide better insight into the NK/CD4 contact site and the local IL-2 secretion.

5.4 The contacts between NK and CD4 cells are not conventional IS

In this study, we found that the NK/CD4 contact is quite different from a conventional IS between NK or T cells with their target cells/APCs in the following aspects: 1) Duration. The former is very transient lasting only for tens of seconds to minutes, whereas the latter is stable for tens of minutes to hours or even days [237, 238]. 2) Morphology. Upon recognition of target cells, NK or T cells will stop migrating and spread symmetrically to form a stable synapse [239, 240]. When NK and T cells come into contact, neither formed symmetric shape and they tend to keep moving. Especially T cells, they were polarized and asymmetrical in shape and formed lamellipodium at the leading edge, and trailing uropod in the rear, which are typical structures for migration [241]. Moreover, NK/CD4 contact is asymmetric and dynamic, starting with the engagement at the T cell leading edge and ending with the interaction between the NK cell and the T cell uropod. This interaction mode is in good agreement with the highly dynamic interactions reported happened between T cells and APCs or tissue stroma [241]. The short-lived interaction between T cells and APCs is named by Michael L. Dustin as "*Kinapses*" for its characterization that lacks stability and polarity [241]. The differences between the NK/CD4 interaction and conventional IS suggest that the molecular pathways involved in establishing physical contact between NK and CD4$^+$ T cells are very likely distinct from the ones for IS formation.

During establishment of the IS between NK or T cells with their target cells, MTOC will is actively reorientated towards the contact site from the cell rear [242]. MTOC is associated with Golgi complex which release several secreted proteins including IL-2 [243]. And in migrating T cells, MTOC is located in the uropod [141]. We found in our study that CD4$^+$ T cells tended to form "*Kinapses*"-like interaction with NK cells using their uropod and the IL-2-containing vesicles in CD4$^+$ T cells were accumulated in the vicinity to the NK/CD4 contact site. We can therefore hypothesize that during the NK/CD4 contact, MTOC in CD4$^+$ T cells is left in the uropod directly in the vicinity of NK cells along with IL-2-containing vesicles adjacent to MTOC. To test this, we may fluorescently label the microtubules and IL-2 in CD4$^+$ T cells by transfection to locate the MTOC and the IL-2-containing vesicles.

5.5 What does the marker profiling of T-boosted NK cells tell us?

Firstly, the subsets of the T-boosted NK cells revealed by our CyTOF data indicate that the co-

culture with CD4$^+$ T cells polarizes NK cells into activated state. To attain their maximum functional status, NK cells must undergo a process of maturation [244]. In human, the presence of CD56 indicates the final step that NK cell precursors (NKPs) differentiate into NK cells. Based on the expression level of CD56, human NK cell maturation is categorized into CD56^{bright} stage and CD56^{dim} stage. CD56^{bright} NK cells are considered to be immature, and with the acquisition of CD16, they can finally develop into CD56^{dim} NK cells [245]. The expression of CD57 defines the final maturation of CD56^{dim} NK cells with the optimal cytolytic activity, higher sensitivity to CD16 and natural cytotoxicity receptors (NCRs) signal, and suppressed sensitivity to cytokines [208, 246]. By interacting with M1 macrophages, CD56^{dim} NK cells can be polarized into fully activated stage characterized by the acquisition of CCR7, a potent secretion of IFN-γ, and high expression of CD69 as well as CD25 (IL-2Rα) [204]. Although our data shows that co-culture with CD4$^+$ T cells doesn't affect the expressions of CD56, CD16, and CD57 on NK cells, expressions of CCR7, CD69, and CD25 (IL-2Rα) were significantly upregulated which suggest that the T-boosted NK cells are polarized into an activated state.

It's also interesting but confusing that the CyTOF data shows expressions of CD3 and CD4 molecule on the surface of the T-boosted NK cells. The RNAseq data, on the other hand, shows a high transcriptional level (RPKM>100) of CD3 delta subunit of T-cell receptor complex (CD3D) as well as CD4 molecule in the T-boosted NK cells. The CyTOF data of the T-boosted NK cells were obtained from NK+T cell mixture and the NK cells for RNAseq were isolated positively from NK+T co-culture using CD56 microbeads. Yet we can't rule out the possibility that these signals were from CD4$^+$ cell contaminations due to unperfect gating or purification, but were can't exclude other possible sources of the CD3/CD4 molecules in T-boosted NK cells such as NKT cells neither. Unlike traditionally defined CD56$^+$/CD3$^-$ NK cells [203], invariant NKT (iNKT) cells and NKT-like cells are some T cell subsets that share the characteristics from both NK and T cells. iNKT cells are a unique subpopulation of T lymphocytes that featured by the simultaneous expressions of serial TCR variable region genes as well as the NK cell marker NK1·1 (NKR-P1C) [247]. The majority of iNKT cells express a semi-invariant TCR that is comprised of an identical α-chain (Vα24-Jα18 in human, Vα14-Jα18 in mouse) and a restricted number of β-chains (Vβ11 in human, Vβ8, Vβ7, Vβ6 or Vβ2 in mouse) [248, 249]. NKT-like cells, on the other hand, are conventional T cells that express NK-associated receptors (NKRs) such as CD56, CD16, CD57, CD161, NKG2D, NKG2A, NKp46, or CD94 [250]. Once upon activation via TCR recognition, iNKT cells proliferate, produce cytokines and regulate immune responses against pathogens [251] while NKT-like cells can mediate cytotoxicity and cytokine production [252]. Given the characteristics of the NKT cells, if the CD3/CD4 signal were really from NK cells, it's still hard to tell whether the current data indicates the presence of NK cells bearing CD3/CD4 molecules or T cells bearing NK markers. Since our RNAseq data shows no expression of the typical semi-invariant TCR molecules for iNKT cells in the T-

boosted NK cells, the CD3$^+$/CD4$^+$/CD56$^+$ are more likely to be the NKT-like cells. However, according to the available literature, it's also possible that there were NK subsets upregulated CD3 and CD4 molecule expressions on their surface after co-culture with activated T cells. CD4$^+$ NK cells have been reported in humans and enriched in lymphoid tissue at a substantially higher level than that in peripheral blood. In-vitro experiments showed that IL-2/PHA-induced CD4$^+$/CD3$^-$/CD56$^+$ NK cells can mediate effective cytotoxicity, enhance cytokine production upon CD4 ligation, and migrate in response to IL-16 [253]. CD3 gamma, delta, and epsilon subunits were also found in the cytoplasm of the cloned human fetal liver NK cells. These subunits can form CD3-epsilon/gamma and CD3-epsilon/delta dimers in the NK cytoplasm but can't be transported to the cell surface [252]. Therefore, to make further insight into the elusive CD3$^+$/CD4$^+$/CD56$^+$ cell population found in our study, their expressions of NKT-specific surface markers and their cytokine profiles upon activation should be checked. The detailed identification of these cells may reveal new NK subpopulations or provide new sight into the source and functions of NKT cells. Moreover, whether the CD3/CD4/CD56 molecule-expressing cells are associated with the boosted NK cytotoxicity and migration is worth to be studied. In future study, we may upregulate/downregulate the expression of CD3/CD4 molecules in NK cells to investigate the impact on NK cytotoxicity and motility.

5.6 How do adhesion molecules participate in the NK/CD4 interaction?

For the formation of both the IS and the "*Kinapses*", LFA-1 is indispensable [241]. LFA-1 is an adhesion molecule abundantly expressed in NK and T cells, which binds to ICAM-1 or extracellular matrix proteins such as fibronectin and collagen [254, 255]. A blockage or deficiency of LFA-1 diminishes expression of cytotoxic proteins and killing capacity of NK cells [256]. Interaction between LFA-1 and ICAM-1 is required to seal the IS, preventing leakage of cytotoxic proteins to jeopardize irrelevant neighboring cells [257]. LFA-1 could serve a similar role concerning NK/CD4 contacts to concentrate IL-2 at the contact site. Notably, blockade of LFA-1 by its neutralizing antibody during 24-hour NK/CD4-co-culture does not impede T-boosted NK killing machinery, but rather affects target recognition. Alteration in expression of inhibitory and/or activating receptors on NK cells could contribute to this deficiency in target recognition. Interestingly, if LFA-1 is blocked for three days, neither IL-2 nor CD4$^+$ T cells could elevate NK killing anymore, suggesting that LFA-1 signaling is upstream of IL-2 and act as a switch to govern IL-2-mediated NK activation.

5.7 Summary

In this study, we aimed to investigate whether and how T cells from the adaptive immune system influence the killing efficiency of NK cells from the innate immune system. Using

human primary T cells and NK cells, we conducted real-time killing assay, live cell imaging, FACS staining, ICC staining, CyTOF, and RNAseq to examine the T cell-induced NK function changes and the underlying mechanism. Our data shows that an *in-vitro* co-culture with activated T cells, both CD4$^+$ and CD8$^+$, can result in a boosted killing efficiency of homologues NK cells against different types of tumor cell lines. This T-induced NK activation was found not attributed to altered expressions of cytolytic proteins (perforin and granzymes) or the degranulation of lytic granules. Instead, the co-culture with T cells greatly enhanced the speed and persistence of NK cell migration as well as NK cell infiltrating capability into 3D collagen matrices. The T-induced NK activation can be achieved in 24-hour-co-culture and lasts for several days. By transwell experiment, I identified physical contact between T cells and NK cells as an indispensable factor for the T-induced NK activation. Blockade of IL-2 receptor using neutralizing antibody abolished the T-boosted NK killing. Nether conditional medium from activated T cells nor addition of IL-2 could resemble the extent of the T-boosted NK killing, indicating that local IL-2 plays a critical role in this regard. Moreover, the ICAM-1/LFA-1 interaction is also involved in boosting NK cell functions by T cells. Our CyTOF data reveals distinct subsets in the T-boosted NK cells and RNAseq data indicates the boosted NK migration is likely related to cytoskeleton molecules and cell metabolism. These results provide us valuable insights into the T-NK cell interaction. By connecting important players from both innate and adaptive immunity, our work underlies the significance of interaction between T and NK cells, shedding light on developing new strategies to enhance efficacy of NK-based adoptive immunotherapy.

It is important to acknowledge the limitations of our study. We used neutralizing antibodies to examine the IL-2 receptor and IFA-1 signaling in the T-induced NK activation. However, both T cells and NK cells express IL-2 receptor and IFA-1 molecules. To further clarify on which side (NK or T) the IL-2 receptor or the LFA-1 is responsible for the T-induced NK activation, siRNA silencing of these molecules may help to address the issue. However, human NK cells are technically difficult to be transfected. Transfecting T cells with corresponding siRNA may provide indirect evidence; Though we explored the mechanism of how T cells boost NK killing and examines the NK cell changes using RNAseq, the data was not solid enough to support any conclusion, and yet we can't establish clear links between the gene expression changes with the NK function promotion. Further analysis focus on candidate molecules revealed by RNAseq data can build upon the current study's findings; Additionally, we only examined the T-NK interaction *in vitro*, we therefore lack evidence to conclude that they perform the same *in vivo*. Future research such as *in vivo* experiments in mouse models is recommended; A detailed test of the CD8-boosted NK killing may further complete our understanding of the T-NK interaction and advance the immunotherapy field.

6. References

1. Nicholson LB. **The immune system**. *Essays Biochem* 2016; 60(3):275-301.

2. Delves PJ, Roitt IM. **The immune system. First of two parts**. *N Engl J Med* 2000; 343(1):37-49.

3. Fearon DT, Locksley RM. **The instructive role of innate immunity in the acquired immune response**. *Science* 1996; 272(5258):50-53.

4. Beutler B, Hoebe K, Du X, Ulevitch RJ. **How we detect microbes and respond to them: the Toll-like receptors and their transducers**. *J Leukoc Biol* 2003; 74(4):479-485.

5. Chaplin DD. **1. Overview of the immune response**. *J Allergy Clin Immunol* 2003; 111(2 Suppl):S442-459.

6. Huston DP. **The biology of the immune system**. *JAMA* 1997; 278(22):1804-1814.

7. Bernardini G, Gismondi A, Santoni A. **Chemokines and NK cells: regulators of development, trafficking and functions**. *Immunol Lett* 2012; 145(1-2):39-46.

8. Kourilsky P, Truffa-Bachi P. **Cytokine fields and the polarization of the immune response**. *Trends Immunol* 2001; 22(9):502-509.

9. Oberholzer A, Oberholzer C, Moldawer LL. **Cytokine signaling--regulation of the immune response in normal and critically ill states**. *Crit Care Med* 2000; 28(4 Suppl):N3-12.

10. Sjoberg AP, Trouw LA, Blom AM. **Complement activation and inhibition: a delicate balance**. *Trends Immunol* 2009; 30(2):83-90.

11. Weissman IL, Cooper MD. **How the immune system develops**. *Sci Am* 1993; 269(3):64-71.

12. Kruisbeek AM. **Introduction: regulation of T cell development by the thymic microenvironment**. *Semin Immunol* 1999; 11(1):1-2.

13. Brodsky FM, Guagliardi LE. **The cell biology of antigen processing and presentation**. *Annu Rev Immunol* 1991; 9:707-744.

14. Davis MM. **T cell receptor gene diversity and selection**. *Annu Rev Biochem* 1990; 59:475-496.

15. Germain RN, Margulies DH. **The biochemistry and cell biology of antigen processing and presentation**. *Annu Rev Immunol* 1993; 11:403-450.

16. Luckheeram RV, Zhou R, Verma AD, Xia B. **CD4(+)T cells: differentiation and functions**. *Clin Dev Immunol* 2012; 2012:925135.

17. Zhang N, Bevan MJ. **CD8(+) T cells: foot soldiers of the immune system**. *Immunity* 2011; 35(2):161-168.

18. Stabile H, Fionda C, Gismondi A, Santoni A. **Role of Distinct Natural Killer Cell Subsets in Anticancer Response**. *Front Immunol* 2017; 8:293.

19. Trinchieri G. **Biology of natural killer cells**. *Adv Immunol* 1989; 47:187-376.

20. Biron CA. **Activation and function of natural killer cell responses during viral infections**. *Curr Opin Immunol* 1997; 9(1):24-34.

21. Fogler WE, Volker K, McCormick KL, Watanabe M, Ortaldo JR, Wiltrout RH. **NK cell infiltration into lung, liver, and subcutaneous B16 melanoma is mediated by VCAM-1/VLA-4 interaction**. *J Immunol* 1996; 156(12):4707-4714.

22. Castriconi R, Carrega P, Dondero A, Bellora F, Casu B, Regis S, et al. **Molecular Mechanisms Directing Migration and Retention of Natural Killer Cells in Human Tissues**. *Front Immunol* 2018; 9:2324.

23. Garrod KR, Wei SH, Parker I, Cahalan MD. **Natural killer cells actively patrol peripheral lymph nodes forming stable conjugates to eliminate MHC-mismatched targets**. *Proc Natl Acad Sci U S A* 2007; 104(29):12081-12086.

24. Moretta L, Moretta A. **Unravelling natural killer cell function: triggering and inhibitory human NK receptors**. *EMBO J* 2004; 23(2):255-259.

25. Stinchcombe JC, Griffiths GM. **Secretory mechanisms in cell-mediated cytotoxicity**. *Annu Rev Cell Dev Biol* 2007; 23:495-517.

26. Krzewski K, Coligan JE. **Human NK cell lytic granules and regulation of their exocytosis**. *Front Immunol* 2012; 3:335.

27. Ljunggren HG, Karre K. **In search of the 'missing self': MHC molecules and NK cell recognition**. *Immunol Today* 1990; 11(7):237-244.

28. Cruz-Munoz ME, Valenzuela-Vazquez L, Sanchez-Herrera J, Santa-Olalla Tapia J. **From the "missing self" hypothesis to adaptive NK cells: Insights of NK cell-mediated effector functions in immune surveillance**. *J Leukoc Biol* 2019; 105(5):955-971.

29. Lanier LL. **NK cell recognition**. *Annu Rev Immunol* 2005; 23:225-274.

30. Lanier LL, Corliss B, Phillips JH. **Arousal and inhibition of human NK cells**. *Immunol Rev* 1997; 155:145-154.

31. Cerwenka A, Baron JL, Lanier LL. **Ectopic expression of retinoic acid early inducible-1 gene (RAE-1) permits natural killer cell-mediated rejection of a MHC class I-bearing tumor in vivo**. *Proc Natl Acad Sci U S A* 2001; 98(20):11521-11526.

32. Diefenbach A, Jensen ER, Jamieson AM, Raulet DH. **Rae1 and H60 ligands of the NKG2D receptor stimulate tumour immunity**. *Nature* 2001; 413(6852):165-171.

33. Biassoni R, Cantoni C, Pende D, Sivori S, Parolini S, Vitale M, et al. **Human natural killer cell receptors and co-receptors**. *Immunol Rev* 2001; 181:203-214.

34. Chiesa S, Tomasello E, Vivier E, Vely F. **Coordination of activating and inhibitory signals in natural killer cells**. *Mol Immunol* 2005; 42(4):477-484.

35. Watzl C, Urlaub D. **Molecular mechanisms of natural killer cell regulation**. *Front Biosci (Landmark Ed)* 2012; 17(4):1418-1432.

36. Anderson P, Caligiuri M, O'Brien C, Manley T, Ritz J, Schlossman SF. **Fc gamma receptor type III (CD16) is included in the zeta NK receptor complex expressed by human natural killer cells**. *Proc Natl Acad Sci U S A* 1990; 87(6):2274-2278.

37. Arneson LN, Leibson PJ. **Signaling in natural immunity: Natural killer cells**. In: *NeuroImmune Biology*: Elsevier; 2005. pp. 151-166.

38. Bottino C, Castriconi R, Moretta L, Moretta A. **Cellular ligands of activating NK receptors**. *Trends Immunol* 2005; 26(4):221-226.

39. Lanier LL, Chang C, Phillips JH. **Human NKR-P1A. A disulfide-linked homodimer of the C-type lectin superfamily expressed by a subset of NK and T lymphocytes**. *J Immunol* 1994; 153(6):2417-2428.

40. Bryceson YT, March ME, Ljunggren HG, Long EO. **Activation, coactivation, and costimulation of resting human natural killer cells**. *Immunol Rev* 2006; 214:73-91.

41. Almeida CR, Davis DM. **Segregation of HLA-C from ICAM-1 at NK cell immune synapses is controlled by its cell surface density**. *J Immunol* 2006; 177(10):6904-6910.

42. Endt J, McCann FE, Almeida CR, Urlaub D, Leung R, Pende D, et al. **Inhibitory receptor signals suppress ligation-induced recruitment of NKG2D to GM1-rich membrane domains at the human NK cell immune synapse**. *J Immunol* 2007; 178(9):5606-5611.

43. Watzl C, Stebbins CC, Long EO. **NK cell inhibitory receptors prevent tyrosine phosphorylation of the activation receptor 2B4 (CD244)**. *J Immunol* 2000; 165(7):3545-3548.

44. Masilamani M, Nguyen C, Kabat J, Borrego F, Coligan JE. **CD94/NKG2A inhibits NK cell activation by disrupting the actin network at the immunological synapse**. *J Immunol* 2006; 177(6):3590-3596.

45. Bryceson YT, Ljunggren HG, Long EO. **Minimal requirement for induction of natural cytotoxicity and intersection of activation signals by inhibitory receptors**. *Blood* 2009; 114(13):2657-2666.

46. Vyas YM, Mehta KM, Morgan M, Maniar H, Butros L, Jung S, et al. **Spatial organization of signal transduction molecules in the NK cell immune synapses during MHC class I-regulated noncytolytic and cytolytic interactions**. *J Immunol* 2001; 167(8):4358-4367.

47. Roda-Navarro P, Vales-Gomez M, Chisholm SE, Reyburn HT. **Transfer of NKG2D and MICB at the cytotoxic NK cell immune synapse correlates with a reduction in NK cell cytotoxic function**. *Proc Natl Acad Sci U S A* 2006; 103(30):11258-11263.

48. Orange JS, Harris KE, Andzelm MM, Valter MM, Geha RS, Strominger JL. **The mature activating natural killer cell immunologic synapse is formed in distinct stages**. *Proc Natl Acad Sci U S A* 2003; 100(24):14151-14156.

49. Liu D, Bryceson YT, Meckel T, Vasiliver-Shamis G, Dustin ML, Long EO. **Integrin-dependent organization and bidirectional vesicular traffic at cytotoxic immune synapses**.

Immunity 2009; 31(1):99-109.

50. Chen S, Kawashima H, Lowe JB, Lanier LL, Fukuda M. **Suppression of tumor formation in lymph nodes by L-selectin-mediated natural killer cell recruitment**. *J Exp Med* 2005; 202(12):1679-1689.

51. Warren HS, Altin JG, Waldron JC, Kinnear BF, Parish CR. **A carbohydrate structure associated with CD15 (Lewis x) on myeloid cells is a novel ligand for human CD2**. *J Immunol* 1996; 156(8):2866-2873.

52. Comerci CJ, Mace EM, Banerjee PP, Orange JS. **CD2 promotes human natural killer cell membrane nanotube formation**. *PLoS One* 2012; 7(10):e47664.

53. Inoue H, Miyaji M, Kosugi A, Nagafuku M, Okazaki T, Mimori T, et al. **Lipid rafts as the signaling scaffold for NK cell activation: tyrosine phosphorylation and association of LAT with phosphatidylinositol 3-kinase and phospholipase C-gamma following CD2 stimulation**. *Eur J Immunol* 2002; 32(8):2188-2198.

54. McNerney ME, Kumar V. **The CD2 family of natural killer cell receptors**. *Curr Top Microbiol Immunol* 2006; 298:91-120.

55. Ben-Shmuel A, Sabag B, Biber G, Barda-Saad M. **The Role of the Cytoskeleton in Regulating the Natural Killer Cell Immune Response in Health and Disease: From Signaling Dynamics to Function**. *Front Cell Dev Biol* 2021; 9:609532.

56. Goode BL, Eck MJ. **Mechanism and function of formins in the control of actin assembly**. *Annu Rev Biochem* 2007; 76:593-627.

57. Pruyne D, Evangelista M, Yang C, Bi E, Zigmond S, Bretscher A, et al. **Role of formins in actin assembly: nucleation and barbed-end association**. *Science* 2002; 297(5581):612-615.

58. Pollard TD, Borisy GG. **Cellular motility driven by assembly and disassembly of actin filaments**. *Cell* 2003; 112(4):453-465.

59. Soderling SH. **Grab your partner with both hands: cytoskeletal remodeling by Arp2/3 signaling**. *Sci Signal* 2009; 2(55):pe5.

60. Smith BA, Padrick SB, Doolittle LK, Daugherty-Clarke K, Correa IR, Jr., Xu MQ, et al. **Three-color single molecule imaging shows WASP detachment from Arp2/3 complex triggers actin filament branch formation**. *Elife* 2013; 2:e01008.

61. Orange JS, Ramesh N, Remold-O'Donnell E, Sasahara Y, Koopman L, Byrne M, et al. **Wiskott-Aldrich syndrome protein is required for NK cell cytotoxicity and colocalizes with actin to NK cell-activating immunologic synapses**. *Proc Natl Acad Sci U S A* 2002; 99(17):11351-11356.

62. Katz P, Zaytoun AM, Lee JH, Jr. **Mechanisms of human cell-mediated cytotoxicity. III. Dependence of natural killing on microtubule and microfilament integrity**. *J Immunol* 1982; 129(6):2816-2825.

63. Wulfing C, Purtic B, Klem J, Schatzle JD. **Stepwise cytoskeletal polarization as a series of checkpoints in innate but not adaptive cytolytic killing**. *Proc Natl Acad Sci U S A* 2003; 100(13):7767-7772.

64. Kovar DR, Harris ES, Mahaffy R, Higgs HN, Pollard TD. **Control of the assembly of ATP- and ADP-actin by formins and profilin**. *Cell* 2006; 124(2):423-435.

65. Mentlik AN, Sanborn KB, Holzbaur EL, Orange JS. **Rapid lytic granule convergence to the MTOC in natural killer cells is dependent on dynein but not cytolytic commitment**. *Mol Biol Cell* 2010; 21(13):2241-2256.

66. Combs J, Kim SJ, Tan S, Ligon LA, Holzbaur EL, Kuhn J, et al. **Recruitment of dynein to the Jurkat immunological synapse**. *Proc Natl Acad Sci U S A* 2006; 103(40):14883-14888.

67. Burkhardt JK, McIlvain JM, Jr., Sheetz MP, Argon Y. **Lytic granules from cytotoxic T cells exhibit kinesin-dependent motility on microtubules in vitro**. *J Cell Sci* 1993; 104 (Pt 1):151-162.

68. Stinchcombe JC, Majorovits E, Bossi G, Fuller S, Griffiths GM. **Centrosome polarization delivers secretory granules to the immunological synapse**. *Nature* 2006; 443(7110):462-465.

69. Andzelm MM, Chen X, Krzewski K, Orange JS, Strominger JL. **Myosin IIA is required for cytolytic granule exocytosis in human NK cells**. *J Exp Med* 2007; 204(10):2285-2291.

70. Liu CC, Perussia B, Cohn ZA, Young JD. **Identification and characterization of a pore-forming protein of human peripheral blood natural killer cells**. *J Exp Med* 1986; 164(6):2061-2076.

71. Voskoboinik I, Smyth MJ, Trapani JA. **Perforin-mediated target-cell death and immune homeostasis**. *Nat Rev Immunol* 2006; 6(12):940-952.

72. Rochel N, Cowan J. **Negative cooperativity exhibited by the lytic amino-terminal domain of human perforin: implications for perforin-mediated cell lysis**. *Chem Biol* 1996; 3(1):31-36.

73. Brennan AJ, Chia J, Browne KA, Ciccone A, Ellis S, Lopez JA, et al. **Protection from endogenous perforin: glycans and the C terminus regulate exocytic trafficking in cytotoxic lymphocytes**. *Immunity* 2011; 34(6):879-892.

74. Voskoboinik I, Thia MC, Fletcher J, Ciccone A, Browne K, Smyth MJ, et al. **Calcium-dependent plasma membrane binding and cell lysis by perforin are mediated through its C2 domain: A critical role for aspartate residues 429, 435, 483, and 485 but not 491**. *J Biol Chem* 2005; 280(9):8426-8434.

75. Uellner R, Zvelebil MJ, Hopkins J, Jones J, MacDougall LK, Morgan BP, et al. **Perforin is activated by a proteolytic cleavage during biosynthesis which reveals a phospholipid-binding C2 domain**. *EMBO J* 1997; 16(24):7287-7296.

76. Kataoka T, Togashi K, Takayama H, Takaku K, Nagai K. **Inactivation and proteolytic degradation of perforin within lytic granules upon neutralization of acidic pH**.

Immunology 1997; 91(3):493-500.

77. Fraser SA, Karimi R, Michalak M, Hudig D. **Perforin lytic activity is controlled by calreticulin**. *J Immunol* 2000; 164(8):4150-4155.

78. Nakata M, Kawasaki A, Azuma M, Tsuji K, Matsuda H, Shinkai Y, et al. **Expression of perforin and cytolytic potential of human peripheral blood lymphocyte subpopulations**. *Int Immunol* 1992; 4(9):1049-1054.

79. Salcedo TW, Azzoni L, Wolf SF, Perussia B. **Modulation of perforin and granzyme messenger RNA expression in human natural killer cells**. *J Immunol* 1993; 151(5):2511-2520.

80. Pandey R, DeStephan CM, Madge LA, May MJ, Orange JS. **NKp30 ligation induces rapid activation of the canonical NF-kappaB pathway in NK cells**. *J Immunol* 2007; 179(11):7385-7396.

81. Zhou J, Zhang J, Lichtenheld MG, Meadows GG. **A role for NF-kappa B activation in perforin expression of NK cells upon IL-2 receptor signaling**. *J Immunol* 2002; 169(3):1319-1325.

82. Wagner JA, Wong P, Schappe T, Berrien-Elliott MM, Cubitt C, Jaeger N, et al. **Stage-Specific Requirement for Eomes in Mature NK Cell Homeostasis and Cytotoxicity**. *Cell Rep* 2020; 31(9):107720.

83. Daussy C, Faure F, Mayol K, Viel S, Gasteiger G, Charrier E, et al. **T-bet and Eomes instruct the development of two distinct natural killer cell lineages in the liver and in the bone marrow**. *J Exp Med* 2014; 211(3):563-577.

84. Grossman WJ, Revell PA, Lu ZH, Johnson H, Bredemeyer AJ, Ley TJ. **The orphan granzymes of humans and mice**. *Curr Opin Immunol* 2003; 15(5):544-552.

85. Chowdhury D, Lieberman J. **Death by a thousand cuts: granzyme pathways of programmed cell death**. *Annu Rev Immunol* 2008; 26:389-420.

86. Griffiths GM, Isaaz S. **Granzymes A and B are targeted to the lytic granules of lymphocytes by the mannose-6-phosphate receptor**. *J Cell Biol* 1993; 120(4):885-896.

87. Metkar SS, Wang B, Aguilar-Santelises M, Raja SM, Uhlin-Hansen L, Podack E, et al. **Cytotoxic cell granule-mediated apoptosis: perforin delivers granzyme B-serglycin complexes into target cells without plasma membrane pore formation**. *Immunity* 2002; 16(3):417-428.

88. Smyth MJ, McGuire MJ, Thia KY. **Expression of recombinant human granzyme B. A processing and activation role for dipeptidyl peptidase I**. *J Immunol* 1995; 154(12):6299-6305.

89. Meade JL, de Wynter EA, Brett P, Sharif SM, Woods CG, Markham AF, et al. **A family with Papillon-Lefevre syndrome reveals a requirement for cathepsin C in granzyme B activation and NK cell cytolytic activity**. *Blood* 2006; 107(9):3665-3668.

90. D'Angelo ME, Bird PI, Peters C, Reinheckel T, Trapani JA, Sutton VR. **Cathepsin H is an additional convertase of pro-granzyme B**. *J Biol Chem* 2010; 285(27):20514-20519.

91. Sutton VR, Brennan AJ, Ellis S, Danne J, Thia K, Jenkins MR, et al. **Serglycin determines secretory granule repertoire and regulates natural killer cell and cytotoxic T lymphocyte cytotoxicity**. *FEBS J* 2016; 283(5):947-961.

92. Law RH, Lukoyanova N, Voskoboinik I, Caradoc-Davies TT, Baran K, Dunstone MA, et al. **The structural basis for membrane binding and pore formation by lymphocyte perforin**. *Nature* 2010; 468(7322):447-451.

93. Keefe D, Shi L, Feske S, Massol R, Navarro F, Kirchhausen T, et al. **Perforin triggers a plasma membrane-repair response that facilitates CTL induction of apoptosis**. *Immunity* 2005; 23(3):249-262.

94. Kurschus FC, Fellows E, Stegmann E, Jenne DE. **Granzyme B delivery via perforin is restricted by size, but not by heparan sulfate-dependent endocytosis**. *Proc Natl Acad Sci U S A* 2008; 105(37):13799-13804.

95. Goping IS, Barry M, Liston P, Sawchuk T, Constantinescu G, Michalak KM, et al. **Granzyme B-induced apoptosis requires both direct caspase activation and relief of caspase inhibition**. *Immunity* 2003; 18(3):355-365.

96. Wang X. **The expanding role of mitochondria in apoptosis**. *Genes Dev* 2001; 15(22):2922-2933.

97. Waterhouse NJ, Sedelies KA, Browne KA, Wowk ME, Newbold A, Sutton VR, et al. **A central role for Bid in granzyme B-induced apoptosis**. *J Biol Chem* 2005; 280(6):4476-4482.

98. Sebbagh M, Hamelin J, Bertoglio J, Solary E, Breard J. **Direct cleavage of ROCK II by granzyme B induces target cell membrane blebbing in a caspase-independent manner**. *J Exp Med* 2005; 201(3):465-471.

99. Gross C, Koelch W, DeMaio A, Arispe N, Multhoff G. **Cell surface-bound heat shock protein 70 (Hsp70) mediates perforin-independent apoptosis by specific binding and uptake of granzyme B**. *J Biol Chem* 2003; 278(42):41173-41181.

100. Weiner OD, Marganski WA, Wu LF, Altschuler SJ, Kirschner MW. **An actin-based wave generator organizes cell motility**. *PLoS Biol* 2007; 5(9):e221.

101. Herrmann H, Bar H, Kreplak L, Strelkov SV, Aebi U. **Intermediate filaments: from cell architecture to nanomechanics**. *Nat Rev Mol Cell Biol* 2007; 8(7):562-573.

102. Carpen O, Virtanen I, Lehto V, Saksela EJTJoI. **Polarization of NK cell cytoskeleton upon conjugation with sensitive target cells**. 1983; 131(6):2695-2698.

103. Dominguez R, Holmes KC. **Actin structure and function**. *Annu Rev Biophys* 2011; 40:169-186.

104. Reicher B, Joseph N, David A, Pauker MH, Perl O, Barda-Saad M. **Ubiquitylation-dependent negative regulation of WASp is essential for actin cytoskeleton dynamics**. *Mol*

Cell Biol 2012; 32(15):3153-3163.

105. Kim AS, Kakalis LT, Abdul-Manan N, Liu GA, Rosen MK. **Autoinhibition and activation mechanisms of the Wiskott-Aldrich syndrome protein**. *Nature* 2000; 404(6774):151-158.

106. Abdul-Manan N, Aghazadeh B, Liu GA, Majumdar A, Ouerfelli O, Siminovitch KA, et al. **Structure of Cdc42 in complex with the GTPase-binding domain of the 'Wiskott-Aldrich syndrome' protein**. *Nature* 1999; 399(6734):379-383.

107. Mace EM, Orange JS. **Lytic immune synapse function requires filamentous actin deconstruction by Coronin 1A**. *Proc Natl Acad Sci U S A* 2014; 111(18):6708-6713.

108. Krummel MF, Bartumeus F, Gerard A. **T cell migration, search strategies and mechanisms**. *Nat Rev Immunol* 2016; 16(3):193-201.

109. Jacobelli J, Friedman RS, Conti MA, Lennon-Dumenil AM, Piel M, Sorensen CM, et al. **Confinement-optimized three-dimensional T cell amoeboid motility is modulated via myosin IIA-regulated adhesions**. *Nat Immunol* 2010; 11(10):953-961.

110. Lauffenburger DA, Horwitz AF. **Cell migration: a physically integrated molecular process**. *Cell* 1996; 84(3):359-369.

111. Mitchison TJ, Cramer LP. **Actin-based cell motility and cell locomotion**. *Cell* 1996; 84(3):371-379.

112. Hartshorne DJ, Ito M, Erdodi F. **Myosin light chain phosphatase: subunit composition, interactions and regulation**. *J Muscle Res Cell Motil* 1998; 19(4):325-341.

113. Kamm KE, Stull JT. **Dedicated myosin light chain kinases with diverse cellular functions**. *J Biol Chem* 2001; 276(7):4527-4530.

114. Somlyo AP, Somlyo AV. **Ca2+ sensitivity of smooth muscle and nonmuscle myosin II: modulated by G proteins, kinases, and myosin phosphatase**. *Physiol Rev* 2003; 83(4):1325-1358.

115. Desai A, Mitchison TJ. **Microtubule polymerization dynamics**. *Annu Rev Cell Dev Biol* 1997; 13:83-117.

116. Brangwynne CP, MacKintosh FC, Kumar S, Geisse NA, Talbot J, Mahadevan L, et al. **Microtubules can bear enhanced compressive loads in living cells because of lateral reinforcement**. *J Cell Biol* 2006; 173(5):733-741.

117. Kloc M, Kubiak JZ, Li XC, Ghobrial RM. **The newly found functions of MTOC in immunological response**. *J Leukoc Biol* 2014; 95(3):417-430.

118. Carlier MF, Pantaloni D. **Kinetic analysis of guanosine 5'-triphosphate hydrolysis associated with tubulin polymerization**. *Biochemistry* 1981; 20(7):1918-1924.

119. Hendricks AG, Lazarus JE, Perlson E, Gardner MK, Odde DJ, Goldman YE, et al. **Dynein tethers and stabilizes dynamic microtubule plus ends**. *Curr Biol* 2012; 22(7):632-637.

120. Desai A, Verma S, Mitchison TJ, Walczak CE. **Kin I kinesins are microtubule-**

destabilizing enzymes. *Cell* 1999; 96(1):69-78.

121. Sproul LR, Anderson DJ, Mackey AT, Saunders WS, Gilbert SP. **Cik1 targets the minus-end kinesin depolymerase kar3 to microtubule plus ends**. *Curr Biol* 2005; 15(15):1420-1427.

122. Mitchison T, Kirschner M. **Dynamic instability of microtubule growth**. *Nature* 1984; 312(5991):237-242.

123. Akhmanova A, Steinmetz MO. **Control of microtubule organization and dynamics: two ends in the limelight**. *Nat Rev Mol Cell Biol* 2015; 16(12):711-726.

124. Akhmanova A, Steinmetz MO. **Tracking the ends: a dynamic protein network controls the fate of microtubule tips**. *Nat Rev Mol Cell Biol* 2008; 9(4):309-322.

125. Howard J, Hyman AA. **Microtubule polymerases and depolymerases**. *Curr Opin Cell Biol* 2007; 19(1):31-35.

126. Wiche G. **Role of plectin in cytoskeleton organization and dynamics**. *J Cell Sci* 1998; 111 (Pt 17):2477-2486.

127. Li J, Wang R, Tang DD. **Vimentin dephosphorylation at ser-56 is regulated by type 1 protein phosphatase in smooth muscle**. *Respir Res* 2016; 17(1):91.

128. Tang DD. **Intermediate filaments in smooth muscle**. *Am J Physiol Cell Physiol* 2008; 294(4):C869-878.

129. Nieminen M, Henttinen T, Merinen M, Marttila-Ichihara F, Eriksson JE, Jalkanen S. **Vimentin function in lymphocyte adhesion and transcellular migration**. *Nat Cell Biol* 2006; 8(2):156-162.

130. Eckes B, Dogic D, Colucci-Guyon E, Wang N, Maniotis A, Ingber D, et al. **Impaired mechanical stability, migration and contractile capacity in vimentin-deficient fibroblasts**. *J Cell Sci* 1998; 111 (Pt 13):1897-1907.

131. Ivaska J, Pallari HM, Nevo J, Eriksson JE. **Novel functions of vimentin in cell adhesion, migration, and signaling**. *Exp Cell Res* 2007; 313(10):2050-2062.

132. Leduc C, Etienne-Manneville S. **Intermediate filaments in cell migration and invasion: the unusual suspects**. *Curr Opin Cell Biol* 2015; 32:102-112.

133. Kong L, Schafer G, Bu H, Zhang Y, Zhang Y, Klocker H. **Lamin A/C protein is overexpressed in tissue-invading prostate cancer and promotes prostate cancer cell growth, migration and invasion through the PI3K/AKT/PTEN pathway**. *Carcinogenesis* 2012; 33(4):751-759.

134. Wu Z, Wu L, Weng D, Xu D, Geng J, Zhao F. **Reduced expression of lamin A/C correlates with poor histological differentiation and prognosis in primary gastric carcinoma**. *J Exp Clin Cancer Res* 2009; 28:8.

135. Paluch EK, Raz E. **The role and regulation of blebs in cell migration**. *Curr Opin Cell Biol* 2013; 25(5):582-590.

136. Charras G, Paluch E. **Blebs lead the way: how to migrate without lamellipodia**. *Nat Rev Mol Cell Biol* 2008; 9(9):730-736.

137. Liu YJ, Le Berre M, Lautenschlaeger F, Maiuri P, Callan-Jones A, Heuze M, et al. **Confinement and low adhesion induce fast amoeboid migration of slow mesenchymal cells**. *Cell* 2015; 160(4):659-672.

138. Renkawitz J, Schumann K, Weber M, Lammermann T, Pflicke H, Piel M, et al. **Adaptive force transmission in amoeboid cell migration**. *Nat Cell Biol* 2009; 11(12):1438-1443.

139. Ruprecht V, Wieser S, Callan-Jones A, Smutny M, Morita H, Sako K, et al. **Cortical contractility triggers a stochastic switch to fast amoeboid cell motility**. *Cell* 2015; 160(4):673-685.

140. Bergert M, Erzberger A, Desai RA, Aspalter IM, Oates AC, Charras G, et al. **Force transmission during adhesion-independent migration**. *Nat Cell Biol* 2015; 17(4):524-529.

141. Ratner S, Sherrod WS, Lichlyter D. **Microtubule retraction into the uropod and its role in T cell polarization and motility**. *J Immunol* 1997; 159(3):1063-1067.

142. Lammermann T, Sixt M. **Mechanical modes of 'amoeboid' cell migration**. *Curr Opin Cell Biol* 2009; 21(5):636-644.

143. Discher DE, Janmey P, Wang YL. **Tissue cells feel and respond to the stiffness of their substrate**. *Science* 2005; 310(5751):1139-1143.

144. Gupta M, Sarangi BR, Deschamps J, Nematbakhsh Y, Callan-Jones A, Margadant F, et al. **Adaptive rheology and ordering of cell cytoskeleton govern matrix rigidity sensing**. *Nat Commun* 2015; 6:7525.

145. Tozluoglu M, Tournier AL, Jenkins RP, Hooper S, Bates PA, Sahai E. **Matrix geometry determines optimal cancer cell migration strategy and modulates response to interventions**. *Nat Cell Biol* 2013; 15(7):751-762.

146. Lammermann T, Bader BL, Monkley SJ, Worbs T, Wedlich-Soldner R, Hirsch K, et al. **Rapid leukocyte migration by integrin-independent flowing and squeezing**. *Nature* 2008; 453(7191):51-55.

147. Artym VV, Matsumoto K. **Imaging cells in three-dimensional collagen matrix**. *Curr Protoc Cell Biol* 2010; Chapter 10:Unit 10 18 11-20.

148. Pedersen JA, Swartz MA. **Mechanobiology in the third dimension**. *Ann Biomed Eng* 2005; 33(11):1469-1490.

149. Harley BA, Kim H-D, Zaman MH, Yannas IV, Lauffenburger DA, Gibson LJJBj. **Microarchitecture of three-dimensional scaffolds influences cell migration behavior via junction interactions**. 2008; 95(8):4013-4024.

150. Grew JC, Ricci JL, Alexander HJJoBMRPAAOJoTSfB, The Japanese Society for Biomaterials,, Biomaterials TASf, Biomaterials tKSf. **Connective-tissue responses to defined biomaterial surfaces. II. Behavior of rat and mouse fibroblasts cultured on microgrooved**

substrates. 2008; 85(2):326-335.

151. Poole K, Khairy K, Friedrichs J, Franz C, Cisneros DA, Howard J, et al. **Molecular-scale topographic cues induce the orientation and directional movement of fibroblasts on two-dimensional collagen surfaces**. *J Mol Biol* 2005; 349(2):380-386.

152. Wolf K, Wu YI, Liu Y, Geiger J, Tam E, Overall C, et al. **Multi-step pericellular proteolysis controls the transition from individual to collective cancer cell invasion**. *Nat Cell Biol* 2007; 9(8):893-904.

153. Butcher DT, Alliston T, Weaver VM. **A tense situation: forcing tumour progression**. *Nat Rev Cancer* 2009; 9(2):108-122.

154. Giannone G, Sheetz MP. **Substrate rigidity and force define form through tyrosine phosphatase and kinase pathways**. *Trends Cell Biol* 2006; 16(4):213-223.

155. Wolf K, Muller R, Borgmann S, Brocker EB, Friedl P. **Amoeboid shape change and contact guidance: T-lymphocyte crawling through fibrillar collagen is independent of matrix remodeling by MMPs and other proteases**. *Blood* 2003; 102(9):3262-3269.

156. Friedl P, Wolf K. **Proteolytic and non-proteolytic migration of tumour cells and leucocytes**. *Biochem Soc Symp* 2003; (70):277-285.

157. Zhao R, Zhou X, Khan ES, Alansary D, Friedmann KS, Yang W, et al. **Targeting the Microtubule-Network Rescues CTL Killing Efficiency in Dense 3D Matrices**. *Front Immunol* 2021; 12:729820.

158. Wolf K, Alexander S, Schacht V, Coussens LM, von Andrian UH, van Rheenen J, et al. **Collagen-based cell migration models in vitro and in vivo**. *Semin Cell Dev Biol* 2009; 20(8):931-941.

159. Brown E, McKee T, diTomaso E, Pluen A, Seed B, Boucher Y, et al. **Dynamic imaging of collagen and its modulation in tumors in vivo using second-harmonic generation**. *Nat Med* 2003; 9(6):796-800.

160. Knorck A, Marx S, Friedmann KS, Zophel S, Lieblang L, Hassig C, et al. **Quantity, quality, and functionality of peripheral blood cells derived from residual blood of different apheresis kits**. *Transfusion* 2018; 58(6):1516-1526.

161. Janeway Jr CA, Travers P, Walport M, Shlomchik MJ. **Macrophage activation by armed CD4 TH1 cells**. In: *Immunobiology: The Immune System in Health and Disease 5th edition*: Garland Science; 2001.

162. Zhu X, Zhu J. **CD4 T Helper Cell Subsets and Related Human Immunological Disorders**. *Int J Mol Sci* 2020; 21(21).

163. Morgan DA, Ruscetti FW, Gallo R. **Selective in vitro growth of T lymphocytes from normal human bone marrows**. *Science* 1976; 193(4257):1007-1008.

164. Kim HP, Imbert J, Leonard WJ. **Both integrated and differential regulation of components of the IL-2/IL-2 receptor system**. *Cytokine Growth Factor Rev* 2006; 17(5):349-

366.

165. Wang X, Rickert M, Garcia KC. **Structure of the quaternary complex of interleukin-2 with its alpha, beta, and gammac receptors**. *Science* 2005; 310(5751):1159-1163.

166. Leonard WJ. **Cytokines and immunodeficiency diseases**. *Nat Rev Immunol* 2001; 1(3):200-208.

167. Henney CS, Kuribayashi K, Kern DE, Gillis S. **Interleukin-2 augments natural killer cell activity**. *Nature* 1981; 291(5813):335-338.

168. Bryceson YT, March ME, Ljunggren HG, Long EO. **Synergy among receptors on resting NK cells for the activation of natural cytotoxicity and cytokine secretion**. *Blood* 2006; 107(1):159-166.

169. Robertson MJ, Caligiuri MA, Manley TJ, Levine H, Ritz J. **Human natural killer cell adhesion molecules. Differential expression after activation and participation in cytolysis**. *J Immunol* 1990; 145(10):3194-3201.

170. Caligiuri MA, Murray C, Robertson MJ, Wang E, Cochran K, Cameron C, et al. **Selective modulation of human natural killer cells in vivo after prolonged infusion of low dose recombinant interleukin 2**. *J Clin Invest* 1993; 91(1):123-132.

171. Ni J, Miller M, Stojanovic A, Garbi N, Cerwenka A. **Sustained effector function of IL-12/15/18-preactivated NK cells against established tumors**. *J Exp Med* 2012; 209(13):2351-2365.

172. Bihl F, Pecheur J, Breart B, Poupon G, Cazareth J, Julia V, et al. **Primed antigen-specific CD4+ T cells are required for NK cell activation in vivo upon Leishmania major infection**. *J Immunol* 2010; 185(4):2174-2181.

173. Fehniger TA, Cooper MA, Nuovo GJ, Cella M, Facchetti F, Colonna M, et al. **CD56bright natural killer cells are present in human lymph nodes and are activated by T cell-derived IL-2: a potential new link between adaptive and innate immunity**. *Blood* 2003; 101(8):3052-3057.

174. Horowitz A, Newman KC, Evans JH, Korbel DS, Davis DM, Riley EM. **Cross-talk between T cells and NK cells generates rapid effector responses to Plasmodium falciparum-infected erythrocytes**. *J Immunol* 2010; 184(11):6043-6052.

175. He XS, Draghi M, Mahmood K, Holmes TH, Kemble GW, Dekker CL, et al. **T cell-dependent production of IFN-gamma by NK cells in response to influenza A virus**. *J Clin Invest* 2004; 114(12):1812-1819.

176. Ferlazzo G, Thomas D, Lin SL, Goodman K, Morandi B, Muller WA, et al. **The abundant NK cells in human secondary lymphoid tissues require activation to express killer cell Ig-like receptors and become cytolytic**. *J Immunol* 2004; 172(3):1455-1462.

177. Ferlazzo G, Pack M, Thomas D, Paludan C, Schmid D, Strowig T, et al. **Distinct roles of IL-12 and IL-15 in human natural killer cell activation by dendritic cells from secondary**

lymphoid organs. *Proc Natl Acad Sci U S A* 2004; 101(47):16606-16611.

178. Lee SH, Fragoso MF, Biron CA. **Cutting edge: a novel mechanism bridging innate and adaptive immunity: IL-12 induction of CD25 to form high-affinity IL-2 receptors on NK cells**. *J Immunol* 2012; 189(6):2712-2716.

179. Gasteiger G, Hemmers S, Firth MA, Le Floc'h A, Huse M, Sun JC, et al. **IL-2-dependent tuning of NK cell sensitivity for target cells is controlled by regulatory T cells**. *J Exp Med* 2013; 210(6):1167-1178.

180. Sojka DK, Bruniquel D, Schwartz RH, Singh NJ. **IL-2 secretion by CD4+ T cells in vivo is rapid, transient, and influenced by TCR-specific competition**. *J Immunol* 2004; 172(10):6136-6143.

181. Abbas AK. **The Surprising Story of IL-2: From Experimental Models to Clinical Application**. *Am J Pathol* 2020; 190(9):1776-1781.

182. Kummerow C, Schwarz EC, Bufe B, Zufall F, Hoth M, Qu B. **A simple, economic, time-resolved killing assay**. *Eur J Immunol* 2014; 44(6):1870-1872.

183. Schoppmeyer R, Zhao R, Hoth M, Qu B. **Light-sheet Microscopy for Three-dimensional Visualization of Human Immune Cells**. *J Vis Exp* 2018; (136).

184. Mortazavi A, Williams BA, McCue K, Schaeffer L, Wold B. **Mapping and quantifying mammalian transcriptomes by RNA-Seq**. *Nat Methods* 2008; 5(7):621-628.

185. Anders S, Huber W. **Differential expression analysis for sequence count data**. *Genome Biol* 2010; 11(10):R106.

186. Wang L, Feng Z, Wang X, Wang X, Zhang X. **DEGseq: an R package for identifying differentially expressed genes from RNA-seq data**. *Bioinformatics* 2010; 26(1):136-138.

187. Huang da W, Sherman BT, Lempicki RA. **Systematic and integrative analysis of large gene lists using DAVID bioinformatics resources**. *Nat Protoc* 2009; 4(1):44-57.

188. Huang da W, Sherman BT, Lempicki RA. **Bioinformatics enrichment tools: paths toward the comprehensive functional analysis of large gene lists**. *Nucleic Acids Res* 2009; 37(1):1-13.

189. Kaech SM, Wherry EJ, Ahmed R. **Effector and memory T-cell differentiation: implications for vaccine development**. *Nat Rev Immunol* 2002; 2(4):251-262.

190. Wang SY, Racila E, Taylor RP, Weiner GJ. **NK-cell activation and antibody-dependent cellular cytotoxicity induced by rituximab-coated target cells is inhibited by the C3b component of complement**. *Blood* 2008; 111(3):1456-1463.

191. Backes CS, Friedmann KS, Mang S, Knorck A, Hoth M, Kummerow C. **Natural killer cells induce distinct modes of cancer cell death: Discrimination, quantification, and modulation of apoptosis, necrosis, and mixed forms**. *J Biol Chem* 2018; 293(42):16348-16363.

192. Zhou X, Zhao R, Schwarz K, Mangeat M, Schwarz EC, Hamed M, et al. **Bystander cells**

enhance NK cytotoxic efficiency by reducing search time. *Sci Rep* 2017; 7:44357.

193. Krzewski K, Gil-Krzewska A, Nguyen V, Peruzzi G, Coligan JE. **LAMP1/CD107a is required for efficient perforin delivery to lytic granules and NK-cell cytotoxicity**. *Blood* 2013; 121(23):4672-4683.

194. Del Prete G. **Human Th1 and Th2 lymphocytes: their role in the pathophysiology of atopy**. *Allergy* 1992; 47(5):450-455.

195. Rothoeft T, Balkow S, Krummen M, Beissert S, Varga G, Loser K, et al. **Structure and duration of contact between dendritic cells and T cells are controlled by T cell activation state**. *Eur J Immunol* 2006; 36(12):3105-3117.

196. Boyman O, Sprent J. **The role of interleukin-2 during homeostasis and activation of the immune system**. *Nat Rev Immunol* 2012; 12(3):180-190.

197. Reina M, Espel E. **Role of LFA-1 and ICAM-1 in Cancer**. *Cancers (Basel)* 2017; 9(11).

198. Li S, Wang H, Peng B, Zhang M, Zhang D, Hou S, et al. **Efalizumab binding to the LFA-1 alphaL I domain blocks ICAM-1 binding via steric hindrance**. *Proc Natl Acad Sci U S A* 2009; 106(11):4349-4354.

199. Aoyama M, Tada M, Yokoo H, Demizu Y, Ishii-Watabe A. **Fcgamma Receptor-Dependent Internalization and Off-Target Cytotoxicity of Antibody-Drug Conjugate Aggregates**. *Pharm Res* 2022; 39(1):89-103.

200. van Unen V, Hollt T, Pezzotti N, Li N, Reinders MJT, Eisemann E, et al. **Visual analysis of mass cytometry data by hierarchical stochastic neighbour embedding reveals rare cell types**. *Nat Commun* 2017; 8(1):1740.

201. Beyrend G, Stam K, Hollt T, Ossendorp F, Arens R. **Cytofast: A workflow for visual and quantitative analysis of flow and mass cytometry data to discover immune signatures and correlations**. *Comput Struct Biotechnol J* 2018; 16:435-442.

202. Rein ID, Noto HO, Bostad M, Huse K, Stokke T. **Cell Cycle Analysis and Relevance for Single-Cell Gating in Mass Cytometry**. *Cytometry A* 2020; 97(8):832-844.

203. Gunesch JT, Dixon AL, Ebrahim TA, Berrien-Elliott MM, Tatineni S, Kumar T, et al. **CD56 regulates human NK cell cytotoxicity through Pyk2**. *Elife* 2020; 9.

204. Bellora F, Castriconi R, Dondero A, Reggiardo G, Moretta L, Mantovani A, et al. **The interaction of human natural killer cells with either unpolarized or polarized macrophages results in different functional outcomes**. *Proc Natl Acad Sci U S A* 2010; 107(50):21659-21664.

205. Tang JJ, Sung AP, Guglielmo MJ, Navarrete-Galvan L, Redelman D, Smith-Gagen J, et al. **Natural Killer (NK) Cell Expression of CD2 as a Predictor of Serial Antibody-Dependent Cell-Mediated Cytotoxicity (ADCC)**. *Antibodies (Basel)* 2020; 9(4).

206. Gasteiger G, Hemmers S, Bos PD, Sun JC, Rudensky AY. **IL-2-dependent adaptive control of NK cell homeostasis**. *J Exp Med* 2013; 210(6):1179-1187.

207. Oberg HH, Wesch D, Grussel S, Rose-John S, Kabelitz D. **Differential expression of CD126 and CD130 mediates different STAT-3 phosphorylation in CD4+CD25- and CD25high regulatory T cells**. *Int Immunol* 2006; 18(4):555-563.

208. Cichocki F, Miller JS, Anderson SK, Bryceson YT. **Epigenetic regulation of NK cell differentiation and effector functions**. *Front Immunol* 2013; 4:55.

209. Gregoire C, Chasson L, Luci C, Tomasello E, Geissmann F, Vivier E, et al. **The trafficking of natural killer cells**. *Immunol Rev* 2007; 220:169-182.

210. Maghazachi AA. **Role of chemokines in the biology of natural killer cells**. *Curr Top Microbiol Immunol* 2010; 341:37-58.

211. Dustin ML, Long EO. **Cytotoxic immunological synapses**. *Immunol Rev* 2010; 235(1):24-34.

212. Shimizu Y, Shaw S. **Lymphocyte interactions with extracellular matrix**. *FASEB J* 1991; 5(9):2292-2299.

213. Zhao Y, Li MC, Konate MM, Chen L, Das B, Karlovich C, et al. **TPM, FPKM, or Normalized Counts? A Comparative Study of Quantification Measures for the Analysis of RNA-seq Data from the NCI Patient-Derived Models Repository**. *J Transl Med* 2021; 19(1):269.

214. Seetharaman S, Etienne-Manneville S. **Cytoskeletal Crosstalk in Cell Migration**. *Trends Cell Biol* 2020; 30(9):720-735.

215. Siton-Mendelson O, Bernheim-Groswasser A. **Functional Actin Networks under Construction: The Cooperative Action of Actin Nucleation and Elongation Factors**. *Trends Biochem Sci* 2017; 42(6):414-430.

216. Wu Y, Tian Z, Wei H. **Developmental and Functional Control of Natural Killer Cells by Cytokines**. *Front Immunol* 2017; 8:930.

217. Bihl F, Germain C, Luci C, Braud VM. **Mechanisms of NK cell activation: CD4(+) T cells enter the scene**. *Cell Mol Life Sci* 2011; 68(21):3457-3467.

218. Horowitz A, Behrens RH, Okell L, Fooks AR, Riley EM. **NK cells as effectors of acquired immune responses: effector CD4+ T cell-dependent activation of NK cells following vaccination**. *J Immunol* 2010; 185(5):2808-2818.

219. Yu S, Li A, Liu Q, Li T, Yuan X, Han X, et al. **Chimeric antigen receptor T cells: a novel therapy for solid tumors**. *J Hematol Oncol* 2017; 10(1):78.

220. Cozar B, Greppi M, Carpentier S, Narni-Mancinelli E, Chiossone L, Vivier E. **Tumor-Infiltrating Natural Killer Cells**. *Cancer Discov* 2021; 11(1):34-44.

221. Goldman RD, Khuon S, Chou YH, Opal P, Steinert PM. **The function of intermediate filaments in cell shape and cytoskeletal integrity**. *J Cell Biol* 1996; 134(4):971-983.

222. Lammerding J, Fong LG, Ji JY, Reue K, Stewart CL, Young SG, et al. **Lamins A and C but not lamin B1 regulate nuclear mechanics**. *J Biol Chem* 2006; 281(35):25768-25780.

223. Wilson DN, Doudna Cate JH. **The structure and function of the eukaryotic ribosome**. *Cold Spring Harb Perspect Biol* 2012; 4(5).

224. Guo Y, Xiao P, Lei S, Deng F, Xiao GG, Liu Y, et al. **How is mRNA expression predictive for protein expression? A correlation study on human circulating monocytes**. *Acta Biochim Biophys Sin (Shanghai)* 2008; 40(5):426-436.

225. Plitzko B, Loesgen S. **Measurement of Oxygen Consumption Rate (OCR) and Extracellular Acidification Rate (ECAR) in Culture Cells for Assessment of the Energy Metabolism**. *Bio Protoc* 2018; 8(10):e2850.

226. Jiang T, Zhou C, Ren S. **Role of IL-2 in cancer immunotherapy**. *Oncoimmunology* 2016; 5(6):e1163462.

227. Skrombolas D, Frelinger JG. **Challenges and developing solutions for increasing the benefits of IL-2 treatment in tumor therapy**. *Expert Rev Clin Immunol* 2014; 10(2):207-217.

228. Fajgenbaum DC, June CH. **Cytokine Storm**. *N Engl J Med* 2020; 383(23):2255-2273.

229. Letourneau S, Krieg C, Pantaleo G, Boyman O. **IL-2- and CD25-dependent immunoregulatory mechanisms in the homeostasis of T-cell subsets**. *J Allergy Clin Immunol* 2009; 123(4):758-762.

230. Kim M, Kim TJ, Kim HM, Doh J, Lee KM. **Multi-cellular natural killer (NK) cell clusters enhance NK cell activation through localizing IL-2 within the cluster**. *Sci Rep* 2017; 7:40623.

231. Malek TR. **The biology of interleukin-2**. *Annu Rev Immunol* 2008; 26:453-479.

232. Huse M, Lillemeier BF, Kuhns MS, Chen DS, Davis MM. **T cells use two directionally distinct pathways for cytokine secretion**. *Nat Immunol* 2006; 7(3):247-255.

233. Reichert P, Reinhardt RL, Ingulli E, Jenkins MK. **Cutting edge: in vivo identification of TCR redistribution and polarized IL-2 production by naive CD4 T cells**. *J Immunol* 2001; 166(7):4278-4281.

234. Poo WJ, Conrad L, Janeway CA, Jr. **Receptor-directed focusing of lymphokine release by helper T cells**. *Nature* 1988; 332(6162):378-380.

235. Kupfer H, Monks CR, Kupfer A. **Small splenic B cells that bind to antigen-specific T helper (Th) cells and face the site of cytokine production in the Th cells selectively proliferate: immunofluorescence microscopic studies of Th-B antigen-presenting cell interactions**. *J Exp Med* 1994; 179(5):1507-1515.

236. Kupfer A, Mosmann TR, Kupfer H. **Polarized expression of cytokines in cell conjugates of helper T cells and splenic B cells**. *Proc Natl Acad Sci U S A* 1991; 88(3):775-779.

237. Miller MJ, Wei SH, Parker I, Cahalan MD. **Two-photon imaging of lymphocyte motility and antigen response in intact lymph node**. *Science* 2002; 296(5574):1869-1873.

238. Stoll S, Delon J, Brotz TM, Germain RN. **Dynamic imaging of T cell-dendritic cell interactions in lymph nodes**. *Science* 2002; 296(5574):1873-1876.

239. Dustin ML, Bromley SK, Kan Z, Peterson DA, Unanue ER. **Antigen receptor engagement delivers a stop signal to migrating T lymphocytes**. *Proc Natl Acad Sci U S A* 1997; 94(8):3909-3913.

240. Culley FJ, Johnson M, Evans JH, Kumar S, Crilly R, Casasbuenas J, et al. **Natural killer cell signal integration balances synapse symmetry and migration**. *PLoS Biol* 2009; 7(7):e1000159.

241. Dustin ML. **Hunter to gatherer and back: immunological synapses and kinapses as variations on the theme of amoeboid locomotion**. *Annu Rev Cell Dev Biol* 2008; 24:577-596.

242. Huse M. **Microtubule-organizing center polarity and the immunological synapse: protein kinase C and beyond**. *Front Immunol* 2012; 3:235.

243. Alcover A, Thoulouze MI. **Vesicle traffic to the immunological synapse: a multifunctional process targeted by lymphotropic viruses**. *Curr Top Microbiol Immunol* 2010; 340:191-207.

244. Di Vito C, Mikulak J, Mavilio D. **On the Way to Become a Natural Killer Cell**. *Front Immunol* 2019; 10:1812.

245. Crinier A, Milpied P, Escaliere B, Piperoglou C, Galluso J, Balsamo A, et al. **High-Dimensional Single-Cell Analysis Identifies Organ-Specific Signatures and Conserved NK Cell Subsets in Humans and Mice**. *Immunity* 2018; 49(5):971-986 e975.

246. Lopez-Verges S, Milush JM, Pandey S, York VA, Arakawa-Hoyt J, Pircher H, et al. **CD57 defines a functionally distinct population of mature NK cells in the human CD56dimCD16+ NK-cell subset**. *Blood* 2010; 116(19):3865-3874.

247. Krovi SH, Gapin L. **Invariant Natural Killer T Cell Subsets-More Than Just Developmental Intermediates**. *Front Immunol* 2018; 9:1393.

248. Gadola SD, Dulphy N, Salio M, Cerundolo V. **Valpha24-JalphaQ-independent, CD1d-restricted recognition of alpha-galactosylceramide by human CD4(+) and CD8alphabeta(+) T lymphocytes**. *J Immunol* 2002; 168(11):5514-5520.

249. Brigl M, van den Elzen P, Chen X, Meyers JH, Wu D, Wong CH, et al. **Conserved and heterogeneous lipid antigen specificities of CD1d-restricted NKT cell receptors**. *J Immunol* 2006; 176(6):3625-3634.

250. Godfrey DI, MacDonald HR, Kronenberg M, Smyth MJ, Van Kaer L. **NKT cells: what's in a name?** *Nat Rev Immunol* 2004; 4(3):231-237.

251. Kim CH, Butcher EC, Johnston B. **Distinct subsets of human Valpha24-invariant NKT cells: cytokine responses and chemokine receptor expression**. *Trends Immunol* 2002; 23(11):516-519.

252. Lanier LL, Chang C, Spits H, Phillips JH. **Expression of cytoplasmic CD3 epsilon proteins in activated human adult natural killer (NK) cells and CD3 gamma, delta, epsilon complexes in fetal NK cells. Implications for the relationship of NK and T lymphocytes**. *J

Immunol 1992; 149(6):1876-1880.

253. Bernstein HB, Plasterer MC, Schiff SE, Kitchen CM, Kitchen S, Zack JA. **CD4 expression on activated NK cells: ligation of CD4 induces cytokine expression and cell migration**. *J Immunol* 2006; 177(6):3669-3676.

254. Kandula S, Abraham C. **LFA-1 on CD4+ T cells is required for optimal antigen-dependent activation in vivo**. *J Immunol* 2004; 173(7):4443-4451.

255. Urlaub D, Hofer K, Muller ML, Watzl C. **LFA-1 Activation in NK Cells and Their Subsets: Influence of Receptors, Maturation, and Cytokine Stimulation**. *J Immunol* 2017; 198(5):1944-1951.

256. Barber DF, Faure M, Long EO. **LFA-1 contributes an early signal for NK cell cytotoxicity**. *J Immunol* 2004; 173(6):3653-3659.

257. Orange JS. **Formation and function of the lytic NK-cell immunological synapse**. *Nat Rev Immunol* 2008; 8(9):713-725.

7. Publications

Published:

- Pagano G, Botana IF, Wierz M, Roessner PM, Ioannou N, **<u>Zhou X</u>**, Al-Hity G, Borne C, Gargiulo E, Gonder S, Qu B, Stamatopoulos B, Ramsay AG, Seiffert M, Largeot A, Moussay E, Paggetti J. Interleukin-27 potentiates CD8+ T-cell-mediated anti-tumor immunity in chronic lymphocytic leukemia. *Haematologica* 2023. doi: 10.3324/haematol.2022.282474.

- Dai X, **<u>Zhou X</u>**, Shao R, Zhao R, Yanamandra AK, Xing Z, Ding M, Wang J, Liu T, Zheng Q, Zhang P, Zhang H, Wang Y, Qu B, Wang Y. Bioactive Constituents of Verbena officinalis Alleviate Inflammation and Enhance Killing Efficiency of Natural Killer Cells. *I Int J Mol Sci* 2023; 24(8). doi: 10.3390/ijms24087144.

- **<u>Zhou X</u>**, Zhang K, Liu L, Zhao Q, Huang M, Shao R, Wang Y, Qu B, Wang Y. Anti-fatigue effect from Ginseng Radix et Rhizoma: a suggestive and promising treatment for long COVID. *Acupuncture and Herbal Medicine* 2022; 2(2): 69. doi: 10.1097/HM9.0000000000000033

- **<u>Zhou X</u>**, Zhao R, Yanamandra AK, Hoth M, Qu B. Light-Sheet Scattering Microscopy to Visualize Long-Term Interactions Between Cells and Extracellular Matrix. *Front Immunol* 2022; 13:828634. doi: 10.3389/fimmu.2022.828634.

- Zhao R, **<u>Zhou X</u>**, Khan ES, Alansary D, Friedmann KS, Yang W, Schwarz EC, Del Campo A, Hoth M, Qu B. Targeting the Microtubule-Network Rescues CTL Killing Efficiency in Dense 3D Matrices. *Front Immunol* 2021; 12:729820. doi: 10.3389/fimmu.2021.729820.

- Jung P*, **<u>Zhou X*</u>**, Iden S, Bischoff M, Qu B. T cell stiffness is enhanced upon formation of immunological synapse. *Elife* 2021; 10. doi: 10.7554/eLife.66643.

- Zhu J, Yang W, **<u>Zhou X</u>**, Zöphel D, Soriano-Baguet L, Dolgener D, Carlein C, Hof C, Zhao R, Ye S, Schwarz EC, Brenner D, Prates Roma L, Qu B. High Glucose Enhances Cytotoxic T Lymphocyte-Mediated Cytotoxicity. *Front Immunol* 2021; 12: 689337. doi: 10.3389/fimmu.2021.689337.

- **<u>Zhou X</u>**, Song X, Huai C, Sun H, Chen H, Lu D. The applications of thermostable ligase chain reaction in facilitating DNA recombination. *Yi Chuan* 2016; 38(2):163-169. doi: 10.16288/j.yczz.15-428.

- Qiu P, Wang J, Bian Y, **Zhou X**, Wang G, Lu D. In utero stem cell transplantation and its preliminary application in hemophilia treatment. *Chinese Journal of Healthy Birth & Child Car*e 2012. doi: 10.3969/j.issn.1007-3434.2012.01.001

In preparation:

- **Zhou X**, Yang W, Gonder S, Zhao R, Kummerow C, Schwarz EC, Paggetti J, Moussay E, Hoth M, Qu B. T cells promote natural killer cell killing efficiency via enhanced migration.

* These authors contributed equally to this work

8. Acknowledgements

First and foremost, I would like to express my sincere gratitude and appreciation to my mentor Prof. Dr. Markus Hoth and my supervisor Dr. Bin Qu. As a highly reputed scholar, Prof. Markus showed respectful expertise and motivation. And as a personable mentor, he also showed noble humanity. It's really a great honor to work under his guidance. His invaluable insights and feedback have greatly contributed to my research. To Dr. Bin, I feel my words can't convey my gratefulness to her. She's not only my PhD supervisor but must be a best friend and most respectable elder in my whole life. She paid so much passion and patience to help my research and writing process. I'm always convinced by her talent and diligent. In science, she taught me how to think and do research as a qualified Ph.D. without reservation. And in life, she also provided me with unwavering support. I can't be more grateful for her valuable input, constructive criticism, and encouragement throughout the development of this work.

I am grateful to my colleagues with special thanks to Wenjuan Yang, Renping Zhao, Rouven Schoppmeyer, and Carsten Kummerow. Wenjuan helped me a lot with FACS staining. She was so warm-hearted and helpful. I would wish the best to her and her baby. Renping introduced many important techniques to me with great patience, and I'm always inspired by his ideas. Rouven and Carsten shared precious experiences on imaging technologies with me. Of course, Archana Yanamandra, Galia Magela Montalvo Bereau, Shulagna Sharma, Denise Dolgener are also the best teammates. They have provided me stimulating discussions, valuable suggestions, and a supportive academic environment. Their collaboration and camaraderie have been instrumental in shaping my ideas and enhancing the quality of this research.

I extend my deepest appreciation to our collaborators in this study who generously shared their time and insights. Jérôme Paggetti, Etienne Moussay, and Anne Largeot in Luxembourg Institute of Health helped me a lot on CyTOF analysis. Without their cooperation and willingness to participate, this research would not have gone so far.

I would like to express my heartfelt appreciation to anyone else who has directly or indirectly contributed to this research. Particularly, Dr. Eva C. Schwarz contributed so much to maintaining the running of the plate reader and the autoMACS. Lea Kaschek helped me with microscopy issues. Sylvia Zöphel shared materials with me. I also apologize for all the trouble I made to you. And thank you very much for your patience. Sen Qiao from Experimental Pharmacology, Center for Molecular Signaling (PZMS) also shared knowledge about RNAseq interpretation with me. Your assistance, encouragement, and support have been instrumental in

shaping the outcome of this work.

I would like to acknowledge the support and resources provided by our lovely technicians, Carmen Hässig, Cora Hoxha, Kathrin Förderer, Sandra Janku, Gertrud Schwär, etc. Their hard work and providing relevant materials have significantly contributed to the completion of this work. My gratitude also goes to our secretary Regine Kaleja, she helped me so many times with documents.

Of course, my thanks go to all the members of our lab. Everyone is an irreplaceable part of this warm and impressive lab. It's a luck to once be a member of this lab. Without the excellent atmosphere in this team, I can't image having finished such exciting work in the past 5 years.

Finally, I am indebted to my family and friends for their unwavering support, understanding, and patience throughout this journey. Their encouragement and belief in me have been a constant source of my motivation.

Thank you all for being a part of this incredible journey!

9. Curriculum Vitae

The curriculum vitae was removed from the electronic version of the doctoral thesis for reasons of data protection.